THE UNIVERSITY OF OKLAHOMA

GRADUATE COLLEGE

HEAT TRANSFER ASPECTS OF CRYOGENIC LIQUID SPILLS

A DISSERTATION

SUBMITTED TO THE GRADUATE FACULTY

in partial fulfillment of the requirements for the

degree of

DOCTOR OF PHILOSOPHY

BY

CHING SE YEN

Norman, Oklahoma

1974

HEAT TRANSFER ASPECTS OF CRYOGENIC LIQUID SPILLS

APPROVED BY

C. M. Sliepcevich

Harry H West

J Reed Welker

F M Townsend

John E Francis

DISSERTATION COMMITTEE

ABSTRACT

A quasilinearization alternating-direction implicit (QADI) numerical method was proposed to solve the differential equations that result from analysis of one- and two-dimensional heat conduction problems with phase change. The finite difference equations of these problems were derived from applying heat and material balances to discrete physical mesh regions rather than from applying an arbitrary finite difference approximation to the partial differential equations. The phase change of the medium was assumed to occur over a finite temperature interval rather than at a fixed temperature. The latent heat was approximated by an error function over this interval. The proposed method can deal with nonlinear boundary conditions and composite media without undue effort. The effects of the heat transfer coefficient between soil and Liquefied Natural Gas (LNG), thermal properties of soil, and latent heat of phase change on the boil-off rate of LNG spilled on soil were studied. The temperature distribution and the location of soil phase change were also examined. The results of the calculations and the convergence rate of the quasilinearization alternating-direction method were independent of the accelerating parameter.

A mathematical model for the heat transfer effects accompanying the application of high expansion foam on LNG spills on land was also developed. The model was used to study the characteristics of high expansion foam in controlling LNG vapor dispersion after a spill and particularly during the transition boiling period. The expansion ratio, boil-off rate of LNG, and foam application rate were found to be important factors on the high expansion foam performance.

ACKNOWLEDGMENTS

I would like to express my sincere gratitude to the following:

Dr. C. M. Sliepcevich, George Lynn Cross Research Professor of Engineering, for his guidance and support.

Dr. H. H. West, for his continual assistance and stimulating discussions throughout the program.

Dr. J. R. Welker, Associate Director of the Flame Dynamics Laboratory; Dr. F. M. Townsend, Professor of Chemical Engineering; and Dr. J. E. Francis, Associate Professor of Aerospace and Mechanical Engineering, for their service on the graduate committee.

Dr. L. E. Brown, for his helpful suggestions.

Ms. Bobbie Everidge and Mrs. Carlotta Wood, for their assistance in the manuscript preparation.

University Engineers, Inc., for providing financial support, and the computer center of the University of Oklahoma, for donating the computer time.

Finally I gratefully acknowledge the encouragement of my parents and wife through these many years of graduate school. Their sacrifice and understanding will not be forgotten.

TABLE OF CONTENTS

LIST OF TABLES

LIST OF ILLUSTRATIONS

Figure Page

Figure Page

CHAPTER I

HEAT TRANSFER OF LNG ON SOIL

For cryogenic inground storage, knowledge of the boil-off rate of the cryogen as a function of time and the temperature distribution of the surrounding soil is essential to the economical design of liquefied gas plants and the boil-off handling system. For all LNG plants, the rate of boil-off of LNG from an accidental spill on land must be known in order to predict the downwind concentration of LNG vapors. The object of this study was to develop a model for analyzing this important heat transfer problem.

Several models were previously proposed by several investigators to calculate the heat transfer rate from soil to a pool of boiling LNG and the temperature profile of soil. Their utility in practical applications was limited because of the following unrealistic assumptions. Burgess and Zabetakis (14) assumed that the heat transfer coefficient between the soil and LNG was infinite, that the medium was a one-dimensional semi-infinite soil without phase change, and that the thermal properties of soil were constant. In 1968, Parker and Spata (74) assumed the boiling heat transfer coefficient was 10 Btu/hr-ft^2-°F between LNG and dry soil; the latter was assumed to have constant thermal properties. Later, Parker (75) treated the same problem using 50 Btu/hr-ft^2-°F as the boiling coefficient. Welker (111) used 100 Btu/hr-ft^2-°F and 50 Btu/hr-ft^2-°F as the heat transfer coefficient to calculate the evaporation rate of LNG spilled on "average" soil, dry soil and polyurethane. Recently, Drake, Harris, and Reid (24) have developed a conduction model to calculate the heat flux from wet soil to LNG. In this model the boiling heat transfer coefficient was taken to be constant and finite, 100 Btu/hr-ft^2-°F, and the soil properties were assumed not to vary with temperature. For treating the latent heat of freezing moisture in soil, they proposed a correction factor. They assumed that the ratio of heat transfer rate between wet soil and LNG with and without boiling resistance was a specified function which depended on the boiling heat transfer coefficient, soil properties, and time. A correction term was thus included in their theoretical model to match the predicted heat flux with experimental data. However, this correction term is not generally applicable. Prior to the TRW (114) study, only a limited amount of experimental data for the evaporation rate of LNG on soil had been reported (49).

For inground LNG storage, a one-dimensional model is not suitable for the real situation. A two-dimensional model with phase change for wet soil was presented by Hashemi and Sliepcevich (45). The predictor-corrector alternating-direction implicit method (43) was employed to investigate the boil-off rate of LNG from an inground storage facility. The thermal properties of the media and the heat transfer coefficient were assumed to be constant.

Actually, the rate of heat transfer from soil to LNG is controlled, in the beginning, by the convection boundary condition at the soil-LNG interface. After the temperature difference decreases, the heat transfer rate is controlled by heat conduction to the interface. Hence, the infinite and the constant finite coefficient of the heat transfer assumption will overestimate or underestimate the heat transfer for some ranges. In reality, the specific heat and thermal conductivity of soil are functions of temperature over a wide range of temperature. The objective of this study is to investigate the influence of the heat transfer coefficient, the thermal properties of the soil, the latent heat of phase transition and the insulation, if present, on the heat transfer between LNG and soil.

For investigating the influence of these factors on the boil-off rate and temperature distribution of soil, a quasi-linearization alternating-direction implicit method is proposed to solve nonlinear one- and two dimensional heat conduction problems involving phase change. The phase change is assumed to occur over a finite temperature range, and the latent heat is approximated by an error function, which is a continuous function. It will be demonstrated that the proposed numerical method can be applied to solve problems involving nonlinear boundary conditions and composite media with phase changes.

CHAPTER II

PREVIOUS WORK ON MOVING BOUNDARY PROBLEMS

There is a large class of important problems involving the solution of transient heat or mass transfer equations with phase change. The location of the phase interface, which is treated as a free boundary, is dependent upon the amount of heat or mass brought into the region of interest. In 1891 Stefan (101) first published his study of the polar ice thickness. For this reason, problems involving phase change transients are referred to as Stefan problems. There are several commonly encountered examples of the Stefan problems, such as the melting or solidifying of metals, the formation of permafrost, underground storage of cryogenic liquids, the tarnishing of metal surfaces, the combustion of solids, the evaporation of liquid droplets into surrounding gas, the penetration of a reactant into a spherical particle with or without chemical reactions, the processing of frozen foods, and the spinning of textile fibers.

Because the free boundary exists, it imposes a nonlinearity on the unsteady state equation. The exact solution can be found only for special cases. Since Lamé and Clapeyron

(56), Neumann (72) and Stefan (101) investigated heat conduction with changes of phase in the nineteenth century, many different techniques such as numerical, variational, graphic, heat balance integral, and Green's function methods have been used. Bankoff (3), Muehlbauer and Sunderland (70), and Rubinstein (85) have given extensive reviews of the Stefan problem.

Recently, various techniques have also been developed to solve the generalized one-dimensional Stefan problems; these methods are briefly reviewed below.

The imbedding technique was first introduced by Boley (5). The essential feature of this method requires a fictitious body whose shape is unchanged and identical with that of the no-phase-change body. The unknown surface heat flux is adjusted to satisfy the boundary conditions of the real problem. Then the solution of the original boundary value problem is replaced by an ordinary integro-differential equation which can be solved by a forward integration scheme or in series form. This approach is equivalent to an inverse heat conduction problem in which the interior conditions are implicitly prescribed.

Boley (6) extended this method to solve heat conduction problems for melting or solidifying slabs with arbitrary heating rate, arbitrary rate of liquid removal and temperature dependent thermal properties. The general starting and short-time analytical solutions were developed. Boley (8) investigated the uniqueness of the solution of a one-dimensional melting slab in which an applied heat input depended on time as well as on position as the melted material was instantaneously moved out. For axisymmetric melting or solidification of circular cylinders, Lederman and Boley (59) showed the analytical short time solutions that were available; they applied the imbedding technique for the long time numerical solution. Guzelsu and Cakmak (40) applied the imbedding technique to obtain a general starting and short time solution of a hollow cylinder with an ablating inner boundary. The numerical procedures based on the same technique were developed for the melting of a sphere (37) and the melting of an infinite body with a spherical cavity (61).

Kehoe (52) used a successive approximation method to solve the moving boundary diffusion equations with variable diffusivity. This method is similar to that of Parlange (76) for handling the infiltration problem. In 1969 Savino and Siegel (88) analyzed the frozen thickness and temperature profile for the transient solidification of a warm liquid passing over an isothermal cold flat plate. First, the transient, one-dimensional heat conduction equation was integrated from any point, x, to the interface of solid-liquid, $\bar{\delta}$, i.e.,

$$k \left.\frac{\partial T}{\partial x}\right|_{\bar{\delta}} - k \left.\frac{\partial T}{\partial x}\right|_{x} = \rho \, c_p \int_{x}^{\bar{\delta}} \frac{\partial T}{\partial t} \, dx \qquad \text{(II-1)}$$

Then substituting the boundary condition at the interface and integrating the equation from 0 to x gives

$$T(x,t) = T_w + \frac{\rho H}{k}\frac{d\bar{\delta}}{dt} + \frac{h}{k}(T_\ell - T_t)\,x - \frac{\rho c_p}{k}\int_0^x\int_0^{\bar{\delta}} \frac{\partial T}{\partial t}\,dx\,dx \qquad \text{(II-2)}$$

The above expression was solved by an analytic iteration procedure. The first order approximate solution was obtained by neglecting the heat capacity and letting $\bar{\delta} = 0$. The approximate solutions were substituted into the integration equation successively until a convergent solution was obtained.

The iterative procedure can be continued to a high order of approximation. However, due to their complexity, the high order expressions are very difficult to obtain. Elmas (29) developed another iterative procedure for the Savine and Siegel solidification problem. Shih, *et al*. (99, 100) applied Savino and Siegel's analytical iteration technique to the solidification of a liquid at the freezing point inside and outside cylinders or spheres. In order to make the analytical iteration technique applicable to the cylindrical and spherical systems, the following coordinate transforms were introduced:

$$\bar{\gamma} = \int_0^{\gamma_o/r} \frac{d\gamma}{\gamma\eta} \qquad \text{(II-3)}$$

and

$$\bar{R} = \int_1^{\gamma_o/R} \frac{d\gamma}{\gamma\eta} \qquad \text{(II-4)}$$

where η = 1 for cylindrical coordinates

η = 0 for spherical coordinates.

γ_o = the radius of cylinder or sphere

r = the radial distance

R = the radial interface of the solid-liquid

They compared the results of analytical iteration techniques with those of finite difference methods by Tao (102), and Tien and Churchill (104).

Khakimov (54) observed that a cold surface has the effect on freezing outside of cylinders only to a finite distance. He assumed the temperatures of the unfrozen part were constant and equal to the initial temperature. Using these assumptions, an approximate method for calculating the freezing outside of cylinders was developed. Gupta (38) extended the same approximate technique to the spherical coordinate system. Pechoc (78) combined the Binder-Schmidt explicit method and the implicit method to deal with the unsteady state heat transfer with phase change in a plate, cylinder and sphere.

Making use of the finite integral transformation, Selim and Seagrave (95, 96, 97) reduced the unsteady state heat or mass transfer equation with a moving boundary in finite slabs, cylinders, and spheres to a system of ordinary differential equations. Then the system of ordinary, first order, nonlinear differential equations was integrated by the predictor-corrector or Runge-Kutta-Gill integration method.

They assumed the reactant penetration into a spherical ion-exchange media was a diffusion controlled model with a moving boundary inside the particle. This model was studied with their solution technique. When the concentration of acid was high, their computational result matched the experimental measurements of Dana (22). At low acid concentrations, the agreement with the data was not good. Presumably, film diffusion could not be neglected and should have been considered in the model when the concentration was low.

The perturbation solution for the Stefan problem was first introduced by Lock (62, 63, 64) in 1969. He assumed time and position were independent variables of the solution. Therefore, the solution temperature distribution and the location of the interface were in a power series of a physical parameter, ϕ, which is the ratio of the product of specific heat and maximum temperature difference and the latent heat. Instead, Pedroso and Domoto (79, 80) assumed the independent variables were time and interface position; thus, it was not necessary to expand the moving front in a power series of the physical parameter. The dimensionless temperature was assumed to be in the form:

$$U(x,x_t;\phi) = U_i(x,x_t)\ \phi^{i-1} \qquad \text{(II-5)}$$

and

$$U(x,x_t) = \lambda_{i,j,1}(x_t)\ x^{j-1} \qquad \text{(II-6)}$$

where $i = 1, 2, \ldots, N$

$j = 1, 2, \ldots, 2i$

where detailed calculation of $\lambda_{i,j,1}$ is shown in Reference 80. Hence, in the process of calculating the temperature distribution of the medium, the velocity of the moving interface and its inverse, the coefficients of the integer powers of the perturbation parameter could be obtained without any numerical method. However, in order to know the interface position as a function of time, they needed the numerical integration. They also found that the Shanks (98) transformation was a useful tool to increase the rate and range of convergence of the perturbation series.

Bonacine, et al. (10) considered that the thermal properties of the medium were a function of temperature and that the phase transition occurred over a small temperature range. The latent heat was expressed in terms of a constant heat capacity over the small temperature interval. Then the finite difference form for the following nonlinear partial differential equation

$$c(T)\,\frac{\partial T}{\partial t} = \frac{\partial}{\partial x}\left[k(T)\,\frac{\partial T}{\partial x}\right] \tag{II-7}$$

was

$$\begin{aligned} c(T_i^h)(T_i^{h+1} - T_i^{h-1}) = \frac{2}{3}\,\frac{\Delta t}{(\Delta x)^2}\,\{k^+[(T_{i+1}^{h+1} - T_i^{h+1}) + (T_{i+1}^h - T_i^{h-1})] \\ - k^-[(T^{h+1} - T_{i-1}^{h-1}) + (T_i^h - T_{i-1}^h) \\ + (T_i^{h-1} - T_{i-1}^{h-1})]\} \end{aligned} \tag{II-8}$$

where the superscript h represents the time level, $t = h\Delta t$, and

$$k^{+} = k(T^{h}_{i+\,1/2}) \simeq k\,\left(\frac{T^{h}_{i+1}\;\;T^{h}_{i}}{2}\right) \qquad \text{(II-9)}$$

$$k^{-} = k(T^{h}_{i-\,1/2}) \simeq k\left(\frac{T^{h}_{i} + T^{h}_{i-1}}{2}\right) \qquad \text{(II-10)}$$

The heat balance integral method (33, 34, 35) was applied by Imber and Huang (50) to solve the phase change problem in a semi-infinite slab initially at the fusion point and with temperature dependent thermal properties.

Habib (41, 42) considered the radiation effect on the change of interface position and the temperature distribution of solidification in a planar or cylindrical medium. For the nonparticipating medium, in which the radiation heat flux is constant for all interfaces, the rate of solidification increases as the absorption coefficient decreases. He also found that higher absorption raised the temperature distribution in the cylindrical medium, but it dropped the temperature distribution in a planar medium. However, the radiation effect could be neglected for the high thermal diffusivity medium.

Although numerous numerical procedures for moving boundary problems are available, the majority of them have been restricted to a one-dimensional case with constant thermal properties. However, the one-dimensional model is not accurate for real situations under some circumstances. Due to the mathematical and geometrical complexities little research has been done on the multidimensional moving boundary problems. The numerical methods for multidimensional Stefan problems are summarized below.

Allen and Severn (1) extended the relaxation method, which was originally developed for the solution of an elliptic partial differential equation, to two-dimensional heat conduction with phase change.

The partial differential equation for heat conduction in two-dimensional space is

$$c\,\frac{\partial T}{\partial t} = k\left(\frac{\partial^2 T}{\partial x^2} + \frac{\partial^2 T}{\partial y^2}\right) + \theta \qquad \text{(II-11)}$$

where T = temperature, a function of orthogonal space coordinates x and y

k = constant thermal conductivity of the uniform medium

c = specific heat of the uniform medium

θ = rate of generation of heat per unit volume in the medium

To make the relaxational procedure suitable for this equation, the following transformation is necessary

$$T = \frac{\partial w}{\partial t} + \frac{k}{c}\left(\frac{\partial^2 w}{\partial x^2} + \frac{\partial^2 w}{\partial y^2}\right) \qquad \text{(II-12)}$$

Therefore,

$$\frac{\partial^2 w}{\partial t^2} - \left(\frac{k}{c}\right)^2 \nabla^4 w - \frac{\theta}{c} = 0 \qquad \text{(II-13)}$$

is obtained, where $\nabla^4 \equiv (\partial^2/\partial x^2 + \partial^2/\partial y^2)^2$. Due to the complexity of the computational procedure, this method has not been used extensively.

The one parameter Karman-Pohlhausen method (32) and the two parameter Tani method (103) of boundary layer theory in fluid dynamics were applied by Poots (82) to two-dimensional solidification in a uniform prism. The prediction from the Tani method agreed within 13 percent of the relaxation solution of Allen and Severn. Friedman (30) discussed the extensive theorems of the Stefan problem in several space variables. The Galerkin method of Douglas and Dupont (28) for nonlinear parabolic equations was introduced by Cannon and Hill (16) to solve multidimensional free boundary problems. The particular short time analytical solutions for two- and three-dimensional Stefan problems were derived by Boley and Yagoda (7, 9). Beyond that short time range the imbedding technique was applied.

For dealing with one-dimensional cases the location of the phase-change interface can be represented by a single point. It can be handled easily. Unfortunately, for the multidimensional case, the determination of the interfacial location and the normal derivative, from one time level to another, complicates the numerical procedures. In reality the occurrence of phase transition is not at a fixed temperature and is over a finite temperature interval. For this realistic situation the latent heat can be expressed by a constant or temperature dependent heat capacity over the phase change interval. Then the impossible task of writing a numerical procedure for the location and normal derivative of interfaces need not be undertaken. In other words, the moving boundary problems under this realistic assumption can be changed immediately to a usual boundary value problem.

The constant heat capacity approximation for latent heat has been employed by several authors (10, 13, 87, 106). Hashemi (43) made a more realistic assumption that the heat capacity, c_t, for the latent heat of transition, H, over the phase change temperature interval between $(T_t - \delta t)$ and $(T_t + \delta t)$ was a normal distribution function, i.e.,

$$c_t = \frac{H\varepsilon}{\sqrt{\pi}} e^{-\varepsilon^2 (T_t - T)^2} \qquad \text{(II-14)}$$

for which

$$\int_{T_t-\delta T}^{T_t+\delta T} c_t \, dt = \operatorname{erf}(\varepsilon \delta T) \qquad \text{(II-15)}$$

and ε is so chosen that $\operatorname{erf}(\varepsilon\delta T) \simeq 1.0$. Then the combination of Douglas and Jones' predictor-corrector method (27) for the one-dimensional equation and Peaceman-Rachford's alternating direction implicit procedure (77) was proposed to handle the nonlinear partial differential equation. The boil-off rate of a two-dimensional underground LNG storage (45) and the effect of seepage stream on artificial soil freezing (46) were studied by this scheme. A special scheme was derived by

Lazaridis (58) for points near the interfaces; for all points far from the interface, the explicit finite difference technique was adopted.

In recent publications by Mayer (67, 68) he assumed the phase-transition was over a temperature range, rather than at a fixed point and the latent heat was approximated by a linear enthalpy relation over the temperature interval. The nonlinear partial differential equation was reduced to nonlinear algebraic equations by an implicit finite difference technique. Making use of the Gauss-Siedel method for simultaneous algebraic equations, the thermal properties are constant in his calculation.

In examining the published techniques for solving moving boundary problems, most of them are limited to constant thermal properties and linear boundary conditions. It is not easy to extend the technique to solve the one- and two-dimensional heat conduction problems with phase change, temperature dependent properties, and nonlinear boundary conditions. In order to develop a simple and useful tool to solve the general heat conduction problems, the quasilinearization technique was employed. Essentially, the quasilinearization algorithm is a generalization of the Newton-Raphson scheme applicable to function equations (4, 60). The advantage of this technique is that recursive solution of the linearized equation has the property of quadratic and monotonic convergence. By quasilinearizing the nonlinear difficulties resulting from variable thermal properties, latent heat of phase change and nonlinear boundary conditions were circumvented. For two-dimensional cases, the convergence rate and results of the quasilinearization alternating-direction implicit method were independent of the accelerating parameter. The versatility of this simple method was demonstrated by solving several one- and two-dimensional moving boundary problems including composite media systems.

CHAPTER III

A PROPOSED NUMERICAL METHOD

For solving numerically transient heat conduction problems, the partial differential equation is usually approximated by a set of appropriate finite difference equations, which is then solved by a suitable method. However, an inconsistent set of finite difference equations may be obtained by this procedure. In adtuality the transient heat and mass differential equations are obtained by taking a heat or mass balance around a finite element and letting the finite dimension be infinitesimally small. The simple and straightforward way for obtaining the consistent and accurate discrete equations is to divide the region of interest into a set of cells of finite dimension and then to develop the necessary heat and mass balance equations for each cell. The following finite difference equations are obtained by this simple procedure, rather than from the generalized transport partial differential equation

$$\frac{\partial}{\partial x} [k(T) \frac{\partial T}{\partial x}] + \frac{\partial}{\partial y} [k(T) \frac{\partial T}{\partial y}] = c(T) \frac{\partial T}{\partial t} \qquad \text{(III-1)}$$

The Two-Dimensional Cases

A typical cell from dividing a two-dimensional and locally isotropic medium into a set of cells is shown in Figure III-1. The intersection of j^{th} horizontal line and i^{th} vertical line is called a mesh point (i,j) and its coordinate is (x_i, y_j). There are N_x lines parallel to the x axis and N_y lines parallel to the y axis. Let the shortest distance between mesh point (i,j) and (i+1,j) be h_i, $1 \le i \le N_x$, and the shortest distance between mesh point (i,j) and (i,j+1) be g_j, $1 \le j \le N_y$. The rectangular mesh region is confined by the lines $x_i - 1/2h_{i-1}$, $x_i + 1/2h_i$, $y_i - 1/2g_{j-1}$ and $y_j + 1/2g_j$.

The thickness of the mesh in the third coordinate is Δz, and the temperature at mesh point (i, j) is T_{ij}. Let the heat transfer rates by conduction or convection into the mesh region (i, j) through sides 1 and 2 be q_1 and q_2, respectively. The heat transfer rates out of the mesh region (i, j) through sides 3 and 4 are q_3 and q_4, respectively.

$$q_1 - q_3 + q_2 - q_4 = \Delta V_{ij} \frac{E_{i,j} - E_{i,j,o}}{\Delta t} \qquad \text{(III-2)}$$

where $E_{i,j,o}$ = total internal energy of the mesh (i,j) at time $t-\Delta t$

$E_{i,j}$ = total internal energy of the mesh (i,j) at time t

ΔV_{ij} = volume of the mesh region (i,j) and is given by

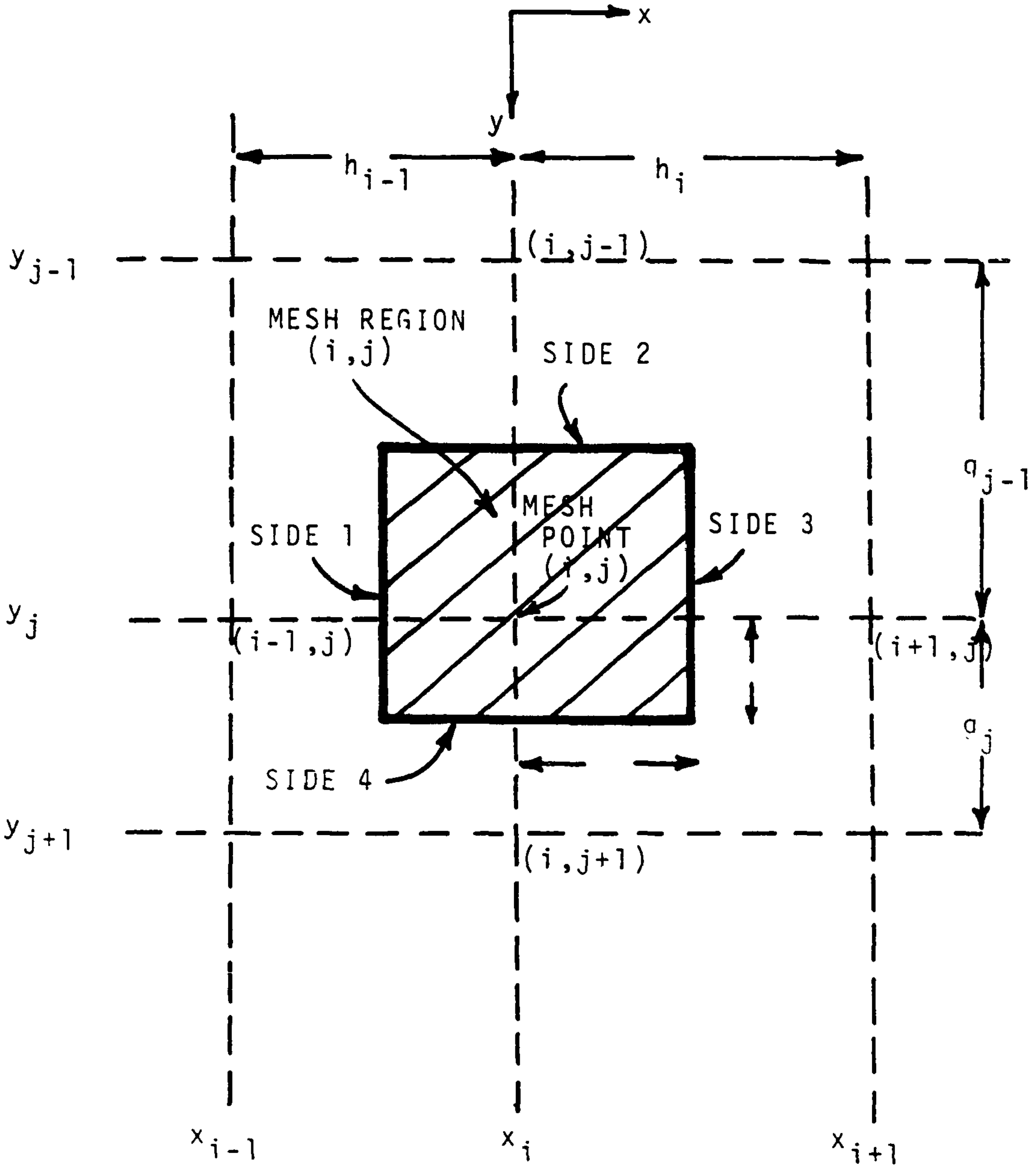

Figure III-1. A Mesh Region (i,j) and Its Adjacent Mesh Points.

$$\Delta V_{i,j} = \Delta z \left(\frac{h_{i-1} + h_i}{2}\right)\left(\frac{g_{j-1} + g_i}{2}\right) \tag{III-3}$$

Following Fourier's law of heat conduction, the rate of heat conduction through side 1 of mesh (i,j) is given by

$$q_1 = -1/2(g_{j-1} + g_j)\Delta z\left(k \frac{\partial T}{\partial x}\right)\Big|_{i-1/2,j} \tag{III-4}$$

Define the dimensionless temperature, $\overline{U}$, by

$$\overline{U} = \frac{T - T_2}{T_1 - T_2} \tag{III-5}$$

where T = actual temperature

T_1, T_2 = two arbitrarily chosen temperatures

The domain of $\overline{U}$ is from 0 to 1. If the thermal conductivity of the medium, k, is temperature dependent, let

$$k(\overline{U}) = k_o\, \alpha(\overline{U}) \tag{III-6}$$

where k_o = thermal conductivity at a reference state

Define

$$U = \frac{\int_o^{\overline{U}} \alpha(\overline{U})\, d\overline{U}}{\int_o^1 \alpha(\overline{U})\, d\overline{U}} \tag{III-7}$$

and

$$I = \int_o^1 \alpha(\overline{U})\, d\overline{U} \tag{III-8}$$

Using the above dimensionless temperatures the expression in Equation III-4 can be modified to

$$q_1 = -1/2(g_{j-1}+g_j)\Delta z(T_1 - T_2)\ k_o I \frac{\partial U}{\partial x}\Big|_{i-1/2,j} \tag{III-9}$$

The dimensionless temperature gradient at point (i-1/2,j), the driving force for heat transport through side 1, is approximated by the temperature difference of mesh points (i-1,j) and (i,j) divided by the distance of these two mesh points, i.e.,

$$\left.\frac{\partial U}{\partial x}\right|_{i-1/2,j} \simeq \frac{U_{i,j} - U_{i-1,j}}{h_{i-1}} \qquad \text{(III-10)}$$

Therefore, the rate which heat is transferred by conduction into the mesh region (i,j) through side 1 approximately is

$$q_1 = -1/2(g_{j-1}+g_j)\Delta z(T_1-T_2)k_oI\,\frac{U_{i,j} - U_{i-1,j}}{h_{i-1}} \qquad \text{(III-11)}$$

Similarly,

$$q_2 = -1/2(h_{i-1}+h_i)\Delta z(T_1-T_2)k_oI\,\frac{U_{i,j} - U_{i,j-1}}{g_{j-1}} \qquad \text{(III-12)}$$

$$q_3 = -1/2(g_{j-1}+g_j)\Delta z(T_1-T_2)k_oI\,\frac{U_{i+1,j} - U_{i,j}}{h_i} \qquad \text{(III-13)}$$

and

$$q_4 = -1/2(h_{i-1}+h_i)\Delta z(T_1-T_2)k_oI\,\frac{U_{i,j+1} - U_{i,j}}{g_j} \qquad \text{(III-14)}$$

The following dimensionless variables are defined as:

$$\bar{h}_i = \frac{h_i}{a}$$

$$\bar{g}_j = \frac{g_j}{a}$$

$$\tau = \frac{k_o t}{c_o a^2}$$

$$\hat{\tau} = \frac{\tau}{\bar{h}\,\bar{g}}$$

$$c_{i,j} = \frac{-2\,\bar{h}\,\bar{g}}{\bar{h}_{i-1}(\bar{h}_{i-1} + \bar{h}_i)}$$

$$b_{i,j} = \frac{-2\,\bar{h}\,\bar{g}}{\bar{h}_i\ (\bar{h}_{i-1}+\bar{h}_i}$$

$$a_{i,j} = -c_{i,j} - b_{i,j}$$

$$f_{i,j} = \frac{-2\,\bar{h}\,\bar{g}}{\bar{g}_{j-1}(\bar{g}_{j-1}+\bar{g}_j)}$$

$$e_{i,j} = \frac{-2\,\bar{h}\,\bar{g}}{\bar{g}_j(\bar{g}_{j-1}+\bar{g}_j)}$$

$$d_{i,j} = -f_{i,j} - e_{i,j} \tag{III-15}$$

where c_o = the heat capacity at a reference state

a = a geometric scaling factor

$\bar{h}$ = arbitrarily chosen from $\bar{h}_i$, $1 \leq i \leq N_x$, $1 \leq j \leq N_y$

$\bar{g}$ = arbitrarily chosen $\bar{g}$, $1 \leq i \leq N_x$, $1 \leq j \leq N_y$

Substituting Equations III-11, III-12, III-13 and III-14 into Equation III-2, the desired difference equation is:

$$c_{i,j}\,U_{i-1,j} + a_{i,j}\,U_{i,j} + b_{i,j}\,U_{i+1,j} + f_{i,j}\,U_{i,j-1} + d_{i,j}\,U_{i,j} + e_{i,j}\,U_{i,j+1} + \frac{1}{c_o(T_1 - T_2)\,I}\,\frac{E_{i,j}}{\Delta\hat{t}} = \frac{1}{c_o(T_1 - T_2)\,I}\,\frac{E_{i,j,o}}{\Delta\hat{t}} \tag{III-16}$$

The purpose of using the transformation in Equation III-7 is to make the difference equation linear in form with respect to dimensionless temperature except the accumulation of internal energy of the mesh. The internal energy, associated with the temperature dependent sensible heat and the latent heat of phase change, is strongly nonlinear.

If there are phase changes in the region of interest, an assumption is made that any phase transition occurs over a finite temperature between $(T_t - \delta T)$ and $(T_t + \delta T)$ rather than at T_t. For impure substances this assumption is more realistic than at a fixed temperature. One logical approximation for latent heat, H, over the transition region is

$$E_t = \frac{H}{2} [1 - \mathrm{erf}\ \varepsilon (T_t - T)] \qquad \text{(III-17)}$$

where erf is an error function and ε is so chosen that $\varepsilon\ \delta T \simeq 1$. The sensible heat of E_t over the transition region is a normal distribution function, i.e.

$$c_t = \left(\frac{\partial E_t}{\partial T}\right)_{\rho,T} = \frac{H\varepsilon}{\sqrt{\pi}} e^{-\varepsilon^2 (T_t - T)^2} \qquad \text{(III-18)}$$

The linear approximation of the latent heat will be

$$E_t = \frac{H}{2\varepsilon'} (T - T_t + \delta T) \qquad \text{(III-19)}$$

where ε' is equal to δT. It can be seen that the sensible heat of E_t between $(T_t - \delta T)$ and $(T_t + \delta T)$ is constant, i.e.,

$$c_t = \frac{H}{2\varepsilon'} \qquad \text{(III-20)}$$

The behavior of the error function and linear approximation is shown in Figure III-2. The solid lines represent the error function approximation, Equation III-17 and Equation III-18. The dotted lines are the linear approximation, Equations III-19 and III-20. In reality Equation III-17 and III-18 are the best approximation for the real phase-transition

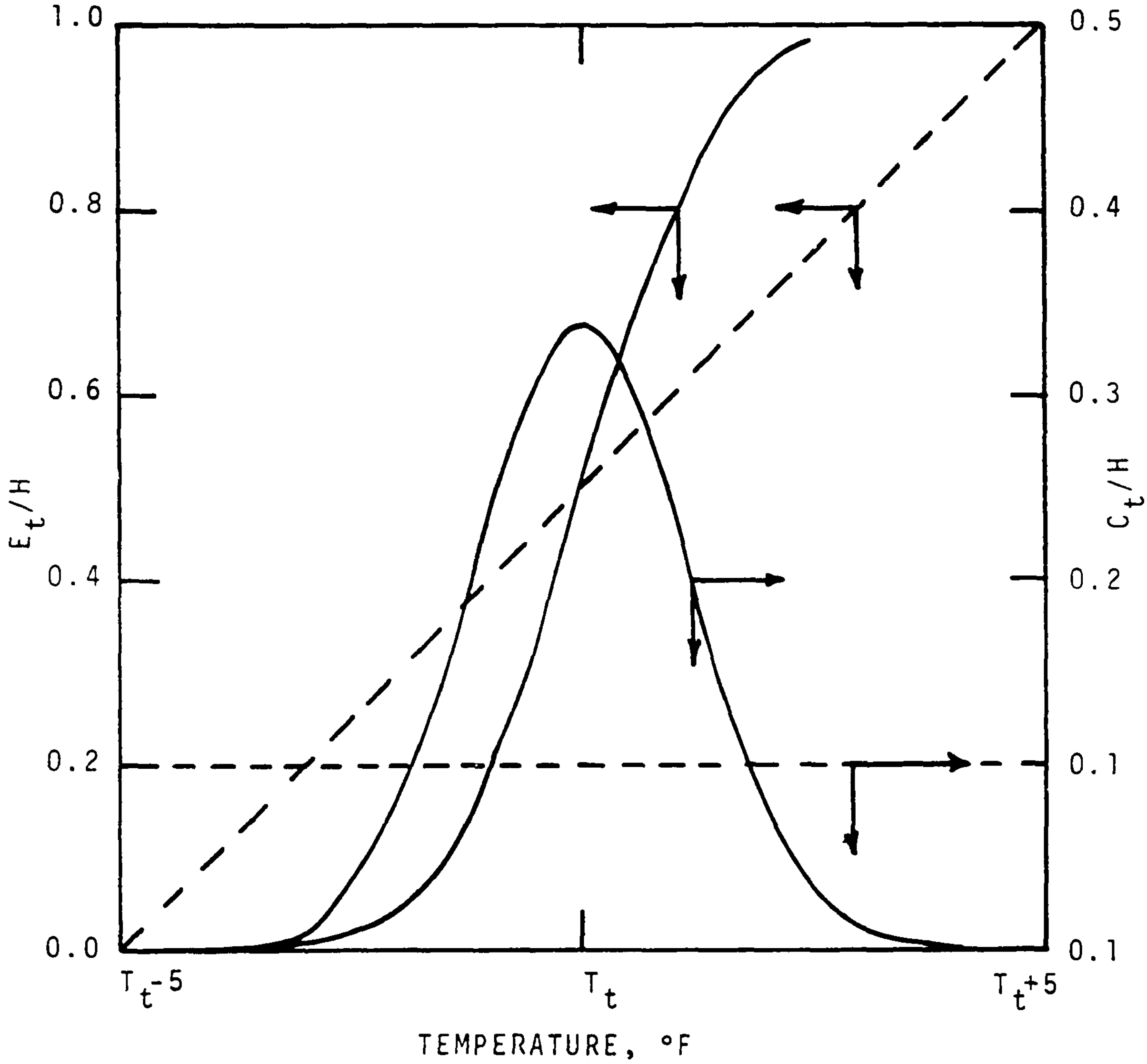

Figure III-2. Comparison of Two Types of Latent Heat Approximations.

behavior. For the present study the error function approximation is employed.

The benefit of the above assumption is that the complexity of finding the positions of the interface and its normal derivatives in multidimensional system with multiplase change is avoided without compromising the realistic model. Therefore, the moving boundary problem can be considered as an initial value problem. However, it is still a strongly nonlinear problem. The total internal energy term, E, can be obtained by the tabular or functional form of the temperature dependent internal energy, for example,

$$E = \int_{T_2}^{T} c(T')\ dT' + \frac{H}{2}\ [1 - \mathrm{erf}\ \varepsilon\ (T_t - T)] \qquad \text{(III-21)}$$

One equation such as Equation III-16 can be obtained for each mesh point. There are N simultaneous equations for N mesh points; consequently, they can be solved for N unknown values of dimensionless temperature simultaneously. The terms of the left hand side of Equation III-16, which are those containing the unknown values of temperature, are moved to the right hand side of Equation III-16.

In order to solve the nonlinear equations the quasilinearization technique is used. This technique is a generalized Newton-Raphson method for functional equations. The quasilinearization technique not only linearizes the nonlinear equation but also possesses two important properties; quadratic convergence and monotonic convergence. More detailed discussion of the advantage and disadvantage of the quasilinearization technique can be found in the literature (4, 60). The linear equations are obtained by using the first and the second terms in the Taylor's series expansion of the original nonlinear equations. Therefore, for the two-dimensional system the nonlinear equations are linearized first by the quasilinearization technique. Then the linearized equations can be solved by the unconditionally stable Peaceman-Rachford alternating-direction implicit method (77). Iteration is continued until satisfactory convergence is obtained.

Making use of the generalized Newton-Raphson method to linearize the nonlinear Equation III-16 results in

$$
\begin{aligned}
& c_{i,j}(U^{n+1}_{i-1,j} - U^{n}_{i-1,j}) + a_{i,j}(U^{n+1}_{i,j} - U^{n}_{i,j}) \\
& + b_{i,j}(U^{n+1}_{i+1,j} - U^{n}_{i+1,j}) + f_{i,j}(U^{n+1}_{i,j-1} - U^{n}_{i,j-1}) \\
& + d_{i,j}(U^{n+1}_{i,j} - U^{n}_{i,j}) + e_{i,j}(U^{n+1}_{i,j+1} - U^{n}_{i,j+1}) \\
& + \frac{\phi_{i,j}}{\Delta\hat{t}}(U^{n+1}_{i,j} - U^{n}_{i,j}) = -S_{i,j} \qquad \text{(III-22)}
\end{aligned}
$$

where the superscript n refers to the n^{th} iteration and the superscript n+1 refers to the $n+1^{th}$ iteration, and

$$\phi_{i,j} = \frac{1}{c_o(T_1 - T_2)I} \frac{dE(U^n_{i,j})}{dU^n_{i,j}} \qquad \text{(III-23)}$$

$$S_{i,j} = c_{i,j}\, U^n_{i-1,j} + a_{i,j}\, U^n_{i,j} + b_{i,j}\, U^n_{i+1,j}$$

$$+ f_{i,j} U^n_{i,j-1} + d_{i,j}\, U^n_{i,j} + e_{i,j}\, U^n_{i,j+1}$$

$$+ \frac{1}{c_o(T_1 - T_2)I}\, \frac{E^n_{i,j} - E_{i,j,o}}{\Delta\hat{\tau}} \qquad \text{(III-24)}$$

To reduce the rounding errors in the numerical calculation (115), define

$$\Gamma^{n+1}_{i,j} = U^{n+1}_{i,j} - U^n_{i,j} \qquad \text{(III-25)}$$

where $\Gamma^{n+1}_{i,j}$ are used as the dependent variables. The linear difference equation can be given by:

$$c_{i,j}\, \Gamma^{n+1}_{i-1,j} + a_{i,j}\, \Gamma^{n+1}_{i,j} + b_{i,j}\, \Gamma^{n+1}_{i+1,j} + f_{i,j}\, \Gamma^{n+1}_{i,j-1}$$

$$+ d_{i,j}\, \Gamma^{n+1}_{i,j} + e_{i,j}\, \Gamma^{n+1}_{i,j+1} + \frac{\phi_{i,j}}{\Delta\hat{\tau}}\, \Gamma^{n+1}_{i,j} = - S_{i,j} \qquad \text{(III-26)}$$

Prescribed Temperature Boundary Condition

Thus far the boundary conditions have not been included in the discussion. There are two categories of boundary conditions: (1) the temperature is prescribed at the boundary; and (2) the heat flux at the boundary is prescribed. The convective boundary condition will be discussed in the next section. If the boundary conditions are prescribed, all boundary temperature dependent terms in Equation III-1 are moved to the right hand side of Equation III-1 before quasilinearization technique is applied.

For N unknown values of $U_{i,j}$, the N simultaneous equations of Equation III-26 can be written in the form

$$\frac{\underline{\phi}}{\Delta\hat{\tau}}\,\underline{\Gamma}^{n+1} + (\underline{H} + \underline{V})\,\underline{\Gamma}^{n+1} = -\underline{S} + \underline{\theta} \qquad \text{(III-27)}$$

where $\underline{\Gamma}$ is an N-dimensional vector whose entries are $\Gamma_{i,j}$. $\underline{\phi}$ and $\underline{S}$ are both N x N diagonal matrices with the diagonal entries $\phi_{i,j}$ and $S_{i,j}$. $\underline{H}$ and $\underline{V}$ are real N x N matrices with positive diagonal entries and nonpositive off-diagonal entries. For each row the matrices $\underline{H}$ and $\underline{V}$ have at most three nonzero entries. If the mesh points are arranged in the x-direction, then $\underline{H}$ is

$$\underline{H} = \begin{pmatrix} H_1 & & & \\ & H_2 & & \\ & & \ddots & \\ & & & H_{N_y} \end{pmatrix} \qquad \text{(III-28)}$$

where

$$\underline{H}_j = \begin{pmatrix} a_{i,j} & b_{i,j} & & \\ c_{2,j} & a_{2,j} & b_{2,j} & \\ \ddots & \ddots & \ddots & \\ & \ddots & \ddots & \ddots \\ & c_{N_x,j} & a_{N_x,j} & \end{pmatrix}$$

If the mesh points are ordered in the y-direction then $\underline{V}$ is

$$\underline{V} = \begin{pmatrix} V_1 & & & \\ & V_2 & & \\ & & \ddots & \\ & & & V_{N_x} \end{pmatrix} \qquad \text{(III-29)}$$

where

$$\underline{V}_i = \begin{bmatrix} d_{i,1} & e_{i,1} & & & \\ f_{i,2} & d_{i,2} & e_{i,2} & & \\ \cdot & \cdot & \cdot & & \\ & \cdot & \cdot & \cdot & \\ & & \cdot & \cdot & \cdot \\ & & & f_{i,N_y} & d_{i,Ny} \end{bmatrix}$$

The properties of $\underline{H}$ and $\underline{V}$ have been discussed by Varga (108). $\underline{\theta}$ is an NxN diagonal matrix composed of entries from all known terms which were moved to the right hand side of Equation III-16.

For each iteration the Peaceman-Rachford variant of the alternating direction implicit procedure (25) is applied. The alternating direction implicit procedure contains two steps, x-direction sweep and y-direction sweep. For the x-direction sweep, the intermediate step, Equation III-27 is rewritten in terms of $\Gamma^*_{i,j}$ and $\Gamma^n_{i,j}$

$$(\frac{\underline{\phi}}{\Delta\hat{\tau}} + \underline{H} + \gamma\underline{I})\underline{\Gamma}^* = -\underline{S} + \underline{\theta} - \underline{V}\ \underline{\Gamma}^n + \gamma\underline{\Gamma}^n \qquad \text{(III-30)}$$

where $\underline{I}$ is the identity matrix. $\underline{\Gamma}^*_{i,j}$ is the dimensionless temperature change over the half iteration, and γ is the accelerating parameter of the alternating direction implicit procedure. More discussion of the accelerating parameter in an alternating direction implicit procedure can be found in the literature (26, 89, 108).

For each j, $1 \leq j \leq N_y$ Equation III-30 becomes

$$\underline{A}_j\ \underline{\Gamma}^*_j = \underline{B}_j \qquad \text{(III-31)}$$

The matrices $\underline{A}_j$, $\underline{B}_j$, and $\underline{\Gamma}_j^*$ can be expressed as

$$\underline{A}_j = \begin{pmatrix} a_{1,j} + \frac{\phi_{1,j}}{\Delta\hat{\tau}} + \gamma & b_{1,j} & & \\ c_{2,j} & a_{2,j} + \frac{\phi_{2,j}}{\Delta\hat{\tau}} + \gamma & b_{2,j} & \\ \ddots & \ddots & \ddots & \\ & c_{N_{x,j}} & a_{N_{x,j}} + \frac{\phi_{N_{x,j}}}{\Delta\hat{\tau}} + \gamma & \end{pmatrix} \tag{III-32}$$

$$\underline{B}_j = \begin{pmatrix} -f_{1,j}\Gamma^n_{1,j-1} - d_{1,j}\Gamma^n_{1,j} - e_{1,j}\Gamma^n_{1,j+1} - S_{1,j} + \theta_{1,j} + \gamma\Gamma^n_{1,j} \\ \vdots \\ -f_{N_{x,j}}\Gamma^n_{N_{x,j-1}} - d_{N_{x,j}}\Gamma^n_{N_{x,j}} - e_{N_{x,j}}\Gamma^n_{N_{x,j+1}} - S_{N_{x,j}} + \theta_{N_{x,j}} + \gamma\Gamma^n_{N_{x,j}} \end{pmatrix} \tag{III-33}$$

$$\underline{\Gamma}_j^* = \begin{pmatrix} \Gamma^*_{1,j} \\ \Gamma^*_{2,j} \\ \vdots \\ \Gamma^*_{N_{x,j}} \end{pmatrix} \tag{III-34}$$

where $\underline{\Gamma}_j^*$ is a vector whose components are the unknown values of $\Gamma^*_{i,j}$ falling on the j^{th} grid-line parallel to the y-axis. Equation III-31 can be solved directly by the Gaussian elimination method (17).

Then, for y-direction sweep, Equation III-27 becomes

$$\left(\frac{\phi}{\Delta\hat{\tau}} + \underline{V} + \gamma\underline{I}\right) \underline{\Gamma}^{n+1} = -\underline{S} + \underline{\theta} - \underline{H\Gamma}^{*} + \gamma\underline{\Gamma}^{*} \qquad \text{(III-35)}$$

Substituting Equation III-30 into Equation III-35 results in

$$\left(\frac{\phi}{\Delta\hat{\tau}} + \underline{V} + \gamma\underline{I}\right) \underline{\Gamma}^{n+1} = (\underline{V} - \gamma\underline{I})\underline{\Gamma}^{n} + \left(2\gamma\underline{I} + \frac{\phi}{\Delta\hat{\tau}}\right)\underline{\Gamma}^{*} \qquad \text{(III-36)}$$

For each i, $1 \leq i \leq N_x$, Equation III-36 will be

$$\underline{D}_i\, \underline{\Gamma}_i^{n+1} = \underline{E}_i \qquad \text{(III-37)}$$

The matrices $\underline{D}_i$, $\underline{E}_i$, and $\underline{\Gamma}_i^{n+1}$ can be expressed as

$$\underline{D}_i = \begin{pmatrix} d_{i,1} + \frac{\phi_{i,1}}{\Delta\hat{\tau}} + \gamma & e_{i,1} & \\ f_{i,2} & d_{i,2} + \frac{\phi_{i,2}}{\Delta\hat{\tau}} + \gamma & e_{i,e} \\ \ddots & \ddots & \ddots \\ & f_{i,N_y} & d_{i,N_y} + \frac{\phi_{i,N_y}}{\Delta\hat{\tau}} + \gamma \end{pmatrix} \qquad \text{(III-38)}$$

$$\underline{E}_i = \begin{pmatrix} f_{i,1}\Gamma^n_{i,0} + d_{i,1}\Gamma^n_{i,1} + e_{i,1}\Gamma^n_{i,2} + \left(\frac{\phi_{i,1}}{\Delta\hat{\tau}} + 2\gamma\right)\Gamma^{*}_{i,1} - \gamma\Gamma^n_{i,1} \\ \vdots \\ f_{i,N_y}\Gamma^n_{i,N_y} + d_{i,N_y}\Gamma^n_{i,N_y} + e_{i,N_y}\Gamma_{i,N_{y+1}} + \left(\frac{\phi_{iN_y}}{\Delta\hat{\tau}} + 2\gamma\right)\Gamma^n_{i,N_y} - \gamma\Gamma_{i,N_y} \end{pmatrix} \qquad \text{(III-39)}$$

$$\underline{\Gamma}_i^{n+1} = \begin{pmatrix} \Gamma^{n+1}_{i,1} \\ \Gamma^{n+1}_{i,2} \\ \vdots \\ \Gamma^{n+1}_{i,N_y} \end{pmatrix} \qquad \text{(III-40)}$$

where the components of vector $\underline{\Gamma}_i^{n+1}$ are the unknown values of $\Gamma_{i,j}^{n+1}$ falling on the i^{th} grid-line parallel to the x-axis. Equation III-37 is also solved by the Gaussian elimination method to get $\underline{\Gamma}_i^{n+1}$. After obtaining the $\Gamma_{i,j}^{n+1}$, for $1 \leq i \leq N_x$ and $1 \leq j \leq N_y$, then one iteration has been accomplished. This iterative procedure is repeated until the convergence criteria are satisfied.

Convective Boundary Condition

So far, only the prescribed temperature boundary conditions have been discussed. The treatment of the nonlinear convective boundary condition is identical to the iterative procedure for the prescribed temperature boundary conditions discussed above. For example, it has the nonlinear convective condition on the side 1 of mesh (i,j), such as

$$q_1 = -h_a(T_{i,j} - T_2)^{h_b} \frac{1}{2}(g_{j-1} + g_j) \qquad \text{(III-41)}$$

where h_a and h_b are arbitrary constants. Following the dimensionless temperature defined in Equations III-5 and III-7, the boundary condition will be

$$q_1 = -h_a(T_1 - T_2)^{h_b} [1 + F(U_{i,j})]^{h_b} \frac{1}{2}(g_{j+1} + g_j) \qquad \text{(III-42)}$$

Taking the heat balance around the mesh (i,j), the difference equation can be written as

$$-b_{i,j}[H_i(1 + F(U_{i,j}))^{h_b} + U_{i,j}] + b_{i,j}\, U_{i+1,j} + f_{i,j}\, U_{i,j-1}$$

$$+ d_{i,j}\, U_{i,j} + e_{i,j}\, U_{i,j+1} + \frac{1}{C_o(T_1-T_2)I}\, \frac{E_{i,j} - E_{i,j,o}}{\Delta\hat{\tau}} = 0 \qquad \text{(III-43)}$$

where

$$H_i = -\frac{h_a a}{k_o I}\, (T_1 - T_2)^{h_b - 1}\, \bar{h}_i \qquad \text{(III-44)}$$

Equation III-43 is similar to Equation III-16. Both the first term and the last term of Equation III-43 are nonlinear forms; the generalized Newton-Raphson method is used to linearize them. The linear finite difference equation is

$$w_{i,j}\Gamma_{i,j}^{n+1} + b_{i,j}\Gamma_{i+1,j}^{n+1} + f_{i,j}\Gamma_{i,j-1}^{n+1} + d_{i,j}\Gamma_{i,j}^{n+1}$$

$$+ e_{i,j}\Gamma_{i,j+1}^{n+1} + \frac{\phi_{i,j}}{\Delta\hat{\tau}}\, \Gamma_{i,j}^{n+1} = -S_{i,j} \qquad \text{(III-45)}$$

where

$$w_{i,j} = -b_{i,j}[H_i h_b (1 + F(U_{i,j}^n))^{h_b - 1}\, \frac{dF(U_{i,j}^n)}{dU_{i,j}^n} + 1] \qquad \text{(III-46)}$$

$$S_{i,j} = -b_{i,j}[H_i(1 + F(U_{i,j}^n))^{h_b} + U_{i,j}^n] + b_{i,j}U_{i+1,j}^n$$

$$+ f_{i,j}U_{i,j-1}^n + d_{i,j}U_{i,j}^n + e_{i,j}U_{i,j+1}^n$$

$$+ \frac{1}{C_o(T_1 - T_2)I}\, \frac{E_{i,j}^n - E_{i,j,o}}{\Delta\hat{\tau}} \qquad \text{(III-47)}$$

Therefore, if the nonlinear boundary condition shown in Equation III-41 is specified on the boundary of the mesh regions $(1,j)$, $1 \leq j \leq N_y$, Equation III-31 and III-37 can be obtained by using the variant alternating direction, implicit procedure. However, the matrix $\underline{A}_j$ of Equation III-31 is now

$$\underline{A}_j = \begin{bmatrix} w_{1,j} + \frac{\phi_{1,j}}{\Delta\hat{\tau}} + \gamma & b_{i,j} & & \\ c_{2,j} & a_{2,j} + \frac{\phi_{2\ j}}{\Delta\hat{\tau}} + \gamma & b_{2,j} & \\ & \ddots & \ddots & \ddots \\ & & c_{N_x,j} & a_{N_x,j} + \frac{\phi_{N_x,j}}{\Delta\hat{\tau}} + \gamma \end{bmatrix} \tag{III-48}$$

Although the first diagonal element of $\underline{A}_j$ for the nonlinear convective boundary condition is different from that for the fixed temperature boundary condition, the elements of $\underline{E}_i$ are all the same for both cases. Herein lies the advantage of using the variant of the alternating direction implicit procedure; it simplifies the computer programming in that the calculations for dealing with different boundary conditions can be included on one computer program. Furthermore, the nonlinear boundary conditions can be treated by the same procedure without any additional difficulty.

Composite Media System

The following demonstration will verify that the same algorithm can be used for solving the transient two-dimensional composite media with phase change and nonlinear boundary conditions. For the composite media system, a typical mesh region adjacent to the conjunction of two different materials is shown in Figure III-3. For the mesh region (i,j), the calculations of q_1, q_2, q_4 and internal energy are from the properties of one medium only. However, the thermal conductivity for calculating q_3 is assumed to be the average thermal conductivity of the two media, i.e.,

$$q_3 = -\frac{1}{2}(g_{j-1} + g_j)\ \Delta z\ \frac{k^{(1)} + k^{(2)}}{2} \left.\frac{\partial T}{\partial x}\right|_{i+\frac{1}{2},j} \qquad \text{(III-49)}$$

where $k^{(1)}$ and $k^{(2)}$ are the thermal conductivities of material 1 and 2, respectively. In order to minimize the error from this assumption, the interval between (i-1,j) and (i,j) is chosen as small as possible.

Define

$$\bar{U}^{(i)} = \frac{T^{(i)} - T_2}{T_1 - T_2} \qquad \text{(III-50)}$$

$$k^{(i)}(\bar{U}^{(i)}) = k_o^{(i)} \alpha^{(i)}(\bar{U}^{(i)}) \qquad \text{(III-51)}$$

and

$$U^{(i)} = \frac{\int_0^{\bar{U}^{(i)}} \alpha^{(i)}(\bar{U}^{(i)})\, d\bar{U}^{(i)}}{I^{(i)}} \qquad \text{(III-52)}$$

where

$$I^{(i)} = \int_0^1 \alpha^{(i)}(\bar{U}^{(i)})\, d\bar{U}^{(i)} \qquad \text{(III-53)}$$

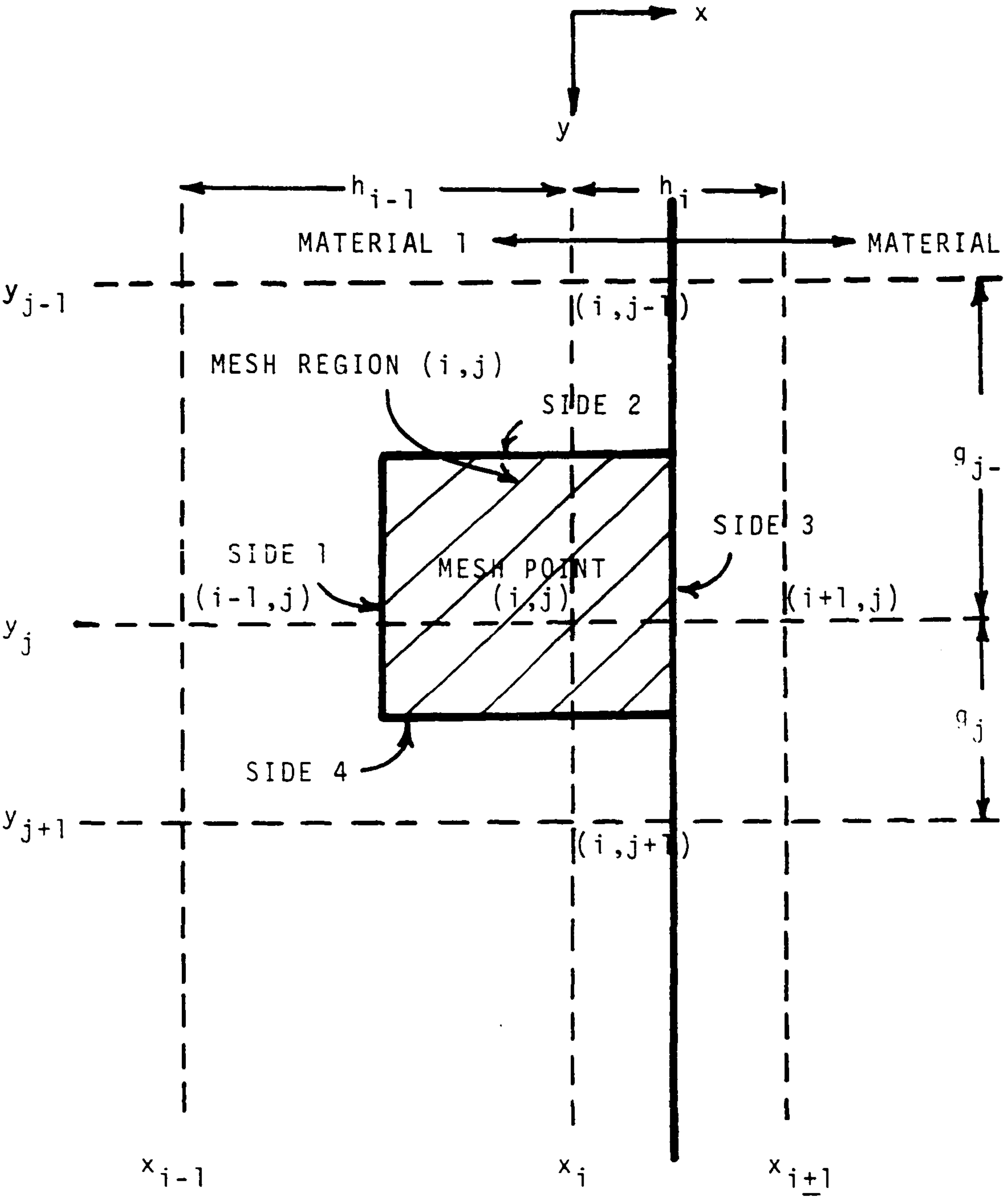

Figure III-3. A Typical Mesh Region (i,j) Adjacent to the Conjunction of Two Different Materials.

From Equation III-49, q_3 is given by

$$q_3 = -\frac{1}{2}(\bar{g}_{j-1} + \bar{g}_j)\ \Delta z\ \frac{T_1 - T_2}{2}$$
$$[k_o^{(1)} I^{(1)}\ \frac{U^{(1)}_{i+1,j} - U^{(1)}_{i,j}}{\bar{h}_i} + k_o^{(2)} I^{(2)}\ \frac{U^{(2)}_{i+1,j} - U^{(2)}_{i,j}}{\bar{h}_i}] \tag{III-54a}$$

or
$$q_3 = -\frac{1}{2}(\bar{g}_{j-1} + \bar{g}_j)\ \Delta z\ \frac{T_1 - T_2}{2}$$
$$[k_o^{(1)} I^{(1)}\ \frac{f(U^{(2)}_{i+1,j}) - U^{(1)}_{i,j}}{\bar{h}_i} + k_o^{(2)} I^{(2)}\ \frac{U^{(2)}_{i+1,j} - f(U^{(1)}_{i,j})}{\bar{h}_i}] \tag{III-54b}$$

where $f(U^{(2)}_{i+1,j})$ is the transformation of $U^{(1)}_{i+1,j}$ from $U^{(1)}$ domain to $U^{(2)}$ domain, and $f(U^{(1)}_{i,j})$ is the transformation of $U^{(2)}_{i,j}$ from $U^{(2)}$ domain to $U^{(1)}$ domain. The equations for q_1, q_2 and q_4 are

$$q_1 = -\frac{1}{2}\ (\bar{g}_j + \bar{g}_j)\ \Delta z\ (T_1 - T_2)\ k_o^{(1)} I^{(1)}\ \frac{U^{(1)}_{i,j} - U^{(1)}_{i+1,j}}{\bar{h}_{i-1}} \tag{III-55}$$

$$q_2 = -\frac{1}{2}\ (\bar{h}_{i-1} + \bar{h}_i)\ \Delta z\ (T_1 - T_2)\ k_o^{(1)} I^{(1)}$$
$$\frac{U^{(1)}_{i,j} - U^{(1)}_{i,j-1}}{\bar{g}_{j-1}} \tag{III-56}$$

$$a_4 = -\frac{1}{2}\ (\bar{h}_{i-1} + \bar{h}_i)\ \Delta z\ (T_1 - T_2)\ k_o^{(1)} I^{(1)}\ \frac{U^{(1)}_{i,j+1} - U^{(1)}_{i,j}}{\bar{g}_j} \tag{III-57}$$

Taking the heat balance around the mesh region (i,j) over the time interval, Δt, results in

$$c_{i,j}\ U^{(1)}_{i-1,j} - \left[c_{i,j}\ U^{(1)}_{i,j} + \frac{b^{(1)}_{i,j}}{2}\ U^{(1)}_{i,j} + \frac{b^{(2)}_{i,j}}{2}\ f\ (U^{(1)}_{i,j})\right]$$

$$+ \left[\frac{b^{(1)}_{i,j}}{2}\ f\ (U^{(2)}_{i+1,j}) + \frac{b^{(2)}_{i,j}}{2}\ U^{(2)}_{i+1,j}\right] + f_{i,j}\ U^{(1)}_{i,j-1} + d_{i,j}\ U^{(1)}_{i,j}$$

$$+ e_{i,j}\ U^{(1)}_{i,j+1} = -\frac{1}{c_o I_o (T_1 - T_2)}\ \frac{E^{(1)}_{i,j} - E^{(1)}_{i,j,o}}{\Delta\hat{t}} \qquad \text{(III-58)}$$

where

$$c_{i,j} = \frac{-\ 2\ \bar{h}\ \bar{g}}{\bar{h}_{i-1}\ (\bar{h}_{i-1}+\bar{h}_i)}\ \frac{k_o^{(1)}\ I^{(1)}}{k_o\ I_o}$$

$$b^{(1)}_{i,j} = \frac{-2\ \bar{h}\ \bar{g}}{\bar{h}_i(\bar{h}_{i-1}+\bar{h}_i)}\ \frac{k_o^{(1)}\ I^{(1)}}{k_o\ I_o}$$

$$b^{(2)}_{i,j} = \frac{-\ 2\ \bar{h}\ \bar{g}}{\bar{h}_i(\bar{h}_{i-1}+\bar{h}_i)}\ \frac{k_o^{(2)}\ I^{(2)}}{k_o\ I_o}$$

$$f_{i,j} = \frac{-\ 2\ \bar{h}\ \bar{g}}{\bar{g}_j(\bar{g}_{j-1}+\bar{g}_j)}\ \frac{k_o^{(1)}\ I^{(1)}}{k_o\ I_o}$$

$$e_{i,j} = \frac{-\ 2\ \bar{h}\ \bar{g}}{\bar{g}_j(\bar{g}_{j-1}+\bar{g}_j)}\ \frac{k_o^{(1)}\ I^{(1)}}{k_o\ I_o}$$

$$d_{i,j} = -\ f_{i,j} - e_{i,j} \qquad \text{(III-59)}$$

k_o = arbitrarily chosen from $k_o^{(i)}$

I_o = arbitrarily chosen from $I^{(i)}$

Applying the generalized Newton-Raphson method to linearize Equation III-58, then

$$c_{i,j}\ \Gamma^{n+1}_{i-1,j} + a_{i,j}\ \Gamma^{n+1}_{i,j} + b_{i,j}\ \Gamma^{n+1}_{i+1,j} + f_{i,j}\ \Gamma^{n+1}_{i,j-1}$$

$$+ d_{i,j}\ \Gamma^{n+1}_{i,j} + e_{i,j}\ \Gamma^{n+1}_{i,j+1} + \frac{\phi_{i,j}}{\Delta\hat{t}}\ \Gamma^{n+1}_{i,j} = -\ S_{i,j} \qquad \text{(III-60)}$$

where

$$a_{i,j} = -\left[c_{i,j} + \frac{b^{(1)}_{i,j}}{2} + \frac{b^{(2)}_{i,j}}{2} \bullet \frac{d\ f(U^{(1),n}_{i,j})}{d\ U^{(1),n}_{i,j}}\right] \qquad \text{(III-61)}$$

$$b_{i,j} = \frac{b^{(1)}_{i,j}}{2} \bullet \frac{d\ f(U^{(1),n}_{i,j})}{d\ U^{(2),n}_{i,j}} + \frac{b^{(2)}_{i,j}}{2} \qquad \text{(III-62)}$$

$$\phi_{i,j} = \frac{1}{c_o(T_1 - T_2)I_o} \bullet \frac{d\ E\ (U^{(1),n}_{i,j})}{d\ U^{(1),n}_{i,j}} \qquad \text{(III-63)}$$

$$\begin{aligned} S_{i,j} &= c_{i,j}\ U^{(1),n}_{i-1,j} - [c_{i,j}\ U^{(1),n}_{i,j} + \frac{b^{(1)}_{i,j}}{2}\ U^{(1),n}_{i,j} \\ &+ \frac{b^{(2)}_{i,j}}{2}\ f(U^{(1),n}_{i,j})] + [\frac{b^{(1)}_{i,j}}{2}\ f(U^{(2),n}_{i+i,j}) \\ &+ \frac{b^{(2)}_{i,j}}{2}\ U^{(2),n}_{i+1,j}] + f_{i,j}\ U^{(1),n}_{i,j-1} + d_{i,j}\ U^{(1),n}_{i,j} \\ &+ e_{i,j}\ U^{(1),n}_{i,j+1} + \frac{1}{c_o\ I_o(T_1 - T_2)}\ \frac{E^{(1)}_{i,j} - E^{(1)}_{i,j,o}}{\Delta\hat{\tau}} \end{aligned} \qquad \text{(III-64)}$$

It is noted that Equation III-60 is the same as Equation III-26 obtained in the previous section, the only difference being the coefficients of $c_{i,j}$, $a_{i,j}$, and $b_{i,j}$ because it has the assumption of taking the average thermal conductivity for calculating q_3. Therefore, the form of Equation III-31 and Equation III-37 can be also obtained for composite media.

One-Dimensional Cases

When the temperature is symmetric with respect to one of the two spatial coordinates, say y, the problem becomes a one-dimensional case. For a one-dimensional case, the finite difference equation can be obtained easily by taking an energy balance around each one-dimensional case discussed above. For the nonlinear equations, the generalized Newton-Raphson method is also employed to linearize them. However, the variant of the alternating direction implicit procedure is not necessary for a one-dimensional case. On the other hand, the finite difference equations given in the above section for a two-dimensional case can be reduced to the one-dimensional case. For example, Equation III-16 for a mesh region becomes

$$c_i\, U_{i-1} + a_i\, U_i + b_i\, U_{i+1} + \frac{1}{c_o(T_1 - T_2)I}\ \frac{E_i}{\Delta\hat{\tau}}$$

$$= \frac{1}{c_o(T_1 - T_2)I}\ \frac{E_{i,o}}{\Delta\hat{\tau}} \qquad \text{(III-65)}$$

Applying the Newton-Raphson method and defining

$$\Gamma_i^{n+1} = U_i^{n+1} - U_i^n \qquad \text{(III-66)}$$

the linearized equation is

$$c_i\, \Gamma_{i-1}^{n+1} + a_i\, \Gamma_i^{n+1} + b_i\, \Gamma_{i+1}^{n+1} + \frac{\phi_i}{\Delta\hat{\tau}}\, \Gamma_i^{n+1} = -\, S_i \qquad \text{(III-67)}$$

where

$$\bar{h}_i = \frac{h_i}{a}$$

$$\hat{\tau} = \frac{\tau}{\bar{h}^2}$$

$$c_i = \frac{-2\ \bar{h}^2}{\bar{h}_{i-1}(\bar{h}_{i-1} + \bar{h}_i)}$$

$$b_i = \frac{-2\ \bar{h}^2}{\bar{h}_i(\bar{h}_{i-1} + \bar{h}_i)}$$

$$a_i = -c_i - b_i$$

$$\phi_i = \frac{1}{c_o(T_1 - T_2)I} \frac{d\,E(U_i^n)}{d\,U_i^n}$$

$$S_i = c_i\,U_{i-1}^n + a_i\,U_i^n + b_i\,U_{i+1}^n + \frac{1}{c_o(T_1 - T_2)I} \frac{E_i^n - E_{i,o}}{\Delta\hat{\tau}} \qquad \text{(III-68)}$$

For all mesh points of the system, it has

$$\underline{A}\,\underline{\Gamma}^{n+1} = \underline{B} \qquad \text{(III-69)}$$

where

$$\underline{A} = \begin{pmatrix} a_1 + \frac{\phi_1}{\Delta\hat{\tau}} & b_1 & & & \\ c_2 & a_2 + \frac{\phi_2}{\Delta\hat{\tau}} & b_2 & & \\ \cdot & \cdot & \cdot & & \\ & \cdot & \cdot & \cdot & \\ & & \cdot & \cdot & \cdot \\ & & & c_{N_x} & a_{N_x} + \frac{\phi_{N_x}}{\Delta\hat{\tau}} \end{pmatrix} \qquad \text{(III-70)}$$

$$\underline{B} = \begin{pmatrix} -S_1 \\ -S_2 \\ \cdot \\ \cdot \\ \cdot \\ -S_{N_x} \end{pmatrix} \qquad \text{(III-71)}$$

$$\underline{\Gamma}^{n+1} = \begin{bmatrix} \Gamma_1^{n+1} \\ \Gamma_2^{n+1} \\ \cdot \\ \cdot \\ \cdot \\ \Gamma_{N_x}^{n+1} \end{bmatrix} \tag{III-72}$$

No matter what kind of boundary conditions exists, Equation III-69 can be obtained for all cases except when the elements of A and B are different from one another.

In the same way, Equation III-60, the representation of a two-dimensional composite media, can be simplified to treat one-dimensional composite regions, i.e.

$$c_i\ \Gamma_{i-1}^{n+1} + a_i\ \Gamma_i^{n+1} + b_i\ \Gamma_{i+1}^{n+1} + \frac{\phi_i}{\Delta \hat{t}}\ \Gamma_i^{n+1} = -S_i \tag{III-73}$$

where

$$c_i = \frac{-2\ \bar{h}^2}{\bar{h}_{i-1}\ (\bar{h}_{i-1} + \bar{h}_i)}\ \frac{k_o^{(1)}\ I^{(1)}}{k_o\ I_o}$$

$$b_i^{(1)} = \frac{-2\ \bar{h}^2}{\bar{h}_i(\bar{h}_{i-1} + \bar{h}_i)}\ \frac{k_o^{(1)}\ I^{(1)}}{k_o\ I_o}$$

$$b_i^{(2)} = \frac{-2\ \bar{h}^2}{\bar{h}_i(\bar{h}_{i-1} + \bar{h}_i)}\ \frac{k_o^{(2)}\ I^{(2)}}{k_o\ I_o}$$

$$a_i = -\ [c_i + \frac{b_i^{(1)}}{2} + \frac{b_i^{(2)}}{2}\ \frac{d\ f(U_i^{(1),n})}{d\ U_i^{(1),n}}]$$

$$b_i = \frac{b_i^{(1)}}{2}\ \frac{d\ f(U_i^{(1),n})}{d\ U_i^{(1),n}} + \frac{b_i^{(2)}}{2}$$

$$\phi_i = \frac{1}{c_o(T_1 - T_2)I_o} \frac{d\,E(U_i^{(1),n})}{d\,U_i^{(1),n}}$$

$$\begin{aligned} S_i = {} & c_i\,U_{i-1}^{(1),n} - [c_i\,U_i^{(1),n} + \frac{b_i^{(1)}}{2}\,U_i^{(1),n} \\ & + \frac{b_i^{(2)}}{2}\,f(U_i^{(1),n})] + [\frac{b_i^{(1)}}{2}\,f(U_{i+1}^{(2),n}) \\ & + \frac{b_i^{(2)}}{2}\,U_{i+1}^{(2),n}] + \frac{1}{c_o(T_1 - T_2)I_o}\,\frac{E_i^{(1)} - E_{i,o}^{(1)}}{\Delta\hat{t}} \end{aligned}$$

(III-74)

For one-dimensional cases, Equation III-69 is obtained and solved by the Gaussian elimination method (17). The iterative procedure is repeated until the convergent criterion is satisfied.

In general, the proposed method is applicable to the general one- and two-dimensional heat conduction problems with and without phase change.

Summary of the Proposed Procedure

1. Linearize the nonlinear simultaneous equation by the quasilinearization technique.
2. Let $\underline{U}$ at time t be the initial guess for calculating $\underline{U}$ of the next time step.
3. The x-direction sweep, $\underline{A}_j\,\underline{\Gamma}_j^* = \underline{B}_j$ for $1 \le j \le N_y$; the tridiagonal system is solved by Gaussian elimination method.
4. The y-direction sweep, $\underline{D}_i\,\underline{\Gamma}_i^{n+1} = \underline{E}_i$ for $1 \le i \le N_x$; the tridiagonal system is solved by Gaussian elimination method.
5. $\underline{U}^{(n+1)} = \underline{U}^{(n)} + \underline{\Gamma}^{(n+1)}$

If the convergence criterion is satisfied, then go to (2) for the next time step. Otherwise, let $\underline{U}^{(n)} = \underline{U}^{(n+1)}$ and $\underline{\Gamma}^{(n)} = \underline{\Gamma}^{(n+1)}$, and then go to (3) for the next iteration.

CHAPTER IV

THE EVAPORATION RATE OF LNG ON SOIL

There are several important factors in the calculation of the boil-off rate of LNG when spilled on soil, such as the physical properties of the soil, the boiling heat transfer coefficient, the dike wall effect, the insulation on the surface of ground, the surface irregularities, the permeability of the soil, and the condition of the weather. In this chapter, fourteen models are discussed to evaluate the influence of the soil properties, boiling coefficient, dike wall effect and insulation on the heat transfer rate between the LNG and the soil. A summary of these fourteen models is listed in Table IV-1. The numerical method proposed in Chapter III is employed to solve some of them. The physical properties of LNG shown in Table IV-2 are taken as those of pure methane for simplicity.

Effect of Thermal Properties of Soil

The heat capacity, thermal conductivity, and density of the soil depend strongly on the moisture content and the temperature of the soil. Soils usually have higher heat capacities, thermal conductivities and densities with increasing water content.

TABLE IV-1

SUMMARY OF MODELS STUDIED FOR EVALUATION OF THE LNG BOIL-OFF RATE

No. of Model	No. of Dim.	Therm. Prop. of Soil	Phase Change	Boiling Heat Trans. Coef. Btu/hr-ft^2-°F	Insulation	Dike Depth-to-Diameter Ratio
I-1	One	Constant	No	Infinite	No	0
I-2	One	Constant	No	100	No	0
I-3	One	Constant	Yes	Infinite	No	0
I-4	One	Temperature Dependent	Yes	Infinite	No	0
I-5	One	Temperature Dependent	Yes	100	No	0
I-6	One	Temperature Dependent	Yes	Temperature Dependent	No	0
I-7	One	Constant	No	Infinite	Yes	0
I-8	One	Constant	No	Finite and Constant	Yes	0
I-9	One	Temperature Dependent	Yes	Infinite	Yes	0
I-10	One	Temperature Dependent	Yes	Temperature Dependent	Yes	0
II-1	Two	Temperature Dependent	Yes	Infinite	No	0.05
II-2	Two	Temperature Dependent	Yes	Infinite	No	0.5
II-3	Two	Temperature Dependent	Yes	Temperature Dependent	No	0.05
II-4	Two	Temperature Dependent	Yes	Temperature Dependent	Yes	0.05

Since the thermal conductivity of water or ice increases with decreasing temperature, the thermal conductivities of frozen and unfrozen soil display the same trend. However, some samples (24) have contrasting behavior, and the conductivities decrease with decreasing temperature.

TABLE IV-2

PROPERTIES OF LNG

Latent Heat of Vaporization	= 220 Btu/lb
Normal Boiling Point	= -260°F
Density of Liquid	= 25.9 lb/ft^3

Because the specific heat of water is nearly constant and the specific heat of ice and dry soils decrease with increasing temperature, the specific heat of wet soil increases as temperature drops.

The effects of temperature, moisture content, density particle size and shape, and mineral composition on the thermal properties of the soil have been extensively investigated by Kersten (53). The thermal properties of three samples of San Clemente soil have been reported by Drake, Harris and Reid (24) recently. The thermal properties of soil over a wide range of temperatures would be expected to vary with temperature. In addition, the latent heat of phase transition of wet soil as a function of temperature needs to be considered in heat transfer analysis.

The properties of ice and water (51, 81) are shown in Tables IV-3A through IV-3C. By making use of the linear least square technique, the properties can be correlated by the following relation:

$$F = a_1 + b_1 T + c_1 T^2 \qquad \text{(IV-1)}$$

where T is in degrees Fahrenheit. The results are shown in Table IV-4. The percentage errors of the regression are presented in the last column of Tables IV-3B and IV-3C.

The properties of soil reported by Hashemi and Sliepcevich (46) are shown in Tables IV-5A through IV-5C. The plot of soil properties versus temperature shown in Figure IV-1 are later adopted for the heat transfer calculations from soil to LNG.

TABLE IV-3A

PROPERTIES OF THE WATER AND ICE (51, 81)

Density of Water = 62.4 lb/ft^3

Density of Ice = 57.2 lb/ft^3

Latent Heat of Freezing = 8985.6 Btu/ft^3

TABLE IV-3B

SPECIFIC HEATS OF WATER AND ICE

Temperature °F	Specific Heat Btu/ft^3-°F	Percentage Error of Regression Equation
32.0∿60.0	62.40	--
28.4	28.71	0.201
23.18	28.22	-0.511
17.42	28.01	-0.027
12.20	27.81	0.365
5.36	27.36	0.195
- 5.44	26.71	0.133
- 10.66	26.31	-0.207
- 23.08	25.68	0.125
- 36.94	24.87	0.074
- 76.0	22.43	-0.922
-148.0	18.82	0.632
-220.0	14.99	0.163
-238.0	14.07	0.098
-256.0	13.16	-0.068
-292.0	11.38	-0.289

TABLE IV-3C

THERMAL CONDUCTIVITIES OF WATER AND ICE

Temperature °F	Thermal Conductivity Btu/hr-ft-°F	Percentage Error of Regression Equation
100	0.3634	-0.106
68	0.3459	0.356
50	0.3392	-0.329
32 (Water)	0.3286	0.078
32 (Ice)	1.2900	2.245
- 13	1.44	-0.734
- 58	1.60	-2.261
-103	1.79	-2.262
-148	2.01	-0.132
-193	2.27	3.285

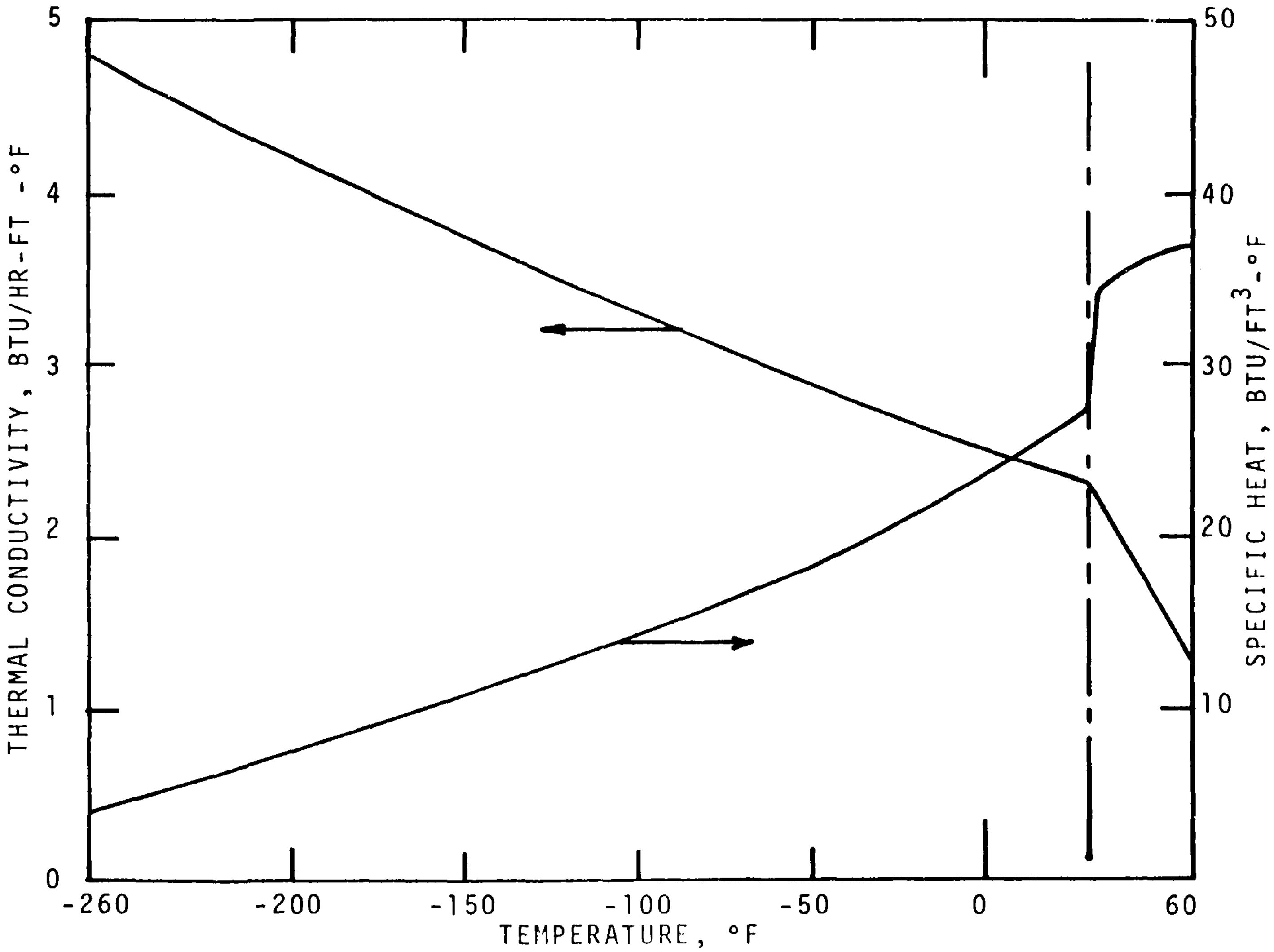

Figure IV-1. Thermal Conductivity and Specific Heat of Soil Versus Temperature.

TABLE IV-4

THE COEFFICIENTS OF A_1, B_1 AND C_1 FOR SPECIFIC HEAT AND THERMAL CONDUCTIVITY OF ICE AND WATER

F	a_1	$b_1 x 10^2$	$c_1 x 10^5$	Temperature Range
Specific Heat Btu/ft^3-°F	62.40	0	0	32°F∿100°F
	26.9942	5.87318	0.184760	-292°F∿ 32°F
Thermal Conductivity Btu/hr-ft-°F	0.312871	0.0502457	0	32°F∿100°F
	1.38578	-0.431746	0	-260°F∿ 32°F

Heat capacities below -30°F are obtained by the extrapolation of the reported values. The thermal properties are also correlated by the linear least squares technique. Percentage errors of regression are shown in the last column of Table IV-5; the coefficients are listed in Table IV-6.

TABLE IV-5A

PROPERTIES OF THE SOIL (46)

Dry Density	116 lb/ft^3
Porosity	30%
Water Content	16.15% dry weight
Latent Heat of Freezing	2700 Btu/ft^3

TABLE IV-5B

SPECIFIC HEAT OF THE SOIL

Temperature °F	Specific Heat Btu/ft^3-°F	Percentage Error of Regression Equation
50	36.5	-3.385
34	34.5	6.647
30 (Frozen)	27.5	1.404
-10	22.2	-1.698
-30	20.2	-1.469

TABLE IV-5C

THERMAL CONDUCTIVITIES OF THE SOIL

Temperature °F	Thermal Conductivity Btu/hr-ft-°F	Percentage Error of Regression Equation
50	1.64	-0.526
30 (Frozen)	2.30	-0.966
- 40	2.80	-1.415
-260	4.80	0.661

TABLE IV-6

THE COEFFICIENTS OF A_1, B_1 AND C_1 FOR SPECIFIC HEAT AND THERMAL CONDUCTIVITY OF SOIL

F	a_1	b_1	$c_1 \times 10^3$	Temperature Range
Specific Heat	-17.6054	2.22633	-22.3903	30°F∿60°F
Btu/ft^3-°F	23.6642	0.110283	0.156776	-260°F∿30°F
Thermal Conductivity	3.33252	-0.00336775	0	30°F∿60°F
Btu/hr-ft-°F	2.48896	-0.00876661	0	-260°F∿30°F

Model I-1

The simplest model, Model I-1, for heat transfer from soil to LNG has the following assumption:

1. The model is the one-dimensional case.
2. The thermal properties of the soil are constant.
3. The soil has no phase change, is homogeneous and of semi-infinite depth.
4. The convective heat transfer coefficient between LNG and soil, h, is infinite.

If LNG is spilled on the soil at T_∞ and boils at a constant temperature, T_L, then the equation for this model is:

$$c \frac{\partial T}{\partial t} = k \frac{\partial^2 T}{\partial x^2} \qquad \text{(IV-2)}$$

and the boundary conditions are:

$$T(x,o) = T_\infty \qquad \text{(IV-3)}$$

$$T(o,t) = T_L \qquad \text{(IV-4)}$$

$$T(\infty,t) = T_\infty \qquad \text{(IV-5)}$$

The solution of temperature distribution (18) is:

$$T = T_\infty + (T_L - T_\infty) \operatorname{erfc} \left(\frac{x}{2\sqrt{\alpha t}}\right) \qquad \text{(IV-6)}$$

where α = thermal diffusivity of soil, k/c

The resulting rate of heat transfer per unit area from the soil to LNG is given as

$$\bar{q} = \frac{k(T_\infty - T_L)}{\sqrt{\pi \alpha t}} \qquad \text{(IV-7)}$$

Integrating Equation IV-7 with respect to t, the accumulation of heat as a function of time is

$$\bar{Q} = 2\, k(T_\infty - T_L) \sqrt{\frac{t}{\pi\alpha}} \qquad \text{(IV-8)}$$

Model I-2

For a finite and constant convection heat transfer coefficient, Model I-1 is modified to Model I-2. The temperature profile is

$$T = T_\infty + (T_L - G_\infty)\left[\operatorname{erfc} \frac{x}{2\sqrt{\alpha t}} - e^{(hx/k) + (2th^2/k^2)} \operatorname{erfc} \left(\frac{x}{2\sqrt{dt}} + \frac{h\sqrt{\alpha t}}{k}\right)\right] \qquad \text{(IV-9)}$$

The heat transfer rate of Model I-2 is

$$\bar{q} = h(T_\infty - T_L)\, e^{\frac{\alpha t h^2}{k^2}} \operatorname{erfc} \left(\frac{h\sqrt{\alpha t}}{k}\right) \qquad \text{(IV-10)}$$

The total heat from the soil to LNG for Model I-2 is

$$\bar{Q} = \frac{c\,k(T_\infty - T_L)}{h}\left[\operatorname{erfc}\left(\frac{h\sqrt{\alpha t}}{k}\right) e^{\frac{\alpha t h^2}{k^2}} + \frac{2h}{k}\sqrt{\frac{\alpha t}{\pi}} - 1\right] \qquad \text{(IV-11)}$$

Model I-3

Model I-3 assumes:

1. The soil is not dry and the phase change of the soil is at a fixed temperature.
2. The thermal properties of frozen and unfrozen soil are different but constant, and no thermal resistance exists between the soil and LNG.

Then this one-dimensional wet soil model is a linear moving boundary problem which can be solved by analytical methods. The equations for Model I-3 are:

$$c_1 \frac{\partial T_1}{\partial t} = k_1 \frac{\partial^2 T_1}{\partial x^2} \qquad \text{(IV-12)}$$

$$c_2 \frac{\partial T_2}{\partial t} = k_2 \frac{\partial^2 T_2}{\partial x^2} \qquad \text{(IV-13)}$$

with initial and boundary conditions

$$T_1(o,t) = T_L \qquad \text{(IV-14)}$$

$$T_1[X(t),t] = T_f = T_2[X(t),t] \qquad \text{(IV-15)}$$

$$T_2(\infty,t) = T_\infty \qquad \text{(IV-16)}$$

$$-k_1 \left.\frac{\partial T_1}{\partial x}\right|_{x = X(t)} = -k_2 \left.\frac{\partial T_2}{\partial x}\right|_{x = X(t)} + H\,\frac{dX(t)}{dt} \qquad \text{(IV-17)}$$

where $X(t)$ = position of unfrozen and frozen soil interface.

H = heat of fusion.

$\frac{dX(t)}{dt}$ = rate at which the interface moves.

Subscripts 1 and 2 represent frozen and unfrozen soil respectively. Following Ruoff's method (86), the analytical solution can be written as follows:

$$\frac{T_1 - T_\infty}{T_L - T_\infty} = 1 - (1-\theta)\,\frac{\operatorname{erf}\dfrac{\bar{z}}{2\sqrt{\alpha_1}}}{\operatorname{erf}\dfrac{Z}{2\sqrt{\alpha_1}}} \tag{IV-18}$$

and

$$\frac{T_2 - T_\infty}{T_L - T_\infty} = \theta\,\frac{1-\operatorname{erf}\dfrac{\bar{z}}{2\sqrt{\alpha_2}}}{1-\operatorname{erf}\dfrac{Z}{2\sqrt{\alpha_2}}} \tag{IV-19}$$

where

$$\theta = \frac{T_t - T_\infty}{T_L - T_\infty} \tag{IV-20}$$

$$\bar{z} = \frac{x}{\sqrt{t}} \tag{IV-21}$$

Z is found by solving the transcendental equation:

$$\frac{1}{k_1\sqrt{\pi\alpha_1}}\,\frac{1-\theta}{\operatorname{erf}\dfrac{Z}{2\sqrt{\alpha_1}}}\,e^{-Z^2/4\alpha_1} = \frac{Z}{2}\,\frac{H}{(T_L - T_\infty)} + \frac{k_2}{\sqrt{\pi\alpha_2}}\,\frac{\theta}{1-\operatorname{erf}\dfrac{Z}{2\sqrt{\alpha_2}}} \times e^{-Z^2/4\alpha_2} \tag{IV-22}$$

Churchill and Evans (20) have presented a tabulated form for Z over a wide range of parameters. The flux and heat equations (similar to Equations IV-10 and IV-11) for Model I-3 are:

$$\bar{q} = \frac{k_1(T_\infty - T_L)}{\sqrt{\pi\alpha_1 t}} \; \frac{1-\theta}{\operatorname{erf}\dfrac{Z}{2\sqrt{\alpha_1}}} \tag{IV-23}$$

and

$$\bar{Q} = 2\, k_1(T_\infty - T_L)\sqrt{\frac{t}{\pi\alpha_1}} \; \frac{1-\theta}{\operatorname{erf}\dfrac{Z}{2\sqrt{\alpha_1}}} \tag{IV-24}$$

For the following calculations, it is assumed that the initial temperature of soil is 60°F and the LNG temperature remains at its initial boiling point, -260°F. By taking the average values of Table IV-5, the specific heat and thermal conductivity of the soil for Model I-1 would be

$$k = 3.0 \text{ Btu/hr-ft-°F}$$

and

$$c = 20.0 \text{ Btu/ft}^3\text{-°F}$$

The thermal properties of frozen and unfrozen soil for Model I-3 are assumed to be

$$k_1 = 3.0 \text{ Btu/hr-ft-°F}$$

$$c_1 = 20.0 \text{ Btu/ft}^3\text{-°F}$$

and

$$k_2 = 2.1 \text{ Btu/hr-ft-°F}$$

$$c_2 = 34.5 \text{ Btu/ft}^3\text{-°F}$$

The phase change temperature of the wet soil is at a fixed temperature, 30°F.

Model I-4

For small temperature ranges, the assumption of constant thermal properties may be proper. However, for a wide temperature range, the assumption is definitely improper. The conditions of Model I-4 are the same as those of Model I-3 except for the constant thermal properties assumption. Because the thermal properties of frozen and unfrozen soil are temperature dependent, there is no exact solution for Model I-4. It can be olved using the numerical method developed in Chapter III.

The soil properties listed on Table IV-5 are employed by Model I-4. It assumes the phase change is over a finite temperature interval, from 35°F to 25°F. Following Equation III-15, the latent heat approximation over the transition interval is in the form:

$$E_t = \frac{H}{2}[1 - \mathrm{erf}\, \varepsilon(30-T)] \qquad \text{(IV-25)}$$

where $H = 2700\ \mathrm{Btu/ft}^3$

$\varepsilon = 0.6(°\mathrm{F})^{-1}$

Effect of Soil Phase Change

The calculated evaporation rate and accumulative boil-off of LNG for Models I-1, I-3, and I-4 are shown in Figure IV-2. The major difference between Model I-1 and Model I-3 is that Model I-3 has a phase change transition. As shown in Figure IV-2,

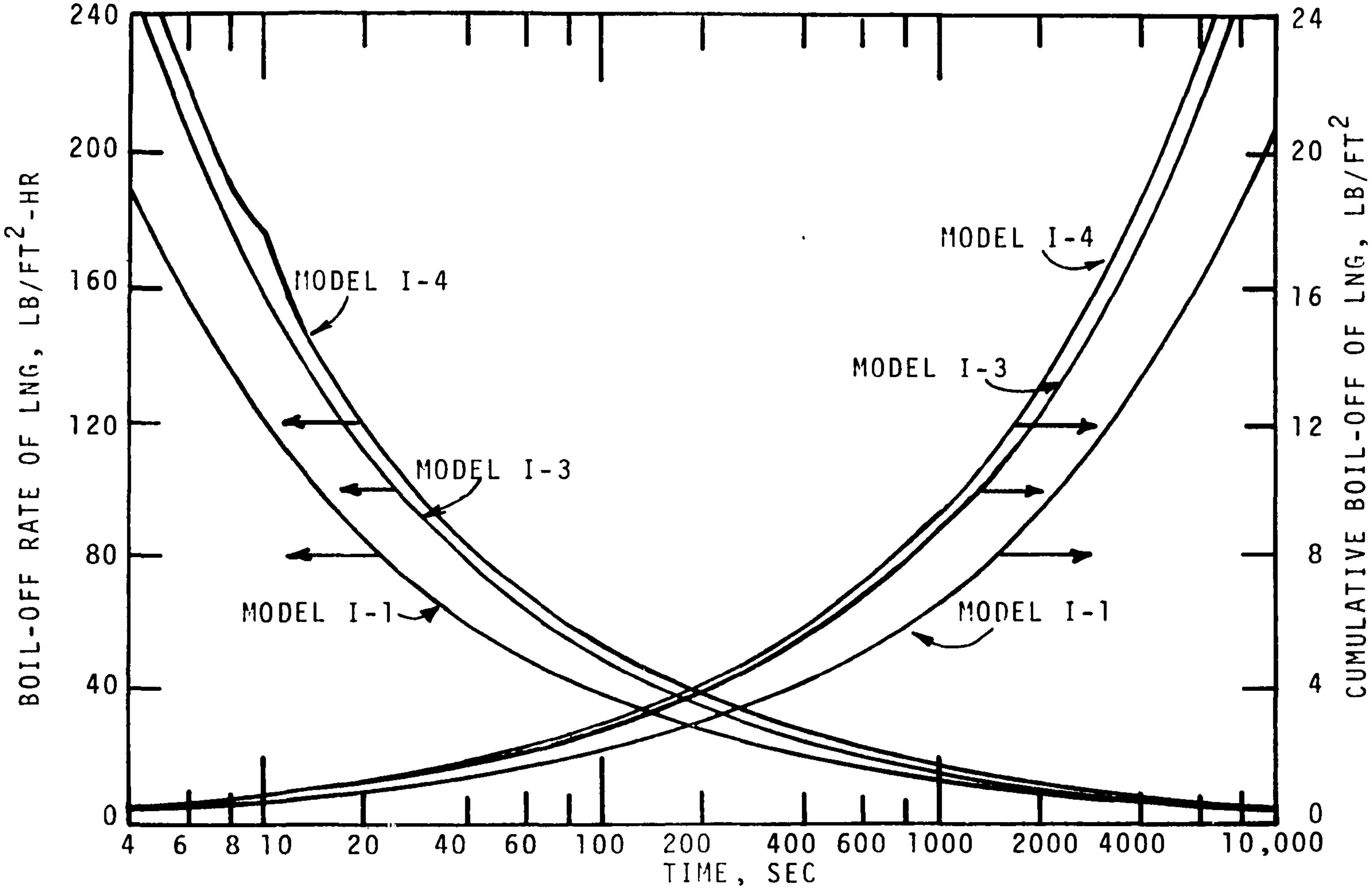

Figure IV-2. Effect of Soil Properties on the LNG Boil-Off of Models I-1, I-3, and I-4.

the boil-off rate and accumulative boil-off of LNG of Model I-3 are about 33 percent higher than those of Model I-1. In other words, the boil-off rates of LNG on the wet soil would be 33 percent higher than on the dry soil if the thermal properties of both the wet and the dry soil are approximately the same. From the comparison of Model I-3 and Model I-4 in Figure IV-2, it can be seen that Model I-4, with temperature-dependent thermal properties of soil, has 5 percent higher boil-off rates of LNG than those of Model I-3 with constant soil properties. Therefore, the model with the assumptions of no phase change occurrence and constant average soil properties would underestimate the LNG boil-off rate by about 38 percent. It should be noted that the above results are under the assumption of no thermal resistance between the LNG and the soil. The soil temperatures of Model I-1, I-3, and I-4 versus $X/(2\sqrt{\alpha t})$, which is called Boltzmann's transformation, are plotted in Figure IV-3. Because the media are semi-infinite and the surfaces are kept at a constant temperature, this type of plot is the best way to present temperature versus time and position. Due to the different thermal properties of frozen and unfrozen soil and the release of latent heat, the temperature distributions of Models I-3 and I-4 have discontinuous points at the freezing temperature. The large amount of latent heat causes the temperature differences of the model with phase change and the model without phase change to be more significant in the neighborhood of the phase transition point.

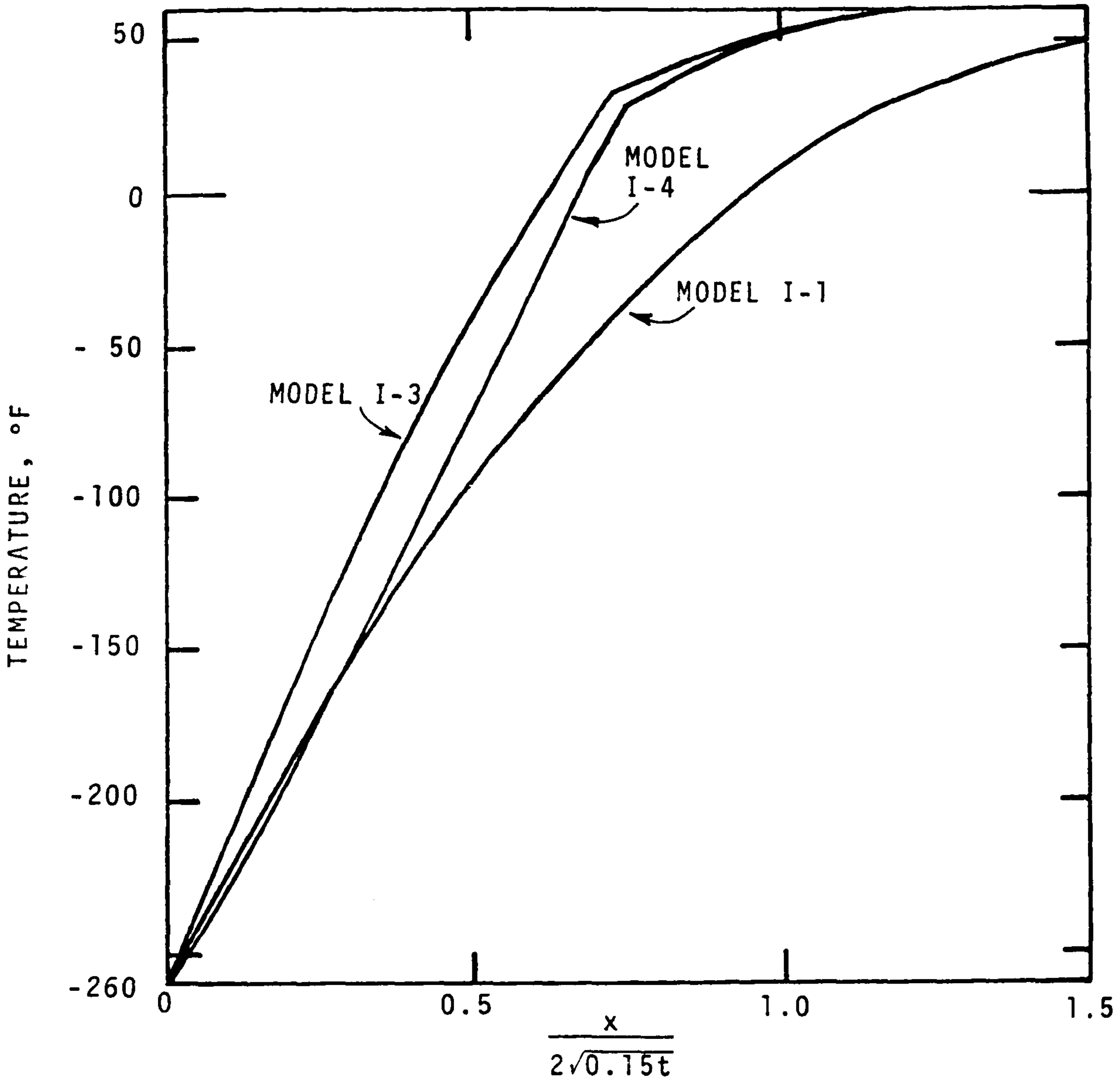

Figure IV-3. Temperature Distributions of Models I-1, I-3 and I-4.

Effect of Constant Heat Transfer Coefficient Between LNG and Soil

Figure IV-4 compares the boil-off rate and accumulative boil-off of Model I-2 and Model I-5. The heat transfer coefficients between the soil and LNG for these two models are finite. The film coefficient, h, is kept constant during the entire boiling period at 100 Btu/hr-ft^2-°F. The properties of the soil for Model I-2 are taken to be those for Model I-1. Model I-5 has the soil properties and phase transition approximation of Model I-4. As previously illustrated in Figure IV-2, Figure IV-4 also shows that the calculated boil-off rates of the wet soil model are greater than those of the dry soil model. However, the percentage of the increase in boil-off rate is dependent upon the time. For all time ranges the difference is from 10 to 60 percent. If there is a thermal resistance between the boiling LNG and the exposed boundary, the heat transfer rate is initially dominated by the boiling heat transfer coefficient. The thermal properties of soil as well as soil latent heat have little effect on the heat transfer rate and the temperature distribution in the short time region. When time is longer, the influence of soil properties becomes more important. Therefore, there is no noticeable difference in the accumulative boil-off of LNG for Models I-2 and I-5 at times less than 10 seconds. But, the difference rises up to 40 percent at 5000 seconds. The plots shown in Figure IV-5 are several temperature profiles of the soil from Model I-2 and Model I-5. The figure indicates that the temperature difference in the neighborhood

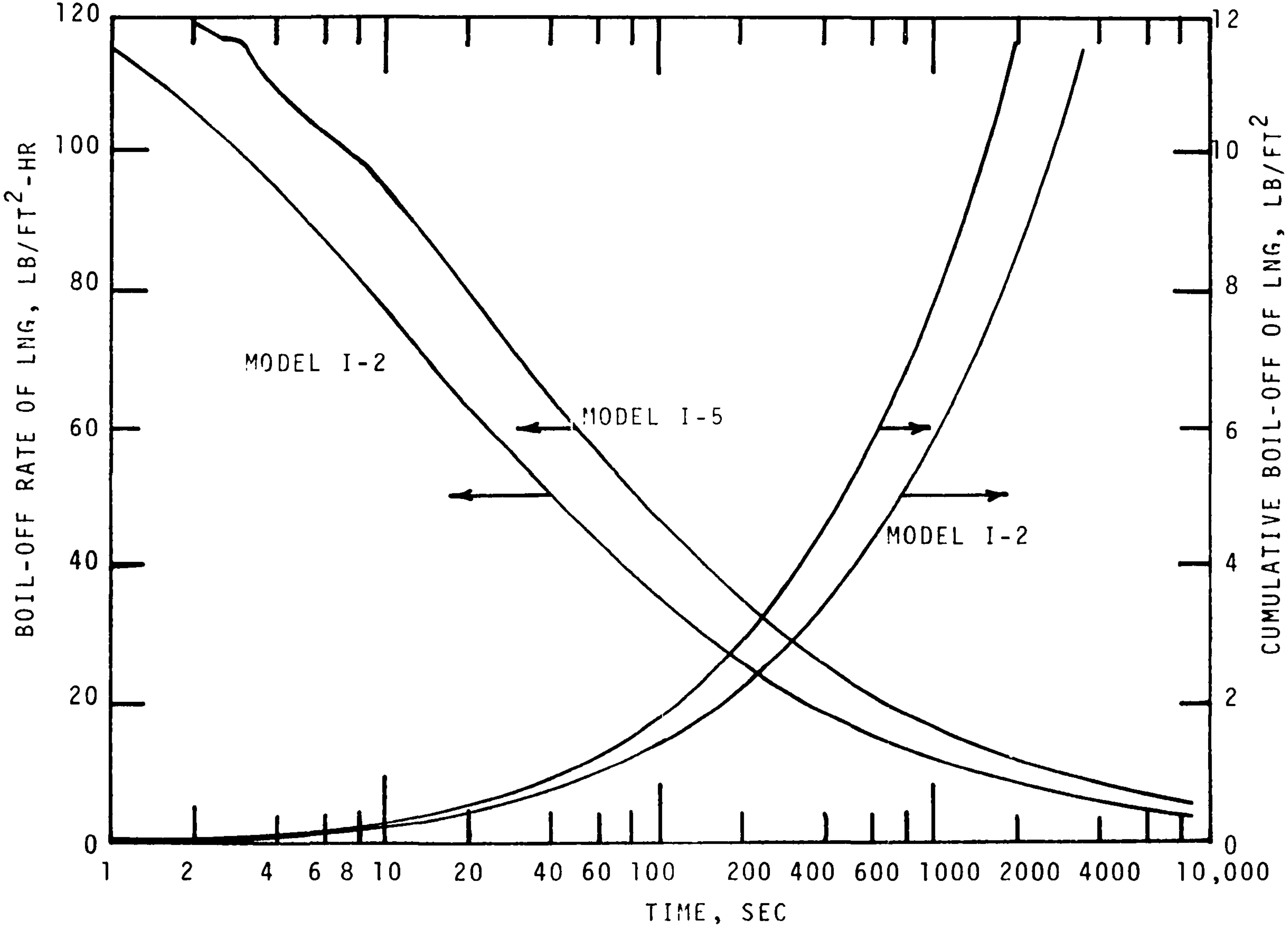

Figure IV-4. Effect of Soil Properties on the LNG Boil-OFF of Models I-2 and I-5.

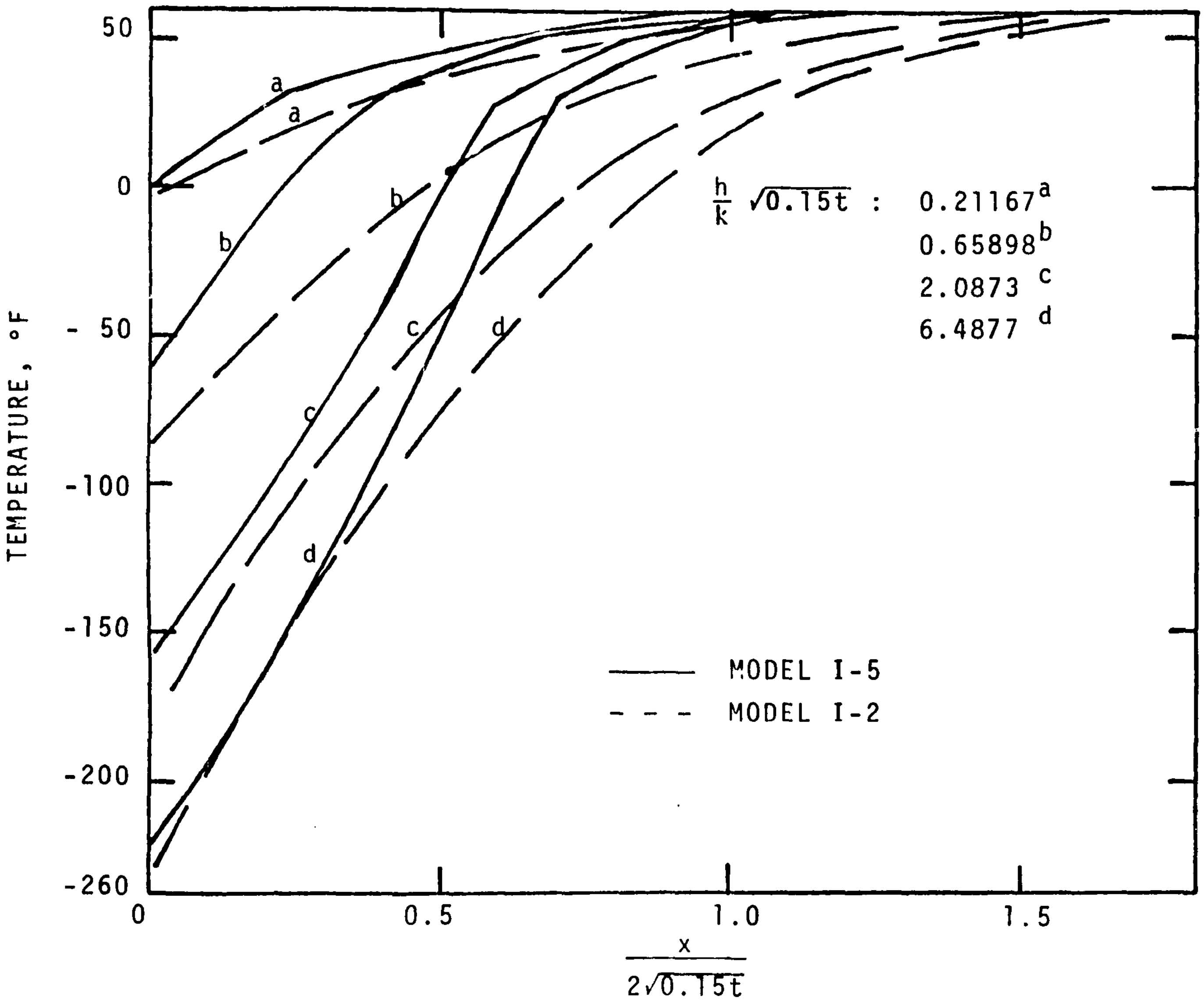

Figure IV-5. Temperature Distributions of Models I-2 and I-5.

of phase transition increases with time. Irregularities are seen in the curves of Model I-5 in the short time range. The large amount of latent heat makes a small change of temperature over the phase change interval. If there is a phase change near the surface, the surface temperature change will be slowed during the phase transition period. The heat transfer rate of Model I-5 is the constant heat transfer coefficient multiplied by the surface temperature difference. These two factors make the heat transfer rate irregular during the initial few seconds of heat transfer, while the curve is smooth for the longer time period. This behavior shows that the occurrence of a phase change far from the surface makes less contribution to the surface temperature change. From the direct comparison for the above models it can be concluded that the thermal conductivity and the heat capacity of the soil have great influence on the temperature distribution and the heat transfer rate. If the latent heat of phase change is neglected for wet soil, the heat transfer rate is underestimated, and the temperature distribution is overestimated.

Effect of Boiling Heat Transfer Coefficient

Film boiling occurs initially because of the large temperature difference between the soil surface and spilled LNG. The thermal resistance is significant, and the accurate boiling heat transfer coefficient is an important factor in the heat transfer calculation within the short time range. The boiling mechanism shifts from film boiling to nucleate boiling when the soil surface temperature drops. If the heat transfer coefficient is higher, then the boiling resistance is less significant. This pool boiling behavior for methane, ethane, propane and butane on a metal cylinder has been investigated by Sciance, Colver and Sliepcevich (91, 92, 93). Later, Brown and Colver (11) reported the nucleate and film boiling heat transfer between LNG and a metal cylinder. According to their report, the temperature differences for the nucleate boiling decreased with increasing pressure for pure methane, but increased with increasing pressure for LNG. The temperature differences for LNG were much larger than those for pure methane. Recently, Vishnev (109) has used the similarity theory and corresponding state principle to develop a generalized correlation for heat transfer during boiling of cryogenic liquids--helium, hydrogen, neon, nitrogen, argon, oxygen and methane.

The real unsteady state heat transfer between soil and LNG is convective-heat-transfer controlled at the onset, and then is conduction-transfer controlled when the temperature difference between the soil and LNG is small. The boiling heat transfer coeffcient is surface-temperature-difference dependent. The heat transfer rate between LNG and soil (12) is

$$q = 7572.621(T_o-T_L)^{0.20837} \qquad \text{(IV-26)}$$

or the heat transfer coefficient is

$$h = 7572.621(T_o-T_L)^{-0.79163} \qquad \text{(IV-27)}$$

where T_o and T_L are the temperatures of the soil surface and LNG respectively. A plot of Equation IV-26 is shown in Figure IV-6. The soil properties of Model I-6 are all identical to those used in Model I-4 and Model I-5. The only difference among these models is the heat transfer coefficient; it is infinite in Model I-4, finite and constant during the entire boiling period in Model I-5, and surface-temperature-difference dependent in Model I-6. The method developed in Chapter III is applied to solve Model I-6 which includes the nonlinear boundary condition, phase change, and temperature dependent soil properties.

To explore the effect of boiling heat transfer coefficient on the boil-off rate of LNG, the calculated results of Models I-4, I-5 and I-6 are compared with each other in Figure IV-7. As expected, the results of these models are quite different in the short time range, i.e., less than 1000 seconds. Beyond 8000 seconds, the three curves plotted in Figure IV-7 are combined, since the soil properties for these three models are the same. There is an indication that the heat transfer mechanism is heat-conduction controlled beyond that point. To consider this fact, the developed computer program as shown in Appendix C is able to deal with both convective and prescribed-temperature boundary conditions. It can be applied not only when the system is convective-heat-transfer controlled but also is heat-conduction controlled.

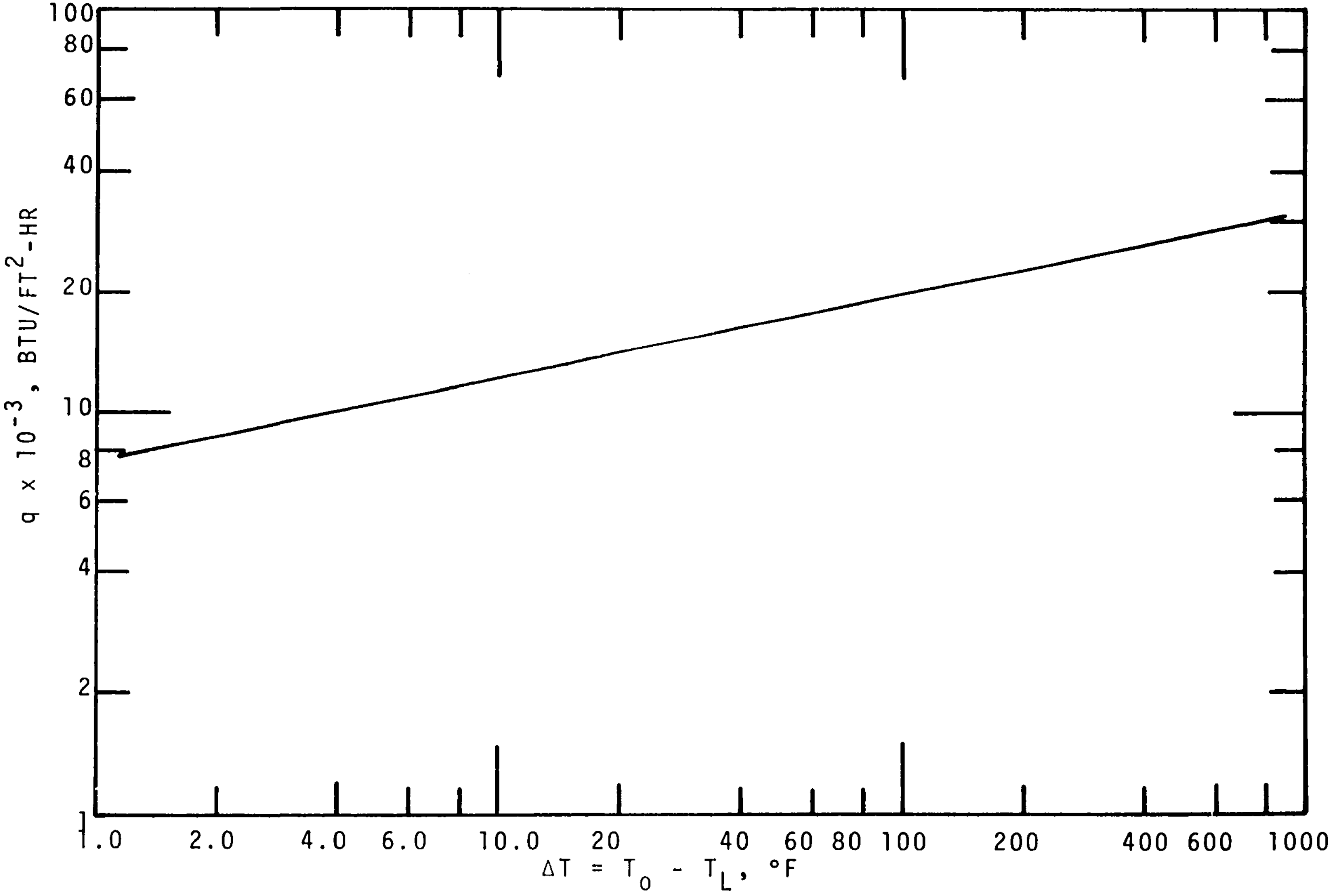

Figure IV-6. Heat Flux of Boiling LNG on Ground.

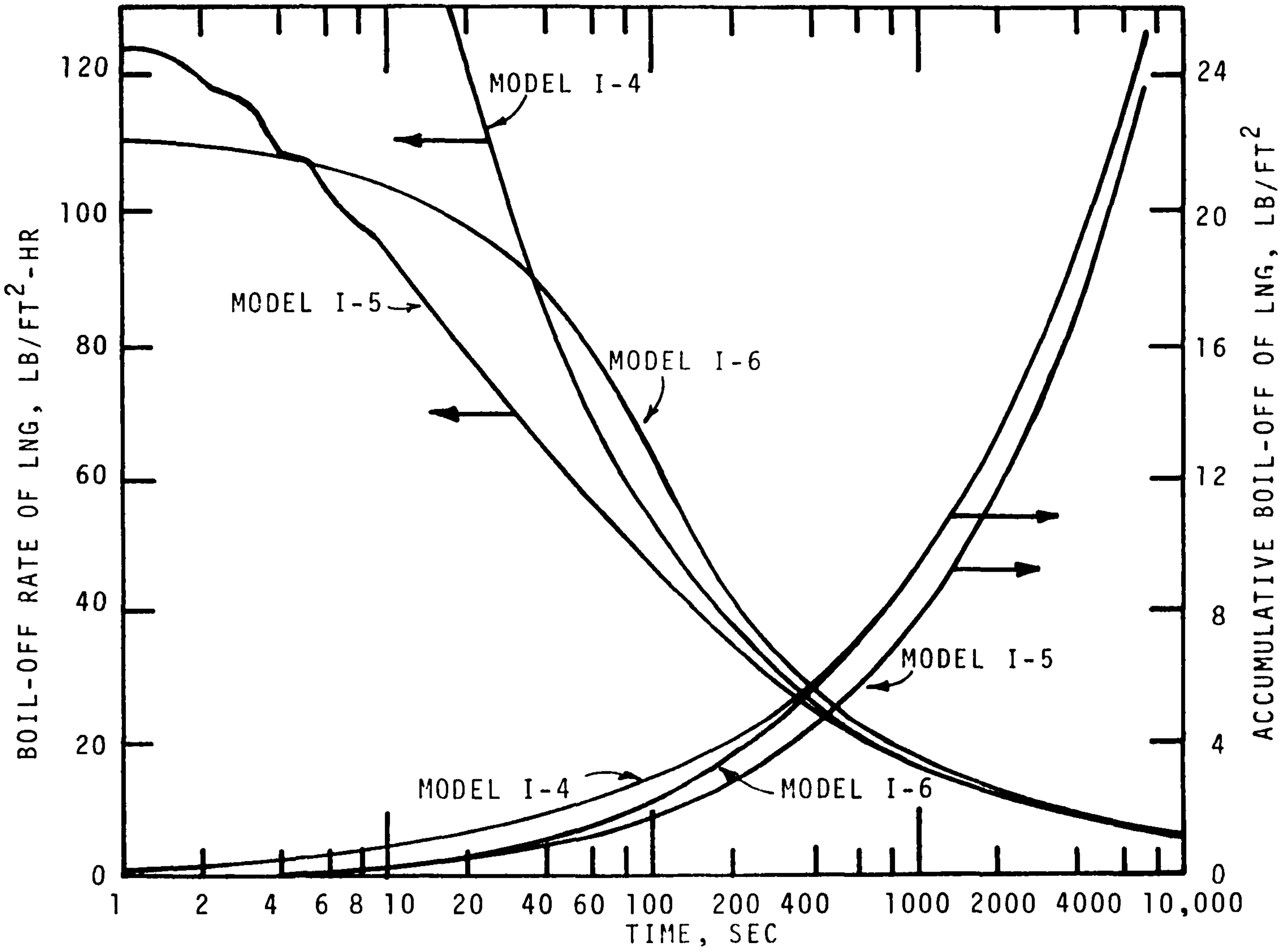

Figure IV-7. Effect of Boiling Heat Transfer Coefficient on LNG Boil-Off of Models I-4, I-5, and I-6.

Since there is no thermal resistance between LNG and the surface of soil in Model I-4, the initial boil-off rate for this model is about 30 times higher than those for Model I-5 and Model I-6. However, it drops to 2 times higher after 6 seconds. As seen in Figure IV-7, the difference in boil-off rate for Model I-4 and Model I-5 decreases with time. For example, Model I-4 has only a 20 percent higher boil-off rate after one minute. The boil-off rates are the same for time greater than about 8000 seconds. Although the boil-off rates for Model I-4 are greater than those for Model I-6 within 0.5 minutes, Model I-6 has higher boil-off rates after 35 seconds. The average discrepancy is about 10 percent.

There is no noticeable difference in the total boil-off between Model I-5 and Model I-6 within 10 seconds. For times longer than 500 seconds, the accumulative boil-off of LNG for Model I-4 and Model I-6 are nearly the same. The total boil-off of LNG for Model I-4 exceeds that for Model I-5 by approximately 1.4 lb/ft^2.

It is reasonable to conclude that the boiling heat transfer is a very important factor for predicting precisely the boil-off rate of LNG spilled on land for all time ranges. The constant boiling coefficient, both infinite and finite, would overestimate or underestimate the boil-off rate at various time ranges beyond the initiation of an LNG spill.

Dike Wall Effect

When the dike wall effect is considered, solution of the LNG/soil heat transfer problem requires a two-dimensional model. Therefore, the simplified one-dimensional model has its limitation in practical application. Due to the geometrical and mathematical complexities, the calculation of a two-dimensional case is much more complicated than that of a one-dimensional case. The proposed numerical method for a two-dimensional heat conduction problem with phase change has been fully discussed in Chapter III. One of the applications of the numerical method is to obtain the boil-off rate of a two-dimensional LNG in-ground storage tank or an LNG spill in an impounding basin as a function of time and the temperature distributions of the surrounding media. Figure IV-8 shows the cross section of the cavity used for the present study. The diameter of the cavity is a; the depth-to-diameter ratio of the cavity is b/a. For calculational purposes, it is a two-dimensional semi-infinite slab. The system can be divided into two symmetrical sub-regions; for convenience in calculation, only one sub-region is considered. Hence, the boundary condition on the central line, y-axis, is a perfect insulation type.

The initial temperature distribution of the surrounding media is uniform and is at 60°F; the air-ground interface is kept at 70°F for the entire period. The depth-to-diameter ratios are 0.05 and 0.5 for Models II-1 and II-2, respectively. The diameter of the storage is 5 ft. The surrounding medium is the

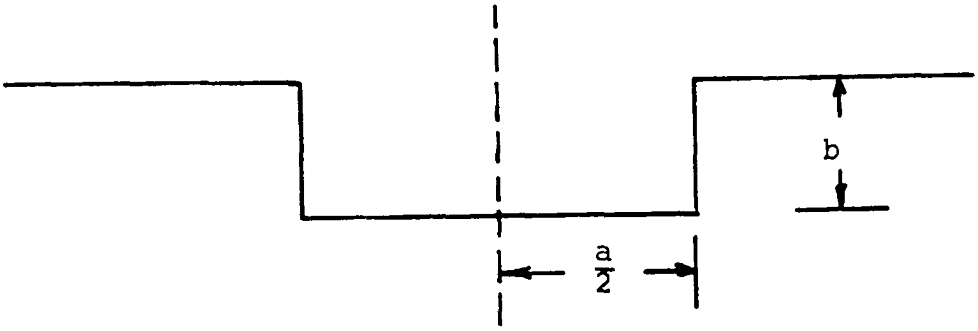

Figure IV-8. Cross Section of Two-Dimensional Model.

soil, and the thermal properties of the soil are listed in Table IV-5. It is assumed that there is no thermal resistance at the exposed boundary of LNG and the soil for Models II-1 and II-2. The temperature of the LNG pool is kept at its boiling point, -260°F.

To solve the two-dimensional problem, first replace the plane region by a network of mesh points and then follow the calculation procedure described in Chapter III. The locations of mesh points and the devised computer program are covered in Appendix C. The positions of the front of frozen soil may be taken to be those of the 30°F isotherm which corresponds to a 50 percent release of the latent heat of transition. Figures IV-9 and IV-10 present the position of the 30°F isotherm for several time levels. It can be seen that the front of the frozen soil for the two-dimensional case is a surface instead of a point. The shape of this surface depends on the geometrical configuration and the boundary conditions. The curves in Figures IV-9 and IV-10 are typical examples of the distribution of isotherms in two-dimensional coordinates. An example of the temperature at a fixed point versus time is shown in

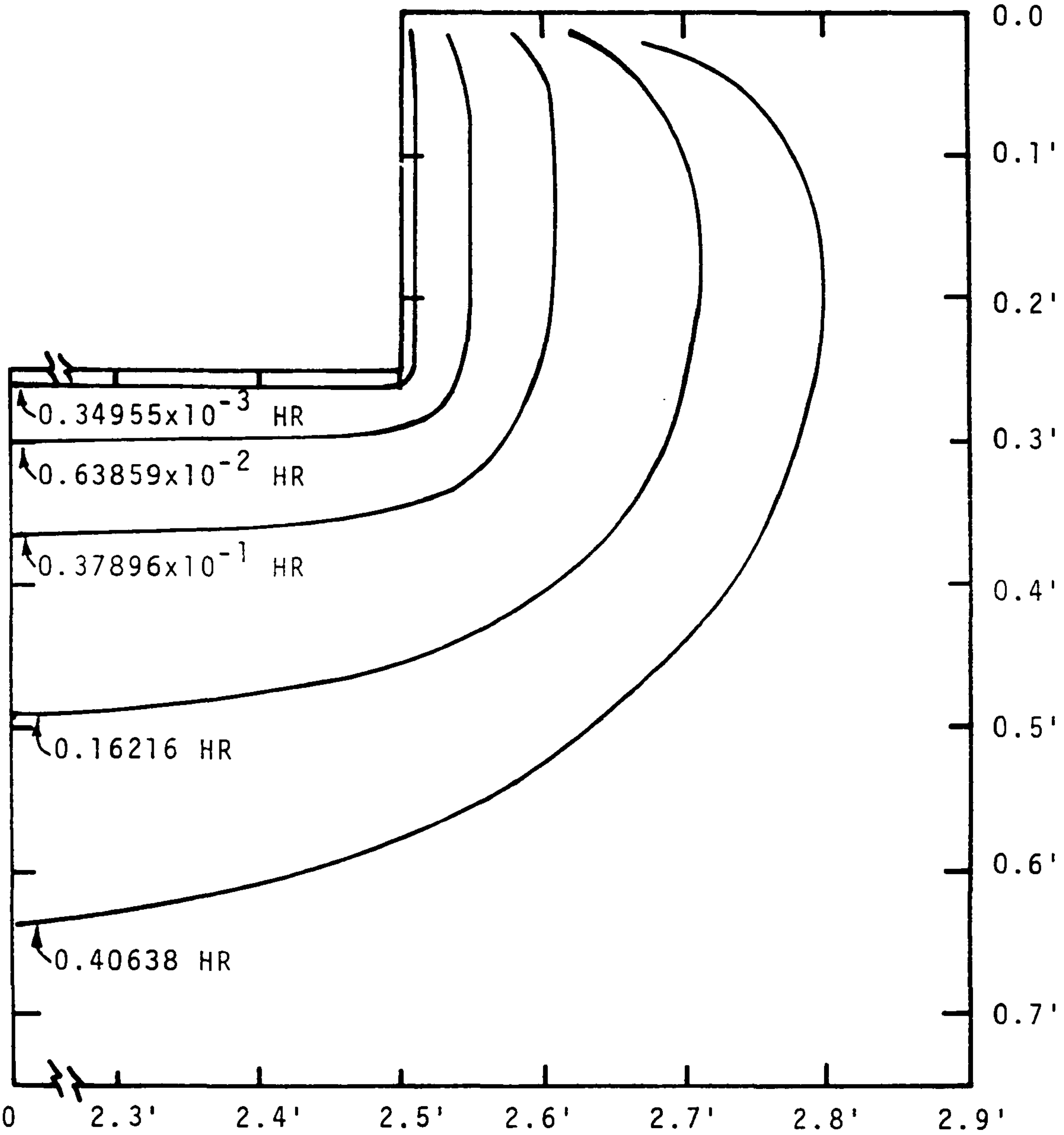

Figure IV-9. The Position of the 30°F Isotherm for Model II-1.

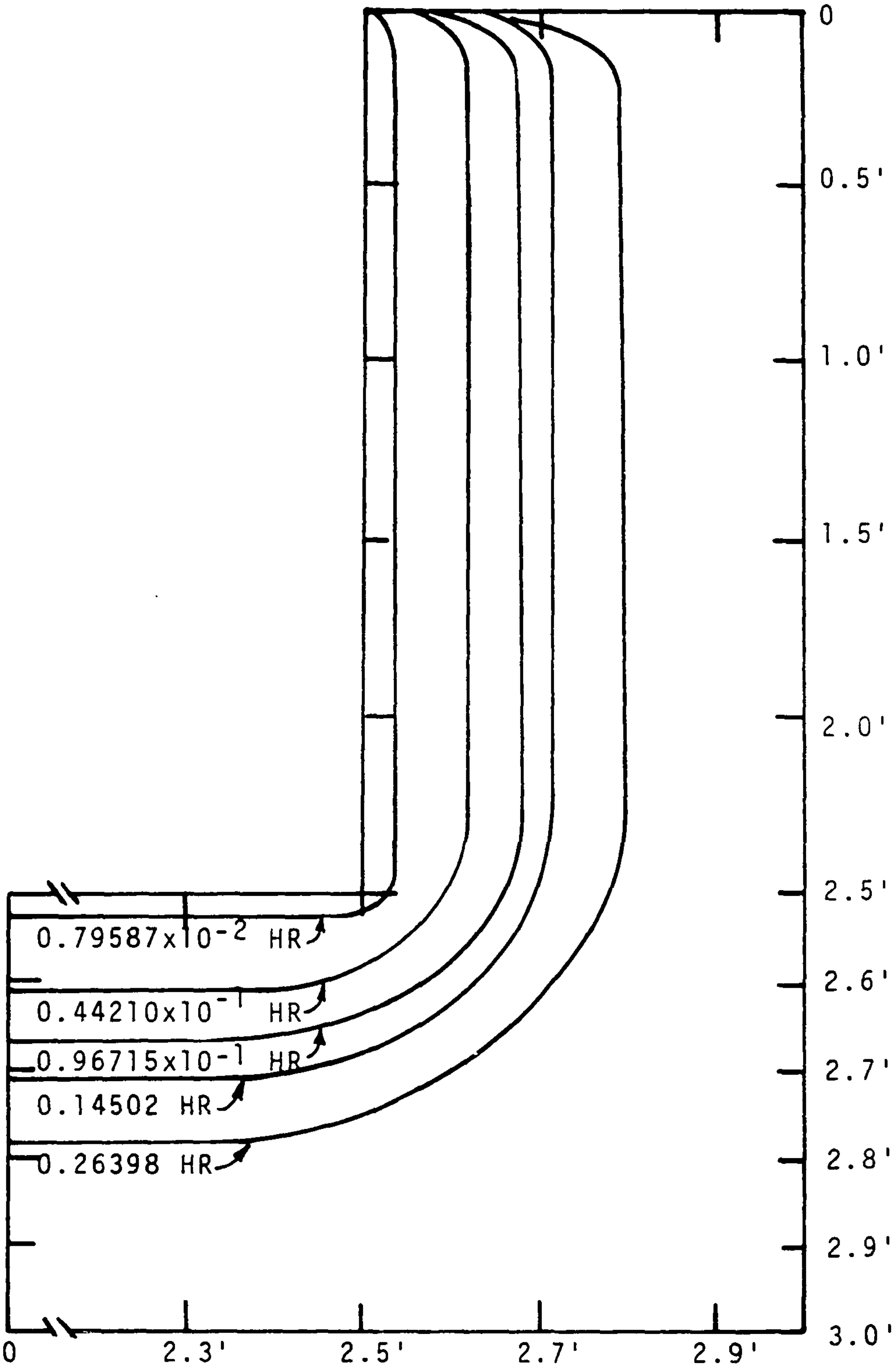

Figure IV-10. The Position of the 30° Isotherm for Model II-2.

Figure IV-20. The situations of Model II-1 and Model II-2 are the same except for a different boiling heat transfer coefficient at the exposed surface of LNG and the soil. The boiling coefficient of Model II-3 follows Equation IV-27.

Figure IV-11 gives the boil-off rates and accumulated evaporation of LNG as a function of time for Model II-1 and Model II-3. This figure shows the effect of the boiling heat transfer coefficient on the boil-off rate of LNG in two-dimensional cases. Figure IV-11 has the same characteristics as those in Figure IV-7. The boil-off rate ratio of Model II-1 and Model II-3 is about 20 at the beginning and drops to 2 after 6 seconds. The difference of boil-off rates predicted by Model II-1 and II-3 decreases with time. For time less than 36 seconds Model II-3 has lower boil-off rates, but it has higher boil-off rates beyond 36 seconds. Therefore, no difference exists between Model II-1 and Model II-3 when time is approximately 2000 seconds; after 2000 seconds, the heat-conduction controls the boil-off rate.

To observe the variation of the boil-off rate for one-dimensional cases under the same physical conditions, the results of Model I-4 and Model II-1 are plotted in Figure IV-12. Similarly, the comparison of Model I-6 and Model II-3 is presented in Figure IV-13. Both of these figures show the same characteristics. In examining the rate of boil-off in Figures IV-12 and IV-13, it is evident that two-dimensional cases have higher heat transfer rate per unit area.

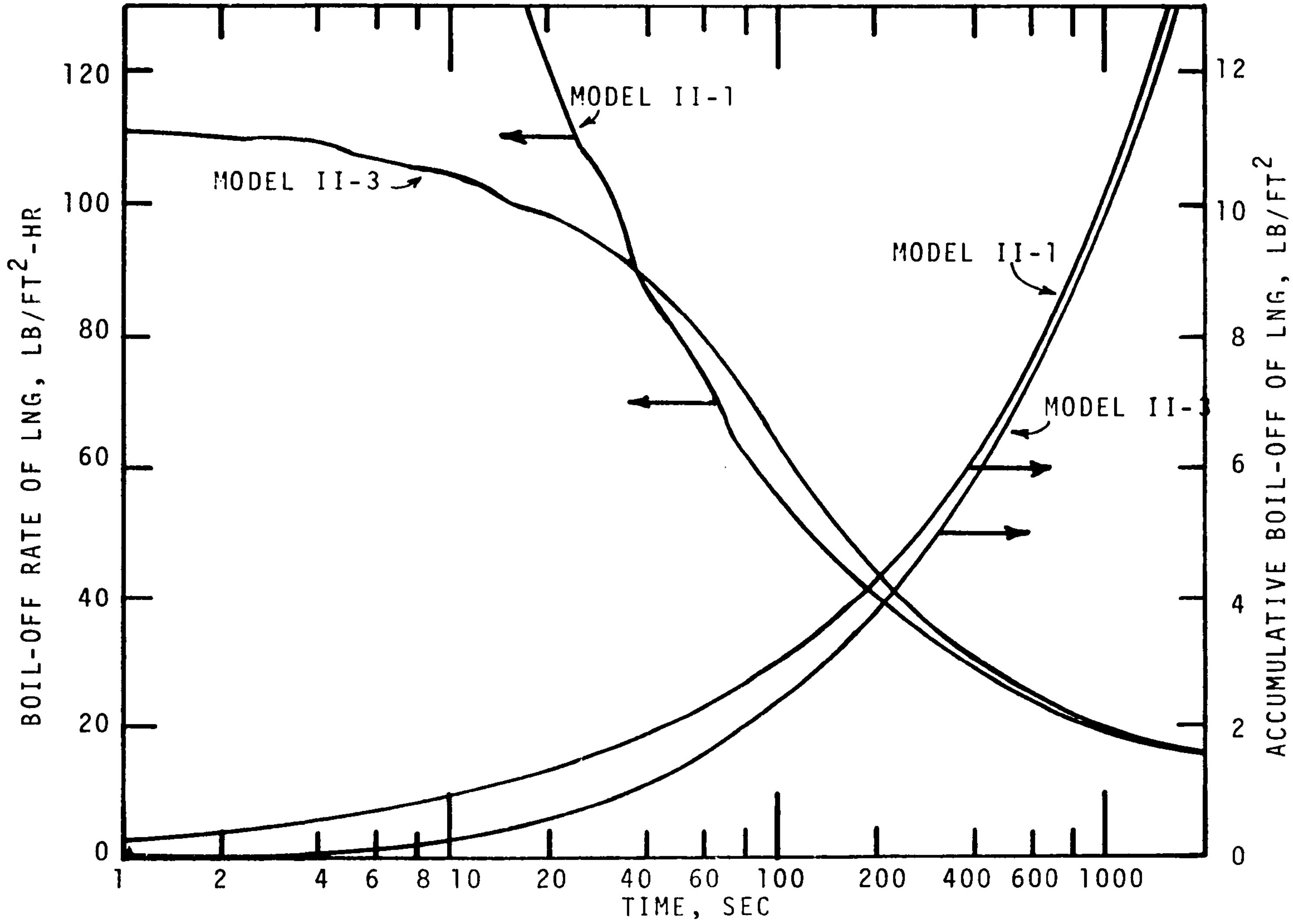

Figure IV-11. Effect of Boiling Heat Transfer Coefficient on LNG Boil-Off of Models II-1 and II-3.

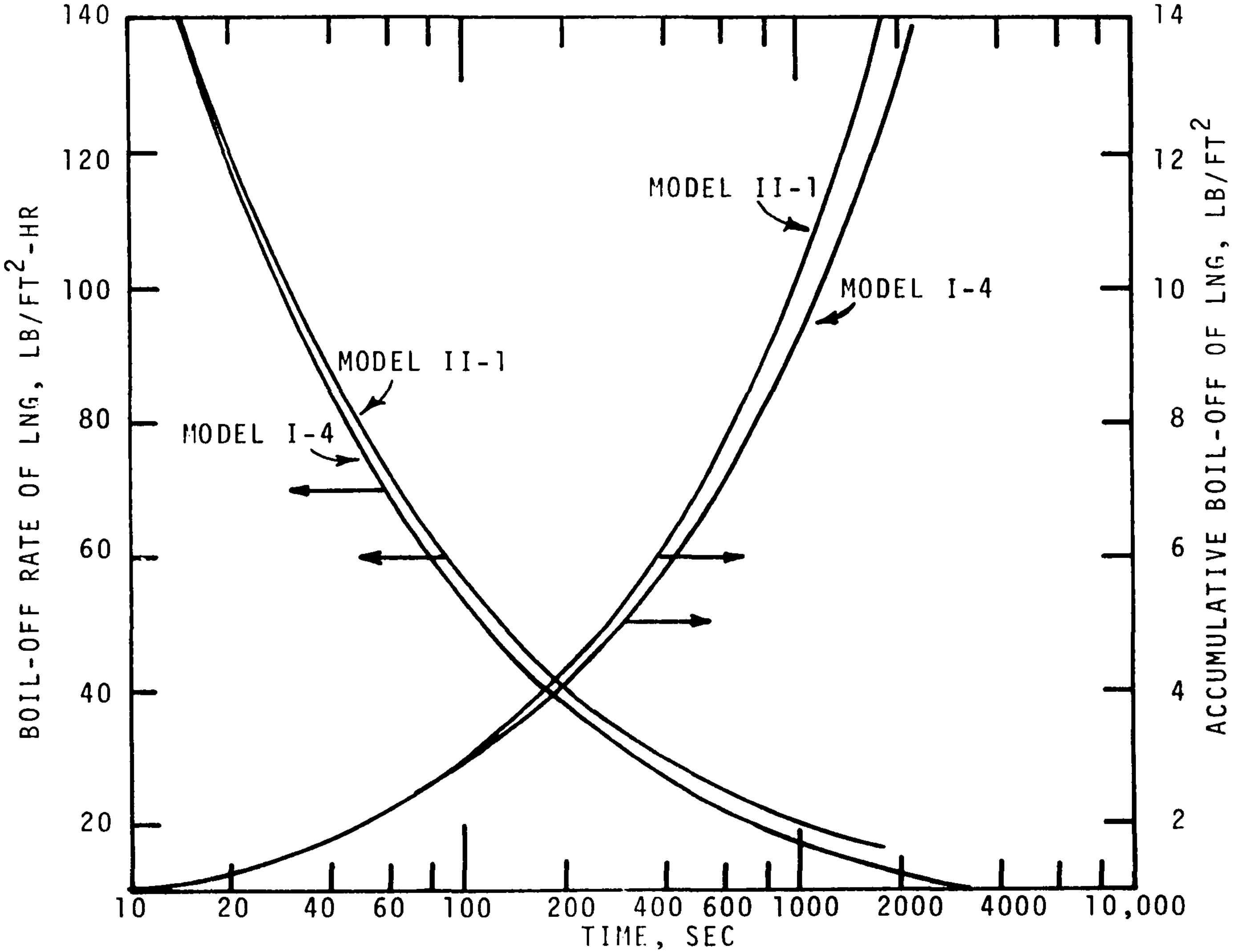

Figure IV-12. Effect of Dike Wall on LNG Boil-Off of Models I-4 and II-1.

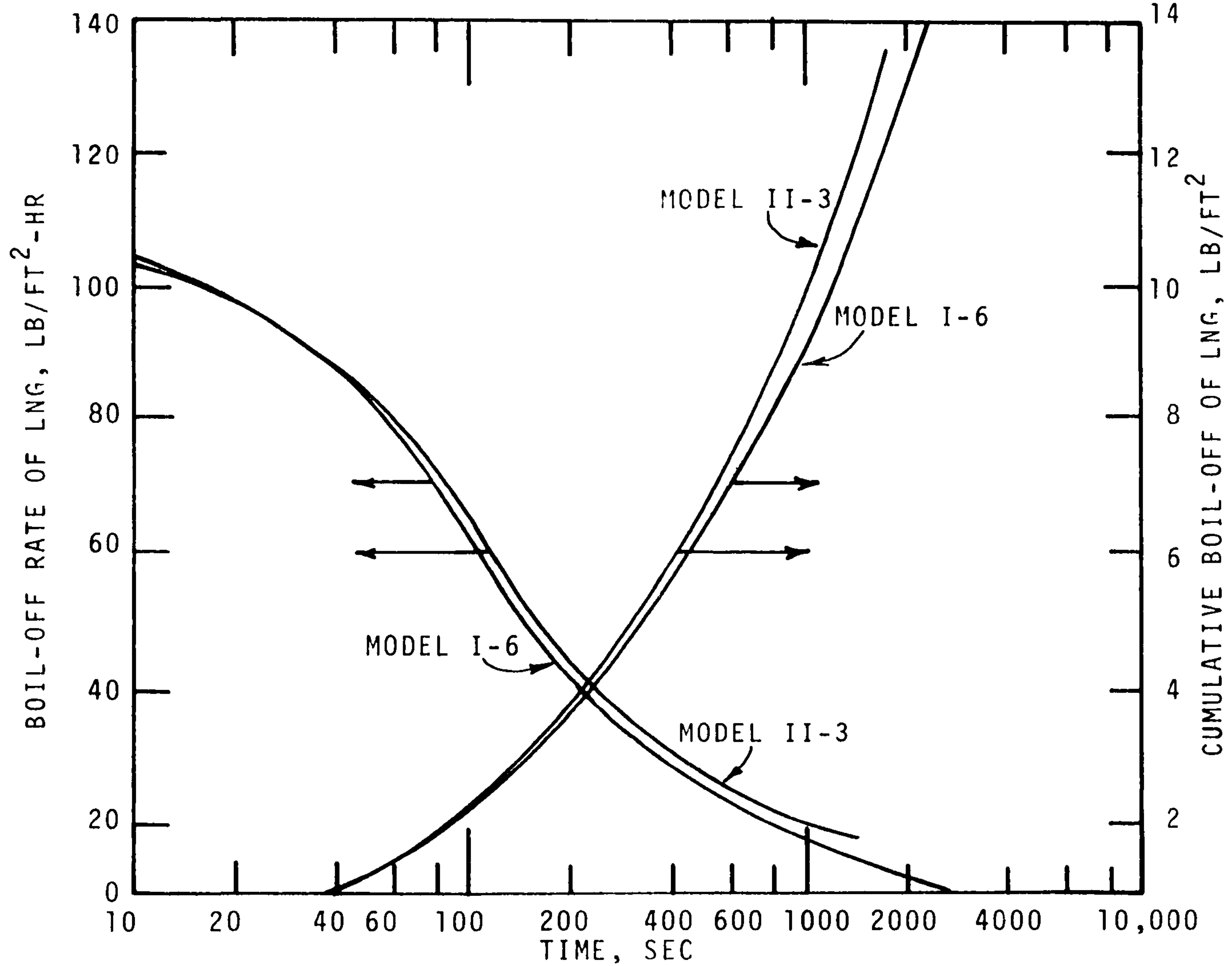

Figure IV-13. Effect of Dike Wall on LNG Boil-Off of Models I-6 and II-3.

For the range shown in Figure IV-12 and Figure IV-13, the two-dimensional cases have 1 to about 25 percent higher boil-off rates than the one-dimensional case. For the accumulative boil-off of LNG, the discrepancy between one-dimensional cases and two-dimensional cases increases with time. For instance, up to 2000 seconds, there is an 11 percent discrepancy. The corner effect and the ground-to-air heat transfer of the surroundings, as demonstrated in Figure IV-10, are responsible for the increased boil-off rate predicted by the two-dimensional model.

The boil-off rates for the two-dimensional models shown in Figures IV-11 through IV-13 are based on the average heat transfer rates of all exposed boundaries, including the dike wall. The two-directional compensation heat transfer in the vicinity of the exposed corner causes the heat transfer rate to be higher than would be predicted from a one-dimensional model. The interfacial heat transfer of air-ground also has an influence on the higher heat transfer rates.

Effect of Insulation

The transient temperature distribution and heat flux in the media composed of several layers are important in some heat transfer problems such as cryogenic thermal insulation (105), rocket thrust chamber lines, fuel elements for nuclear reactors, and reentry bodies. Carslaw and Jaeger (18) used the Laplace transformation method to solve multilayer heat transfer problems. However, the difficulty of the inversion transformation limits the application of the Laplace transformation to this type of problem. Another method which does not have the difficulty of inversion was introduced by Tittle (107) in 1965. He used the method of variable separation and employed a technique for orthogonal expansion of functions over the one-dimensional composite region. This method was also used by Bulavin and Kascheev (15) in 1965 to solve the transient heat conduction problem with heat generation in a multilayer system for plates, cylinders, and spheres. The analysis of heat conduction problems in composite media has been reviewed by Ozisik (73).

Recently, Mulholland and Cobble (71) treated the problems of multilayer media with convective boundary conditions at the external boundaries and with temperature continuities or discontinuities at the interfacial boundaries. A unique dependent variable transformation was developed and used to obtain a new partial differential equation with homogeneous external boundary conditions. Then the quasi-orthogonality was employed to solve the new partial differential equation. For the two-dimensional case Lockwood and Mulholland (65) applied a Fourier integral transformation and a dependent variable substitution to obtain a new partial differential equation with homogeneous boundary conditions.

The problem of one-dimensional underground LNG storage thermally insulated from the dry soil by a thickness of insulation was first attacked by Churchill (19). Then Seider and

Churchill (94) presented a numerical method to investigate the temperature profile and the freezing boundary motion of the wet soil in contact with insulation. For these one-dimensional cases it was assumed that physical properties were uniform and constant. The two-dimensional heat conduction in a composite medium with phase change was studied by Hashemi and Sliepcevich (44). In 1971, Yansinsky (116) used the synthesis method to deal with the three-dimensional composite heat conduction problem.

For the present study of the insulation effect on the boil-off rate of LNG, the proposed procedure developed in Chapter III will be used. Polyurethane is used for the insulation material in the following study and its properties are listed in Table IV-7.

TABLE IV-7

PROPERTIES OF POLYURETHANE (81)

Density	7 lb/ft^3
Thermal Conductivity	1.9×10^{-2} Btu/hr-ft-°F
Specific Heat	0.147 Btu/lb-°F

The simplest model of LNG storage thermally insulated from the earth by a finite thickness of insulation is a one-dimensional semi-infinite slab with constant thermal properties and without phase change, i.e., Model I-7. The initial temperatures of both insulation ($-\delta<x<0$) and soil ($0<x<\infty$) are assumed to be at a uniform temperature, T_∞. No interfacial resistance exists between insulation and soil. The surface temperature at x = o is maintained at the boiling point of LNG, T_L. The analytical temperature distributions in the insulation, T_I, and in the soil, T_2, are described by the following equation (18).

$$\frac{T_I - T_\infty}{T_L - T_\infty} = \sum_{n=o}^{\infty} \beta^n \left\{ \operatorname{erfc}\frac{(2n+1)\ \delta + x}{2\sqrt{\alpha_I t}} - \beta \operatorname{erfc}\frac{(2n+1)\ \delta - x}{2\sqrt{\alpha_I t}} \right\} \tag{IV-28}$$

and

$$\frac{T_s - T_\infty}{T_L - T_\infty} = \frac{2}{1+a} \sum_{n=o}^{\infty} \beta^n \operatorname{erfc}\frac{(2n+1)\ \delta + \kappa x}{2\sqrt{\alpha_I t}} \tag{IV-29}$$

where

$$\kappa = \frac{\alpha_I}{\alpha} \tag{IV-30}$$

$$\sigma = \frac{k_S\ \kappa}{k_I} \tag{IV-31}$$

$$\beta = \frac{\sigma - 1}{\sigma + 1} \tag{IV-32}$$

The heat transfer rate, $\bar{q}$, is

$$\bar{q} = - \frac{k_I}{\sqrt{\pi \alpha_I t}} \left\{ 1 + 2 \sum_{n=1}^{\infty} \beta^n e^{-n^2\ \delta^2/\alpha_I t} \right\} \tag{IV-33}$$

The boil-off rates of LNG of Model I-7 for several insulation thicknesses are plotted in Figure IV-14. The following soil properties are used in the calculation:

$$k_S = 2.1 \text{ Btu/hr-ft-°F}$$

$$c_S = 34.5 \text{ Btu/ft}^3\text{-°F}$$

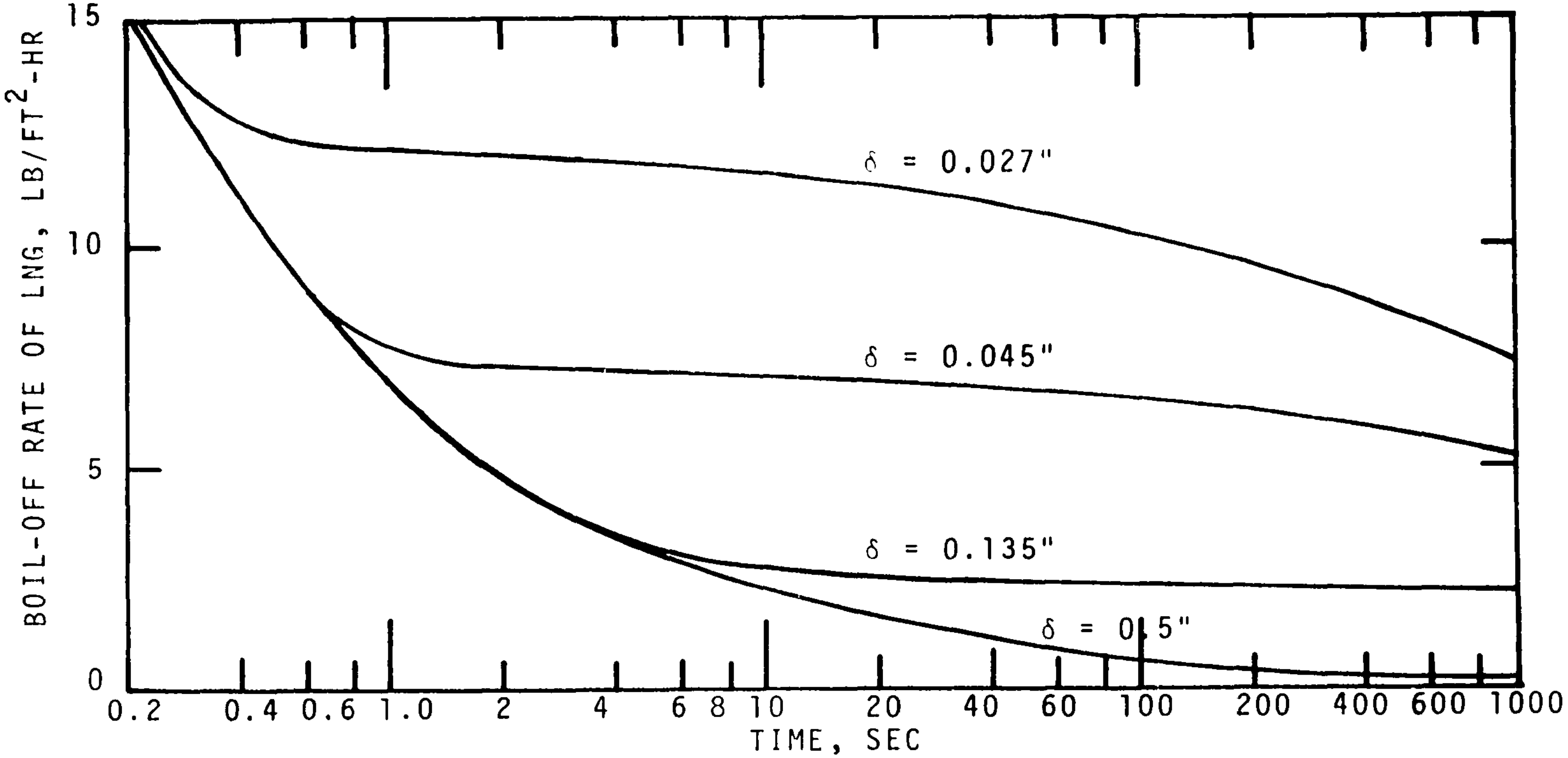

Figure IV-14. Effects of Thickness of Insulation on LNG Boil-Off of Model I-7.

Griffith and Horton (36) used the Laplace transformation technique to solve the transient heat flow in a nonhomogeneous two-layer medium with constant heat flux into the surface. A complete analytic solution for the Griffith and Horton problem with constant heat transfer coefficient on the surface, i.e., Model I-8, does not appear to have been developed. The analytical methods for solving Model I-8 are discussed in Appendix B. The soil properties of Model I-9 and Model I-10 are temperature-dependent as shown in Table IV-5. There is no thermal resistance between insulation and LNG for Model I-9, while the heat transfer coefficient on the surface of Model I-10 follows Equation IV-27. The numerical solution method used for these two models is the proposed procedure described in Chapter III.

Figure IV-15 presents the boil-off rates and the accumulated evaporation of LNG for Model I-10 with the thickness of polyurethane as parameters. As shown in this figure, 1.5∿2.0 inches of polyurethane can reduce the boil-off of LNG significantly. The comparison of Models I-9 and I-10 is shown in Figure IV-16. Notice that the surface temperature of insulation drops to the boiling point of LNG after 0.6 seconds. But it takes 8000 seconds approximately for wet soil as shown in Figure IV-7. Also, the heat transfer coefficient has a great influence on the transfer rate when the time is less than 0.1 sec. The characteristic of these results is that the heat transfer rates of Model I-9 with infinite heat transfer coefficient are

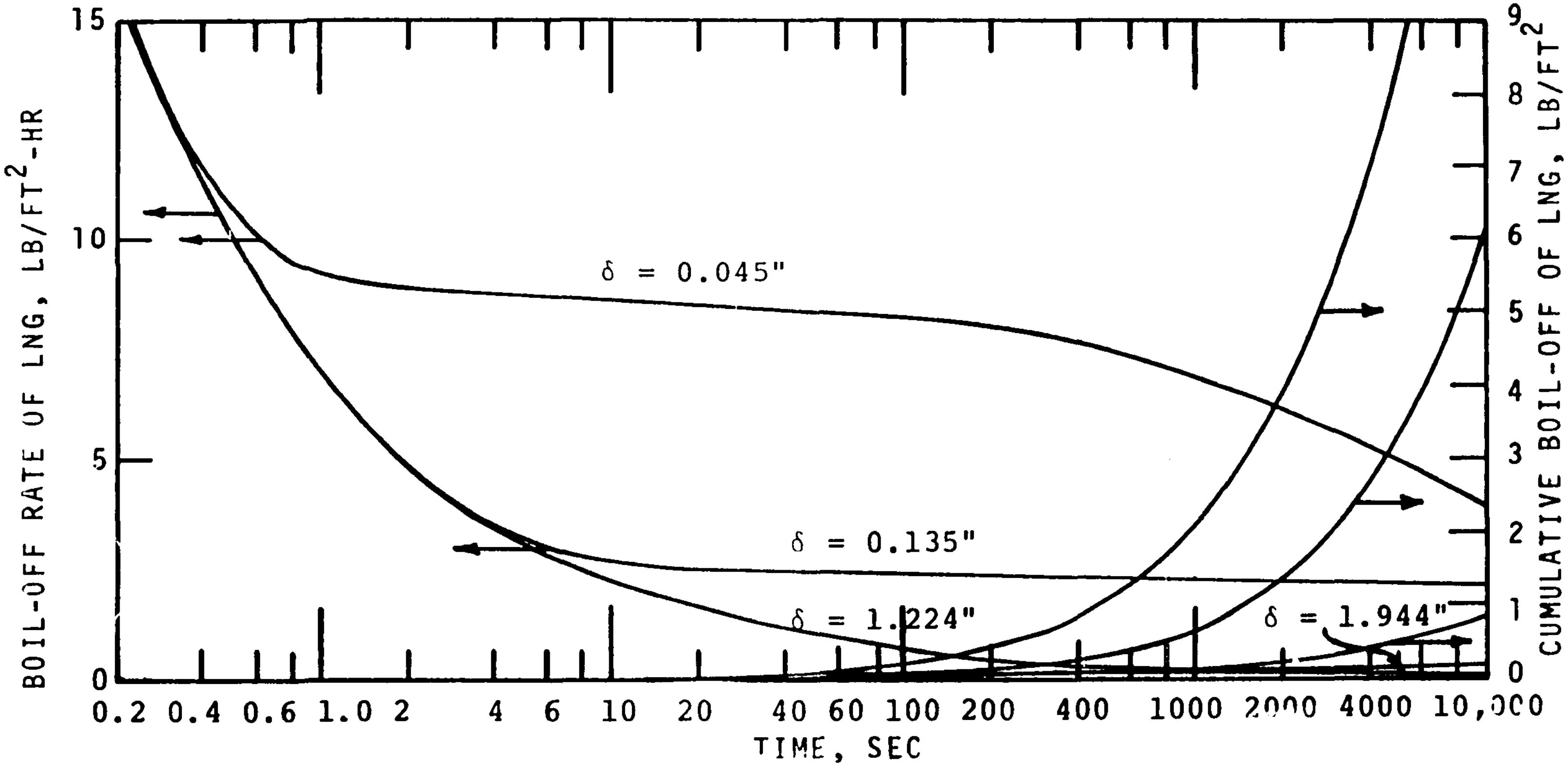

Figure IV-15. Effects of Thickness of Insulation on LNG Boil-Off of Model I-10.

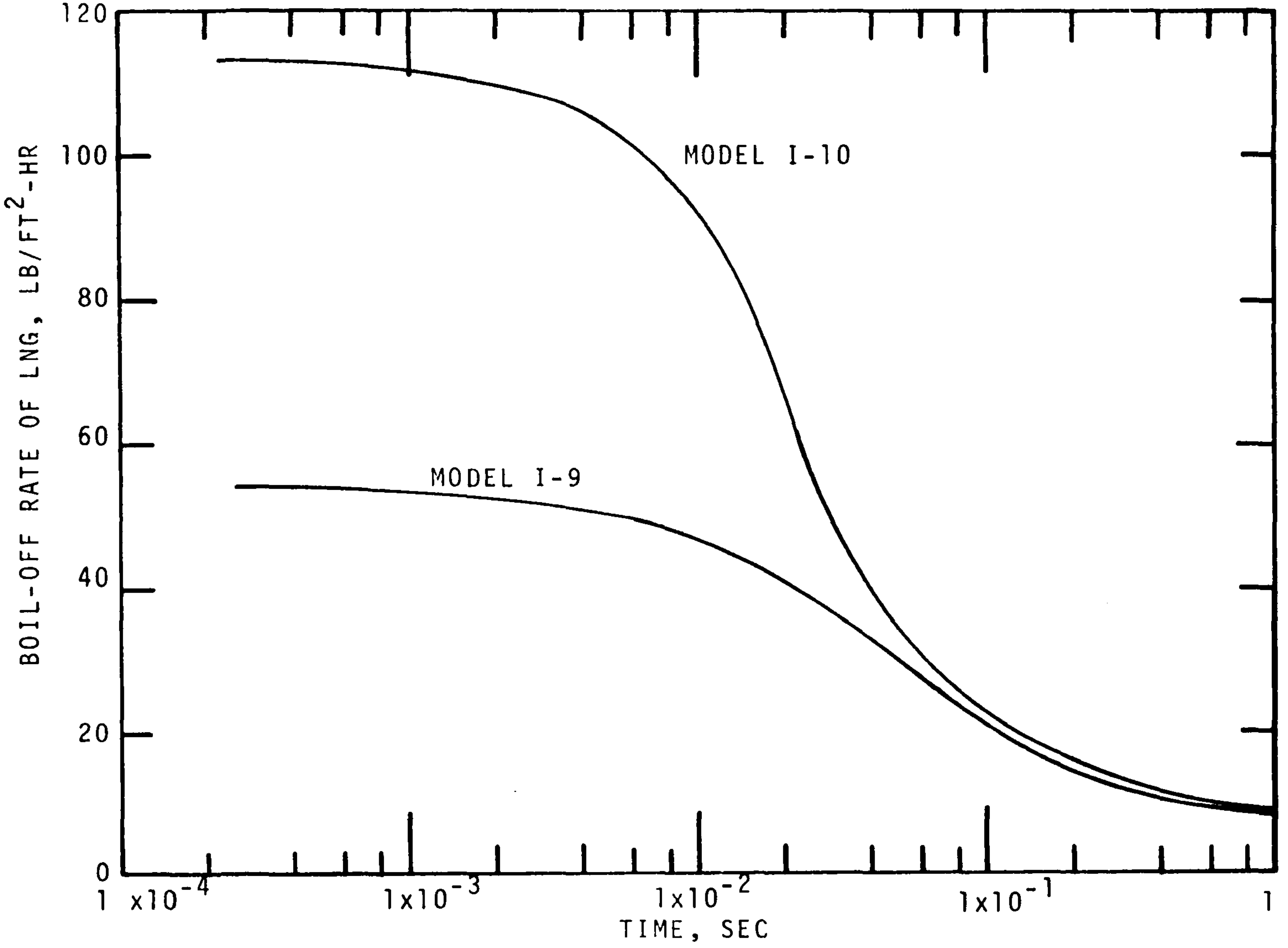

Figure IV-16. Effect of Heat Transfer Coefficient on LNG Boil-Off of Models I-9 and I-10 with 0.045 in Polyurethane Insulation.

lower than those of Model I-10 with thermal resistance initially, because the low thermal conductivity of the insulation causes this system to act in an opposite manner to the models without insulation. It is necessary to compare Model I-7 with Model I-10 to obtain the effect of soil properties on the boil-off rate. One of these comparisons is shown in Figure IV-17 where the thickness of insulation is 0.045 inch. For the initial period up to 0.5 seconds the boil-off rate is heat transfer coefficient controlled and then it switches to a soil properties controlled system. As shown previously in Figure IV-2, the wet soil makes the heat transfer rate higher than the heat transfer rate from dry soil. It can be concluded that the thermal properties of soil have no effect on the heat transfer rate when the polyurethane on the soil is about 1.2 inches thick or greater.

Other Effects

The surface irregularities and the permeability of the soil would increase the heat transfer area and heat flux. Because of this complexity, the true heat transfer area is difficult to predict exactly. When LNG spills on the ground, the high velocity vapor can carry some small liquid drops away from the spill. This effect of losing liquid is important initially, but it can be neglected as the evaporation rate decreases. The heat contribution from solar radiation is small compared with the heat flux from the soil. It is significant at a long time after spill initiation, as the boil-off reaches steady

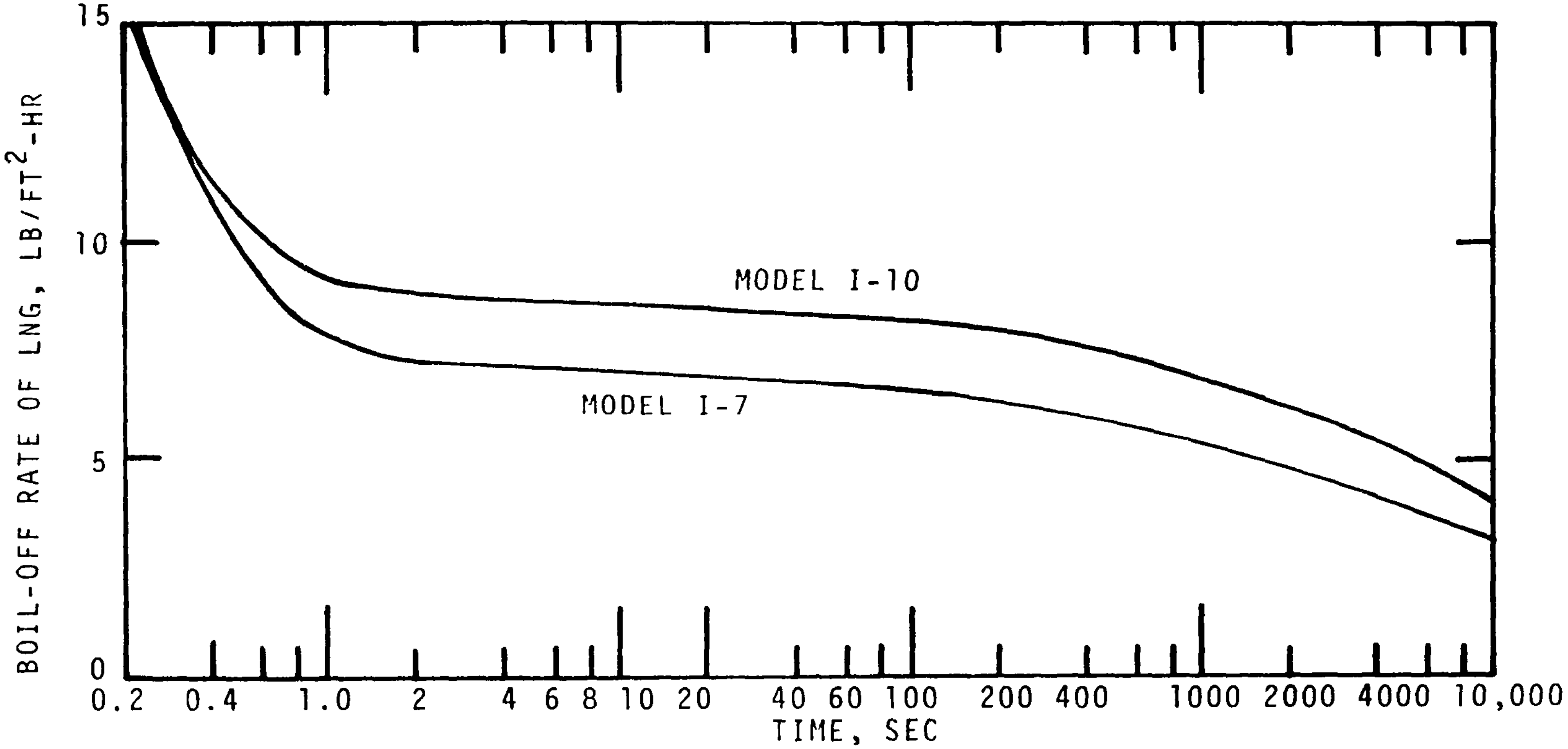

Figure IV-17. Effect of Soil Properties on the LNG Boil-Off of Models I-7 and I-10 with 0.045 in Polyurethane Insulation.

state. The forced convection heat transfer between LNG and the warmer air flowing over a LNG pool will also increase the steady state rate of evaporation. Both solar radiation and the forced convection between air and LNG will be important heat sources for the LNG pool with insulated walls. The contribution of solar radiation flux and the forced convective heat flux to the evaporation of LNG has been discussed by Drake, Harris, and Reid (24). They estimated that the solar heat flux was about 300 Btu/hr-ft^2 and the forced convective heat flux was slightly larger at about 450 Btu/hr-ft^2. The contributions of the solar radiation and the forced convective heat transfer are much less than the heat conduction flux from soil, but they become more significant as steady state approaches. The solar radiation or the forced convection might enhance the liquid regression rate about 0.01 inch/min. For some special cases the effects of snow, rain, or pools of water may be important.

The effect of flow of ground water in the soil on the temperature distribution of frozen and unfrozen soil has been discussed by Hashemi and Sliepcevich (46). Gupta and Churchill (39) have investigated extensively the moisture migration in the wet sand during the freezing. However, the influences of these two factors--bulk flow and moisture migration on the boil-off rate of LNG spilled on ground have not been included in the present study. Hashemi and Sliepcevich (46) have shown that moisture migration is inherent in the measured values of soil thermal conductivity. Ground water flow is more important in inground storage problems than in cryogenic spill problems.

Discussion of the Numerical Method

One way to investigate the accuracy of a proposed numerical method is to compare the numerical result with the exact solution. Model I-3 has an exact solution, i.e., Equations IV-18 and IV-19. Figure IV-18 is a plot of some of the numerical and exact solutions. The solid line in this figure is the numerical solution. The dotted line is the exact solution. The departure of the solid line from the analytic solution increases at the phase change region. It is essentially due to the assumption that the phase change occurs over a finite temperature interval for the numerical solution. However, the phase change is at a fixed temperature for the exact solution. The size of phase change interval not only is an important factor for obtaining accurate results but also has the influence on the stability of numerical method. The latent heat causes the internal energy to have a steep change over the small phase change interval and the slope of internal energy at this interval has a great change. Because of this phenomenon, the proposed iterative method requires a small time increment during the phase change occurrence. Otherwise, it is unstable and produces unrealistic results, for example negative dimensionless temperatures. It should have procedures to make the time interval smaller in the computer program when unrealistic results occur. The size of the time increment, the number of mesh

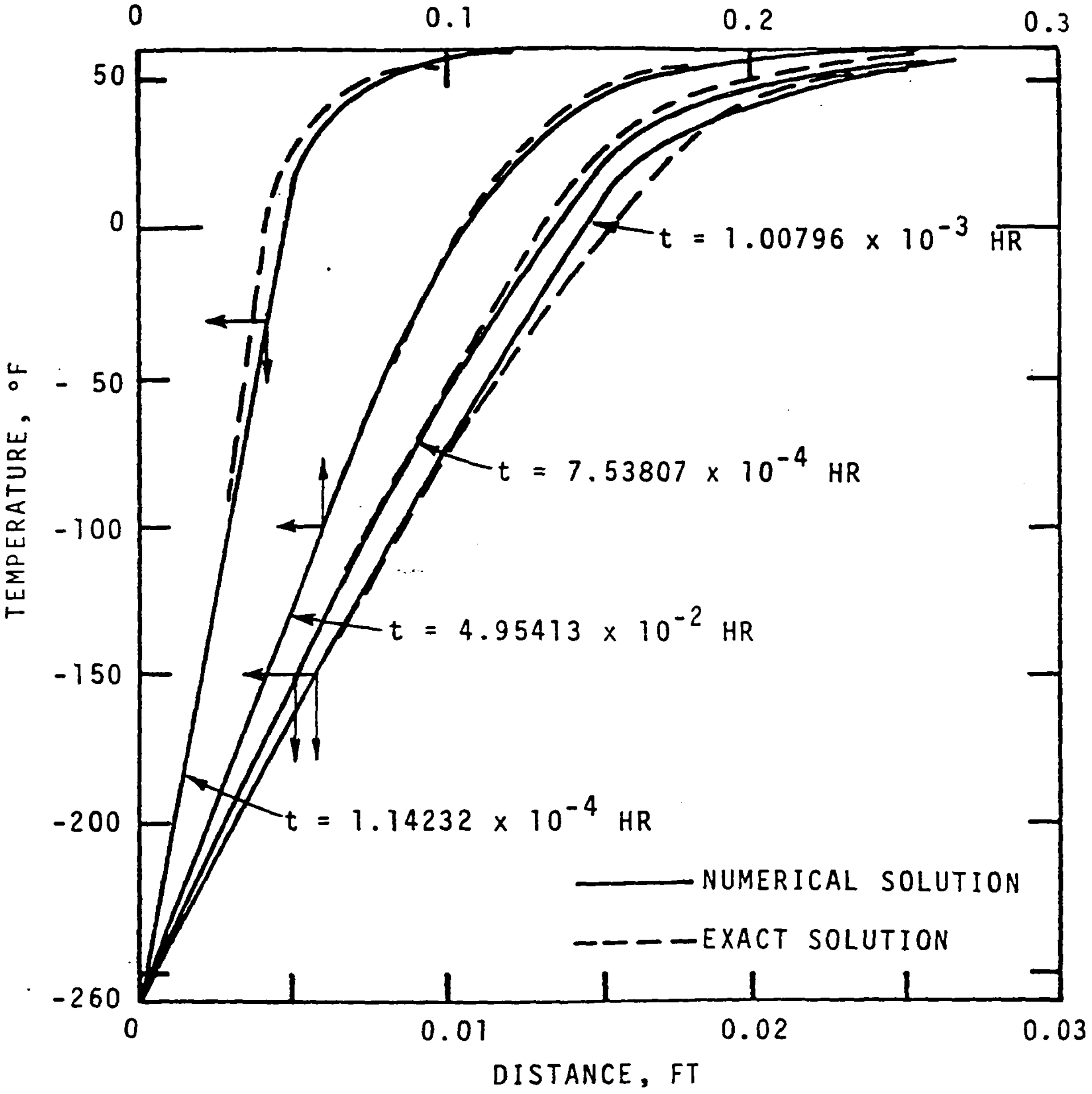

Figure IV-18. Comparison of Numerical and Exact Solutions of Model I-1.

points and variable mesh spacing are indeed important in solving the heat conduction problem in a semi-infinite region. Unequal mesh spacings are usually chosen. The smaller mesh regions are needed only near the surfaces of the LNG and soil and the interfaces of composite media. The time increment is larger when time increases without any sacrifice in the accuracy of the solution. Because the heat transfer rate and temperature change decrease as time increases, the number of mesh points depends on the temperatures of meshes far from the surface.

To confirm the proposed numerical procedure and the devised computer program capable of solving two-dimensional cases and to obtain an idea of the accuracy of two-dimensional systems, the devised program for two-dimensional cases are employed to solve a one-dimensional case first. The test problem is shown in Figure IV-19. It was perfect insulation on two sides, and because the temperature is symmetric to the y axis, it is essentially a one-dimensional case.

In Chapter III, the function form of internal energy rather than the specific heat was introduced for the rate of change of accumulative energy term in the region of interest. Use of the internal energy can substantially improve the accuracy and efficiency of the numerical solution. As can be seen from Figure IV-20, there are variations in the temperature distributions for Model II-1 by using specific heat (dotted line) and internal energy (solid line) for the accumulative energy term.

The temperatures are those of the second mesh point on the control line of a two-dimensional LNG pool as shown in Figure IV-20. Due to the latent heat of phase change, the temperature changes are slowed down in some regions.

From the above tests, the convergence rate is dependent upon the time increment and is independent of the accelerating parameter. Due to the variable time increment in the calculation, the convergent solution is obtained in two to nine iterations with an accuracy to 1×10^{-3} in dimensionless temperature.

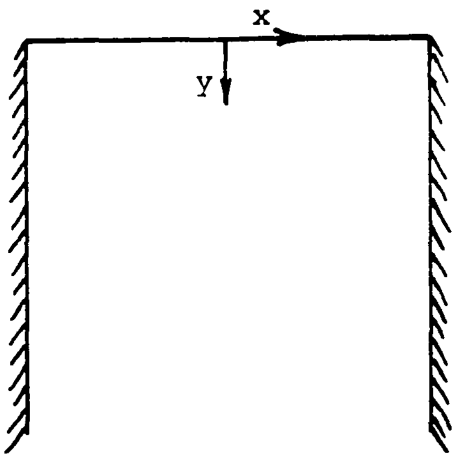

Figure IV-19. A Semi-Infinite Slab with Perfect Insulation on Two Sides.

Comparison of LNG Spill Tests and Theoretical Models

Some experimental data and theoretical predictions of LNG regression rates as a function of time are plotted in Figure IV-21. Humbert-Basset and Montet (49) reported the evaporation rate of LNG from several tests on both wet and dry soil under two different initial temperatures. The evaporation

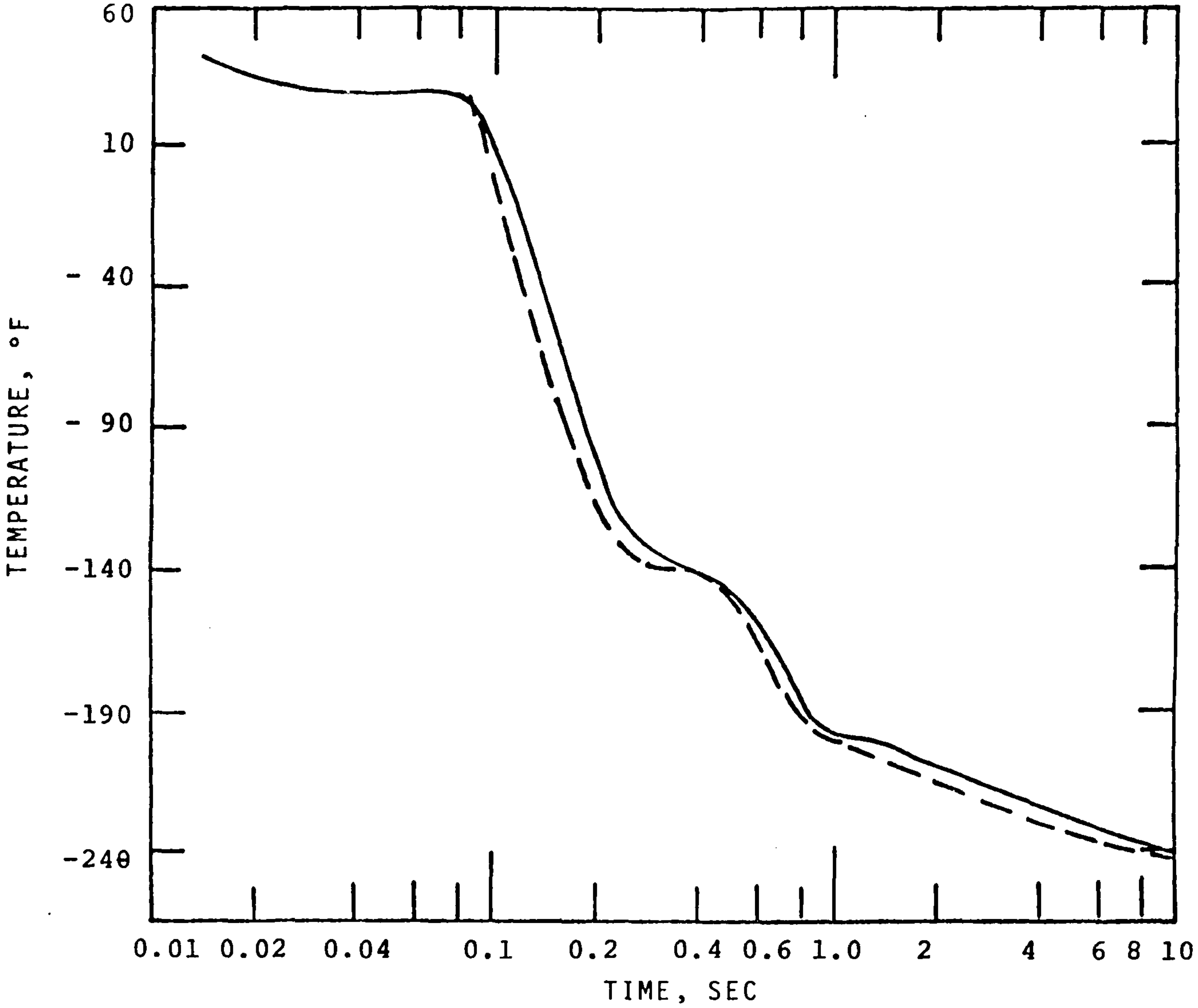

Figure IV-20. Comparison of Temperature Distribution for Model II-1 by Using Specific Heat (Dashed Line) and Internal Energy (Solid Line) for the Accumulative Energy Term.

rates of interest were at the short times. However, there were no thermal properties of soil or other properties reported in their paper. Figure IV-21 also shows some of evaporation rates of LNG carried out by TRW (114) on dry clays. The dotted line of Figure IV-21 represents the AGA-San Clemente data reported recently by Drake, Harris and Reid (24). They proposed a conduction model and added a correction term to the proposed model to match the experimental data. This semiempirical model is not applicable to the general cases. For comparative purposes the calculated results of the models of Parker (75) and Welker (111) are also presented in Figure IV-21. The applications of their models to predict the vaporization of spilled LNG suffer from their limiting assumptions.

As seen in Figure IV-21, the predicted LNG regression rate from Model I-4 at short times are in very close agreement with the AGA-San Clemente data, while, at long times, they do not match very well. The discrepancy results from the different soil properties. As mentioned earlier, the boiling heat transfer coefficient dominates the heat transfer rate between the soil and LNG at the initial time period. The boiling coefficient of Model I-4 follows the experimental data extremely well. Hence, the results are in accord with the AGA-San Clemente data at short times. At longer times after the spill, the boil-off rate is soil-properties controlled. Thus different soil properties result in different regression rates.

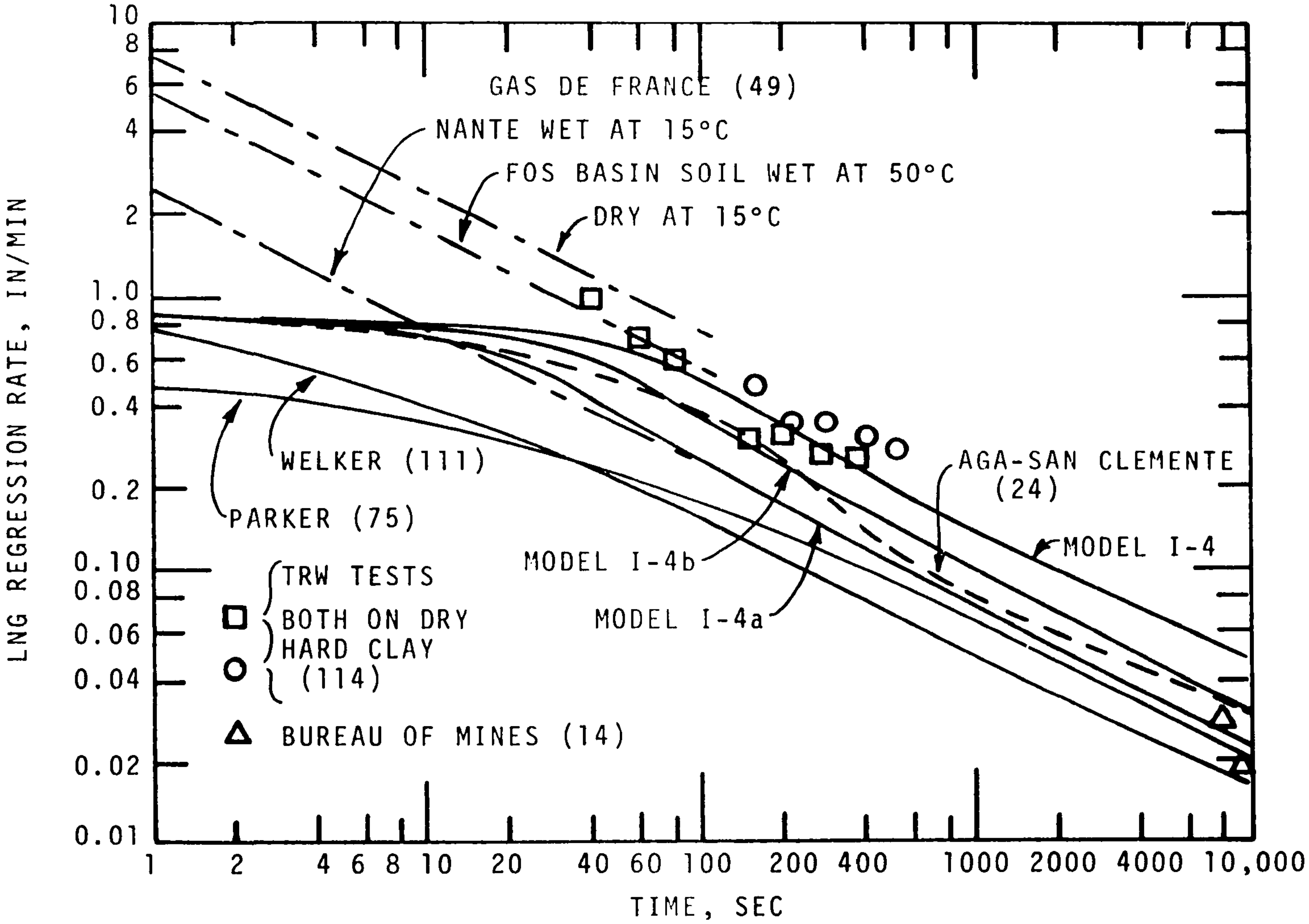

Figure IV-21. Comparison of LNG Spill Tests and Theoretical Models.

There are two modified models of Model I-4: Model I-4-a and Model I-4-b. The physical conditions are all the same with the exception that the soil properties for Model I-4-a are those chosen by Drake, Harris and Reid (24), i.e., k = 0.83 Btu/hr-ft-°F and c = 20 Btu/ft^3. The results of Model I-4-a do not agree well with the AGA - San Clemente data at long times either. There are two reasons for the discrepancies. First, the actual thermal properties of the soil are temperature dependent rather than constant, whereas, constant soil properties were chosen in Model I-4-a. Second, the contributions of the solar radiation flux and forced convection heat flux between air and LNG have been excluded from the prediction of evaporation rate, and the solar radiation and forced convection are important factors at the long-time period. Changing the soil properties of Model I-4-a to k = 1.6 Btu/hr-ft-°F and c = 29 Btu/ft^3 gives Model I-4-b. The LNG regression rates of Model I-4-b are in the middle of those of Model I-4 and Model I-4-a. Examination of these results reveals that more accurate soil properties are required in Model I-4 to obtain more precise regression rates as the LNG spill approaches steady state.

CHAPTER V

A MATHEMATICAL MODEL OF LNG PASSING THROUGH A HIGH EXPANSION FOAM

Recently, some investigations of high expansion foam to control Liquefied Natural Gas (LNG) spill fires have been published (112, 113). When the LNG vapor passes through the high expansion foam, the foam freezes quickly. The frozen foam is usually light enough to float on the LNG surface and strong enough to support the additional foam above it without collapsing into the LNG. The comparison of the efficiency of the same quality foams with different expansion ratios showed the 500:1 expansion ratio foam was the optimum one. The foam application rate on the LNG was an important factor to control the fire. The conditions of these investigations were under steady state evaporation rate of LNG.

A layer of foam applied on the surface of spilled LNG initially warms the upward flowing boil-off LNG vapor. If the temperature of warmed LNG vapor rises higher than about -170°F, the LNG vapor will be lighter than air at ambient temperature. Consequently, it will continue to rise and disperse vertically due to its buoyancy, rather than hugging the ground and traveling downwind near grade level. Therefore, in the event of an accidental release of LNG, high expansion foam can be used to reduce the potential hazard from flammable vapors traveling downwind. The duration of LNG hazard control from high expansion foam depends on the thickness of foam, vapor boil-off rate, foam expansion ratio and foam application rate. A mathematical model for analyzing the effect of depth of foam, vapor boil-off rate and foam application rate on the temperature change of boil-off LNG vapor as it exists from the top of the foam blanket is proposed in the following.

Given a layer of foam, z, initially at a uniform temperature, cold LNG vapors pass upward through the foam at a time-dependent flow rate. It is convenient to think that there are two continuous phases existing side by side for the layer of foam as shown in Figure V-1. The liquid foam is considered to be a stationary liquid phase. The boil-off vapor is a moving vapor phase. It is assumed that the rate of heat transfer from the liquid phase to the vapor phase at any point is proportional to the difference of temperature, that heat conduction can be neglected, and that no mass transfer resistance exists for vapor passing through foam. The model will be set up by the energy balance for two phases over a shell of thickness δz, the section between z and $z + \delta z$. The volume fraction of the high expansion foam occupied by the vapor is f. The cross-sectional area per unit length is S.

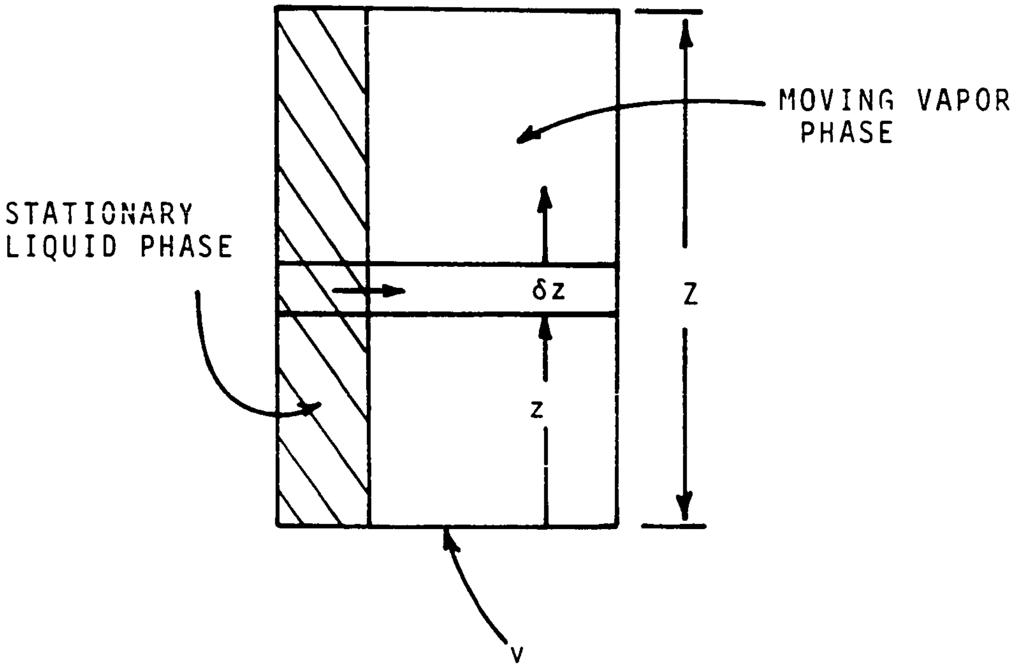

Figure V-1. Scheme Model of a High Expansion Foam on the Surface of Boiling LNG.

The heat balance equation for the liquid phase over a short time period, δt is

$$[\rho_f c_f + \frac{\varepsilon H}{\sqrt{\pi}} e^{-\varepsilon^2 (T_t - T_f)^2}] (1-f) S \delta z \frac{\partial T_f}{\partial t}$$

$$= -(h_f a) (T_f - T_g) S \delta z \qquad \text{(V-1)}$$

where the subscript f refers to the liquid phase, the subscript g refers to the vapor phase. The heat transfer coefficient between the liquid phase and vapor phase is $h_f a$ which is dependent on temperature and vapor flow rate. ρ is density, c is specific heat, and T represents temperature. It is also assumed that the phase change is over a finite temperature interval. This assumption has already been made in Chapter III for the moving boundary problem. During the phase change interval, the internal energy includes the sensible heat and the latent heat, H. The heat capacity of latent heat is assumed to be a normal distribution function over the finite temperature interval. The determination of ε has been discussed in Chapter III. These two terms are within the brackets on the left hand side of Equation V-1.

$$\rho_g c_g f \frac{\partial T_g}{\partial t} = v \frac{c_g T_g\big|_z - c_g T_g\big|_{z+\delta z}}{\delta z} + (h_f a)(T_f - T_g) \qquad \text{(V-2)}$$

where v is the vapor flow rate and is dependent on time. The thermal properties of the liquid phase and the vapor phase are also a function of temperature. Then, if δz and δt approach zero, Equations V-1 and V-2 become

$$[\delta_f c_f + \frac{\varepsilon H}{\sqrt{\pi}} e^{-\varepsilon^2 (T_r - T_f)^2}](1-f) \frac{\partial T_f}{\partial t} = -(h_f a)(T_f - T_g) \tag{V-3}$$

and

$$\rho_g c_g f \frac{\partial T_g}{\partial t} = v \frac{\partial c_g T_g}{\partial z} + (h_f a)(T_f - T_g) \tag{V-4}$$

As the previous discussion in Chapter III revealed, for obtaining consistent and accurate finite difference equation for two-dimensional heat transfer problems, Equations V-1 and V-2 are more reliable than Equations V-3 and V-4 from the physical point of view. Rosenbrock and Storey (84) presented an example that showed a nonsense solution would be obtained if Equations V-3 and V-4 were replaced by a finite difference approximation without consideration of the physical meaning of the dependent variables. Such difference equations should always be set up from a suitable discrete physical model.

Divide region, z, into N_z sections. Equations V-1 and V-2 can then be rearranged in the following form:

$$\frac{dT_{fi}}{dt} = \frac{-(h_f a)(T_{fi} - T_{gi})}{[\rho_{fi} c_{fi} + \frac{\varepsilon H}{\sqrt{\pi}} e^{-\varepsilon^2 (T_t - T_{fi})^2}](1-f)} \tag{V-5}$$

and

$$\frac{dT_{gi}}{dt} = \frac{h_f a}{\rho_{ig} c_{gi} f} (T_{fi} - T_{gi}) + \frac{v}{\Delta z \, \rho_{gi} c_{gi} f} (c_{gi-1} T_{gi-1} - c_{gi} T_{gi}) \tag{V-6}$$

for $i = 1, 2, \ldots, N_z$

These simultaneous, nonlinear, ordinary differential equations cannot be solved by analytical methods. They can be integrated numerically by the Runge-Kutta-Gill method (57). The numerical method and results of these equations are shown and discussed in the next chapter. The stability of the numerical method is also examined.

CHAPTER VI

NUMERICAL RESULTS OF THE HIGH EXPANSION FOAM MODEL

There are many industrially important processes in which mass or heat transfer takes place between fluids and solids. The form of their mathematical models is typically simultaneous first-order partical differential equations. Examples are the fixed bed gas absorber, fixed bed ion exchange resin, heat exchanger and filter cake washing performance (55). More examples have been presented recently by Aris and Amundson (2).

Exact Solution of the Simplest Model

The model developed previously can be simplified, if the following assumptions are made:

1. The thermal properties of water and ice are independent of temperature.
2. The heat transfer coefficient between liquid and vapor phase is constant.
3. The vapor flow rate is time independent.
4. There is no phase transition in the system.

Then, Equations V-3 and V-4 and boundary conditions turn out to be linear partial differential equations.

$$\frac{\partial T_f}{\partial t} = - \frac{(h_f a)_o}{(\rho_f c_f)_o (1-f)} (T_f - T_g) \qquad \text{(VI-1)}$$

$$\frac{\partial T_g}{\partial t} = \frac{v_o c_{go}}{(\rho_g c_g)_o f} \frac{\partial T_g}{\partial z} + \frac{(h_f a)_o}{(\rho_g c_g)_o f} (T_f - T_g) \qquad \text{(VI-2)}$$

with boundary conditions,

$$t = o, T_f = T_\infty, \text{ for all } z \qquad \text{(VI-3)}$$

$$t > o, T_g = T_L, \text{ at } z = o \qquad \text{(VI-4)}$$

where the variables with subscript o are all constants.

Exact solution of Equations VI-1 through VI-4 can be obtained by one-dimensional Laplace transformation techniques (60). However, this kind of simultaneous, first-order, partial differential equation can be solved more easily by two-dimensional Laplace transformations (110). Before solving these equations, the modified position and time variables are introduced,

$$t' = t - z \left[\frac{f(\rho_g c_g)_o}{v_o c_{go}}\right] \qquad \text{(VI-5)}$$

Then Equations VI-1 and VI-2 are rewritten in terms of the following dimensionless variables:

$$X = \frac{T_f - T_\infty}{T_L - T_\infty} \qquad \text{(VI-6)}$$

$$Y = \frac{T_g - T_\infty}{T_L - T_\infty} \qquad \text{(VI-7)}$$

$$\xi = \frac{z'(h_f a)_o}{v_o c_{go}} \qquad \text{(VI-8)}$$

$$\mu = \frac{(h_f a)_o t'}{(\rho_f c_f)_o (1-f)} \qquad \text{(VI-9)}$$

They become

$$\frac{\partial X}{\partial \mu} = - (X - Y) \qquad \text{(VI-10)}$$

$$\frac{\partial Y}{\partial \xi} = + (X - Y) \qquad \text{(VI-11)}$$

The boundary conditions are

$$X = 0, \text{ at } \mu = 0, \text{ for all } \xi \qquad \text{(VI-12)}$$

$$Y = 1, \text{ at } \xi = 0 \text{ for all } \mu \qquad \text{(VI-13)}$$

Take the two-dimensional Laplace transformations with respect to ξ and μ. Let p and q be the transformed variables corresponding to ξ and μ, respectively. $\bar{X}$ and $\bar{Y}$ represent x and y in p and q domain. Equations VI-10 and VI-11 result in

$$\bar{Y} = \frac{1}{p\,q} - \frac{1}{p(p\,q + p + q)} \qquad \text{(VI-14)}$$

$$\bar{X} = \frac{\bar{Y}}{q + 1} \qquad \text{(VI-15)}$$

Three inverse formulas given below are necessary for inverting Equations VI-14 and VI-15 into the ξ and μ domain.

$$L^{-1}_{pq} \left[\frac{1}{pq}\right] = 1 \qquad \text{(VI-16)}$$

$$L^{-1}_{pq} \left[\frac{1}{pq + p + q}\right] = e^{-(\mu + \xi)} J_o(i\sqrt{4\,\xi\,\mu}) \qquad \text{(VI-17)}$$

$$L^{-1}_{p} \left[\frac{1}{p}\right] = 1 \qquad \text{(VI-18)}$$

$$Y(\xi, \mu) = 1 - \int_0^{\xi} e^{-(\mu+\xi)} J_o(i\sqrt{4\mu\,\xi})\, d\xi \qquad \text{(VII-19)}$$

and

$$X(\xi, \mu) = 1 - e^{-(\tau+\xi)} J_o(i\sqrt{4\mu\,\xi}) - \int_0^{\xi} e^{-(\mu+\xi)}$$

$$\times\, J_o(i\sqrt{4\mu\xi})\, d \qquad \text{(VI-20)}$$

where J_o (ix) is a zero-order Bessel function of the first kind. Several references (48, 31, 90) have presented the integral relations given by Equations VI-19 and VI-20 graphically.

Using Equation VI-19, the LNG vapor temperatures of five cases of the simplest high expansion foam model have been calculated. The parameter values used for these cases are summarized in Table VI-1. Figure VI-1 presents the temperature profiles of LNG for Run A-1. It is a typical result of the simplest high expansion foam model. For each fixed thickness of foam the exact solution for the LNG vapor has a discontinuous point at which time the first LNG vapor which entered the high expansion foam at $t = 0$ just reaches the top surface of the foam.

Numerical Results of Nonlinear Equations

The evaporation rate of LNG within a short time period after a spill on land is much higher than the corresponding steady state situation. The transient boil-off rates of LNG on land for various cases have been calculated and discussed in Chapter IV. For the transient period the vapor flow rate should not be assumed to be a constant. The boil-off rates

TABLE VI-1

SUMMARY OF SEVERAL TESTS OF THE SIMPLEST HIGH EXPANSION FOAM MODEL

Run No.	Vapor Flow Rate V_o (16/ft -hr)	Foam Expansion Ratio, f	Heat Transfer Coefficient $(h_f a)_o$ (Btu/hr-ft^2-°F)	Thermal Prop. of Water $(c_f \rho_f)_o$ (Btu/ft^3-°F)	Heat Capacity of LNG, c_g (Btu/lb-°F)	Density of LNG, ρ_g (lb/ft^3)
A-1	100	500:1	15	30	0.5	0.05
A-2	100	500:1	5	30	0.5	0.05
A-3	300	500:1	15	30	0.5	0.05
A-4	100	500:1	15	60	0.5	0.05
A-5	100	500:1	15	30	0.5	0.10

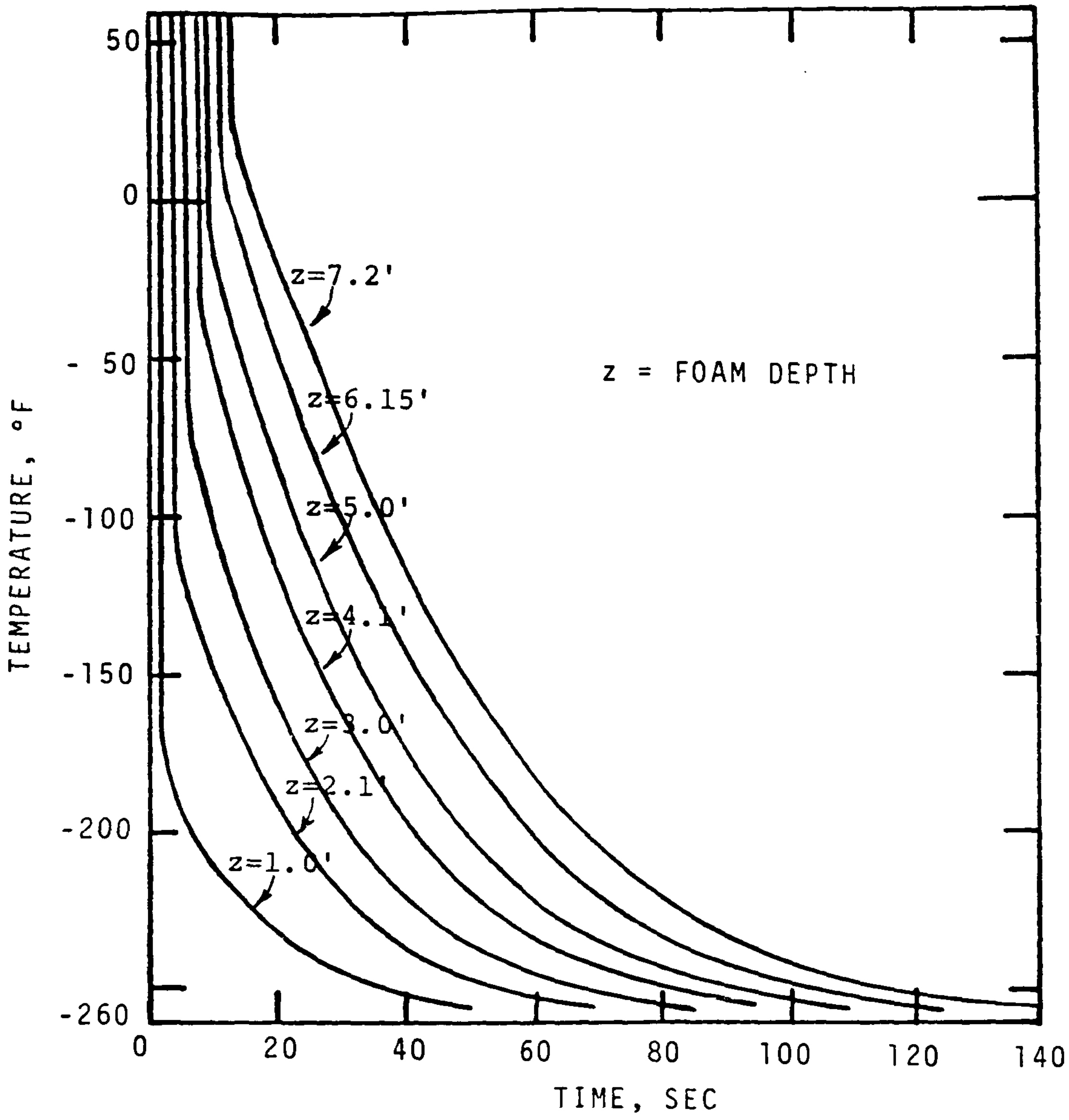

Figure VI-1. LNG Vapor Exit Temperature Versus Time for Run A-1.

as a function of time of Model I-4 and I-6 in Chapter IV are used later in the foam model calculations.

Since the temperature of the boil-off LNG vapor is so cold, it results in the freezing of the foam blanket quickly. Therefore there is a phase change with the frozen foam supporting the additional foam on top. The thermal properties of high expansion foam can be assumed to be those of ice and water. Over a wide range of temperatures, the thermal properties of ice and water are temperature-dependent.

The correlation for thermal properties of ice and water as a function of temperature have been presented in Chapter IV. The density and specific heat of LNG vapor for the present foam model are assumed to be those of pure methane at one atmosphere. For simplicity the volume and specific heat data of methane at one atmosphere by Din (23) are correlated by a polynomial relation in terms of temperature rather than by a complex Equation of State, that is

$$F = a_1 + b_1 T + c_1 T^2 + d_1 T^3 \tag{VI-21}$$

The values of the coefficients a_1, b_1, c_1 and d_1 for density and specific heat are summarized in Table VI-2.

Due to the lack of heat-transfer coefficient data of LNG vapor-water contact, the heat-transfer coefficient between air and water in a packed tower is used for the present foam model calculation. McAdams, Pohlenz, and St. John (66) reported the results of an investigation of air-water heat

TABLE VI-2

THE COEFFICIENTS OF A_1, B_1, C_1 AND D_1 FOR DENSITY AND SPECIFIC HEAT OF METHANE AT 1 ATM

	$a_1 \times 10$	$b_1 \times 10^3$	$c_1 \times 10^7$	$d_1 \times 10^8$
Specific heat Btu/lb-°F	5.15217	0.153397	5.79155	0.0
Density lb/ft^3	0.476306	-0.125204	-0.956163	-0.217108

transfer coefficients. Their correlation for gas and liquid film coefficients were in the form

$$h_g a = 1.78\ v^{0.70}\ \ell^{0.07}\ e^{0.0023T} \tag{VI-22}$$

and

$$h_\ell a = 0.82\ v^{0.7}\ \ell^{0.5} \tag{VI-23}$$

where $h_g a$ and $h_\ell a$ are heat transfer coefficients for the gas and liquid films, respectively. v is the air flow rate and ℓ is the water flow rate. The overall heat-transfer coefficient, $h_f a$, in terms of $h_g a$ and $h_\ell a$ is

$$\frac{1}{h_f a} = \frac{1}{h_g a} + \frac{1}{h_\ell a} \tag{VI-24}$$

Yoshida and Tanaka (117) presented the following similar correlation

$$h_g a = 0.117\ v\ \ell^{0.2} \tag{VI-25}$$

and

$$h_\ell a = 8.0\ \ell^{0.8} \tag{VI-26}$$

The data given by Hensel and Treybal (47) were not in a simple equation and shown in a plot. The correlations given by Equations VI-22 and VI-23, and Equations VI-25 and VI-26 are employed in the following calculation. The heat transfer coefficient is not only flow rate-dependent but also is temperature-dependent. It is obvious that the simplest model may not hold for the actual behavior of the high expansion foam on the spilled LNG.

Without the four assumptions of the simplest model, the nonlinear, hyperbolic, partial differential Equations V-3 and V-4 have no exact solutions. There are two types of numerical methods for solving hyperbolic equations. One is the method of characteristics (83). This method requires specification of characteristic curves first and then evaluation of the solution along these characteristic curves. The other method is the finite difference method (83). When it is applied, the original hyperbolic equations are changed into a set of ordinary differential equations. The physical significance must be considered at this point. Otherwise, the results could sometimes be absurd. Finding the characteristic curves is cumbersome for nonlinear hyperbolic equations, so the more straightforward finite difference method was adopted for studying high expansion foam on the spilled LNG model. The equations deriving from this physical situation, Equations V-5 and V-6 (rather than from partial differential equations regarded abstractly as defining the system) are solved by the Runge-Kutta-Gill method (57).

A summary of several tests of the high expansion foam model during the transition boil-off period is in Table VI-3. The purposes of these tests is to understand the performance of the mathematical, high expansion foam model and to evaluate the characteristics of high expansion foam on LNG spills on land. The principle test variables included LNG boil-off rates, foam application rates and the thickness of foam. Foam quality and expansion ratio are important variables, too, but they were not included as variables in this study.

A high expansion foam, with an expansion ratio of 500:1, is assumed to be placed on the spilled LNG with an infinite application rate right after the LNG is spilled on land. Under this circumstance, the boundary conditions for Equations V-5 and V-6 are

$$t = 0, \quad T_{fi} = T_{gi} = T_\infty, \quad i = 1, 2, \ldots, N_z \qquad \text{(VI-27)}$$

and

$$t > 0, \quad T_{gi} = T_L, \quad i = 0 \qquad \text{(VI-28)}$$

where the initial foam temperature, T_∞, is 60°F and the boiling point of LNG, T_L, is kept constant at -260°F. It is assumed that the transient boil-off rate of LNG on soil is calculated from Model I-4 in Chapter IV. This case is designated Run B-1. Then the calculated temperature distributions of LNG vapor passing through the high expansion foam versus time for various thicknesses of foam are shown in Figure VI-2. If the boil-off rate

TABLE VI-3

SUMMARY OF SEVERAL TESTS OF NONLINEAR HIGH EXPANSION FOAM MODEL

Run No. N	Vapor Flow Rate (lb/ft^2-hr)	Foam Application Rate (cfm/ft^2)	Foam Expansion Ratio	Time Delay of Applying Foam (sec)	Overall Heat Transfer Coefficient (Btu/hr-ft^2-°F)	Comment
					Equations	
B-1	Model I-4	Infinite	500:1	0	VI-22 & VI-23	
B-2	Model I-6	Infinite	500:1	0	VI-22 & VI-23	
B-3	Model I-6	Infinite	500:1	10	VI-22 & VI-23	
B-4	Model I-6	7.5	500:1	10	VI-22 & VI-23	
B-5	Model I-6	15	500:1	10	VI-22 & VI-23	
B-6	Model I-6	24	500:1	10	VI-22 & VI-23	
B-7	Model I-6	96	500:1	10	VI-22 & VI-23	
B-8	Model I-6	96	500:1	10	VI-22 & VI-23	Latent Heat of Phase Change Neglected
B-9	Model I-6	96	500:1	10	VI-25 & VI-26	

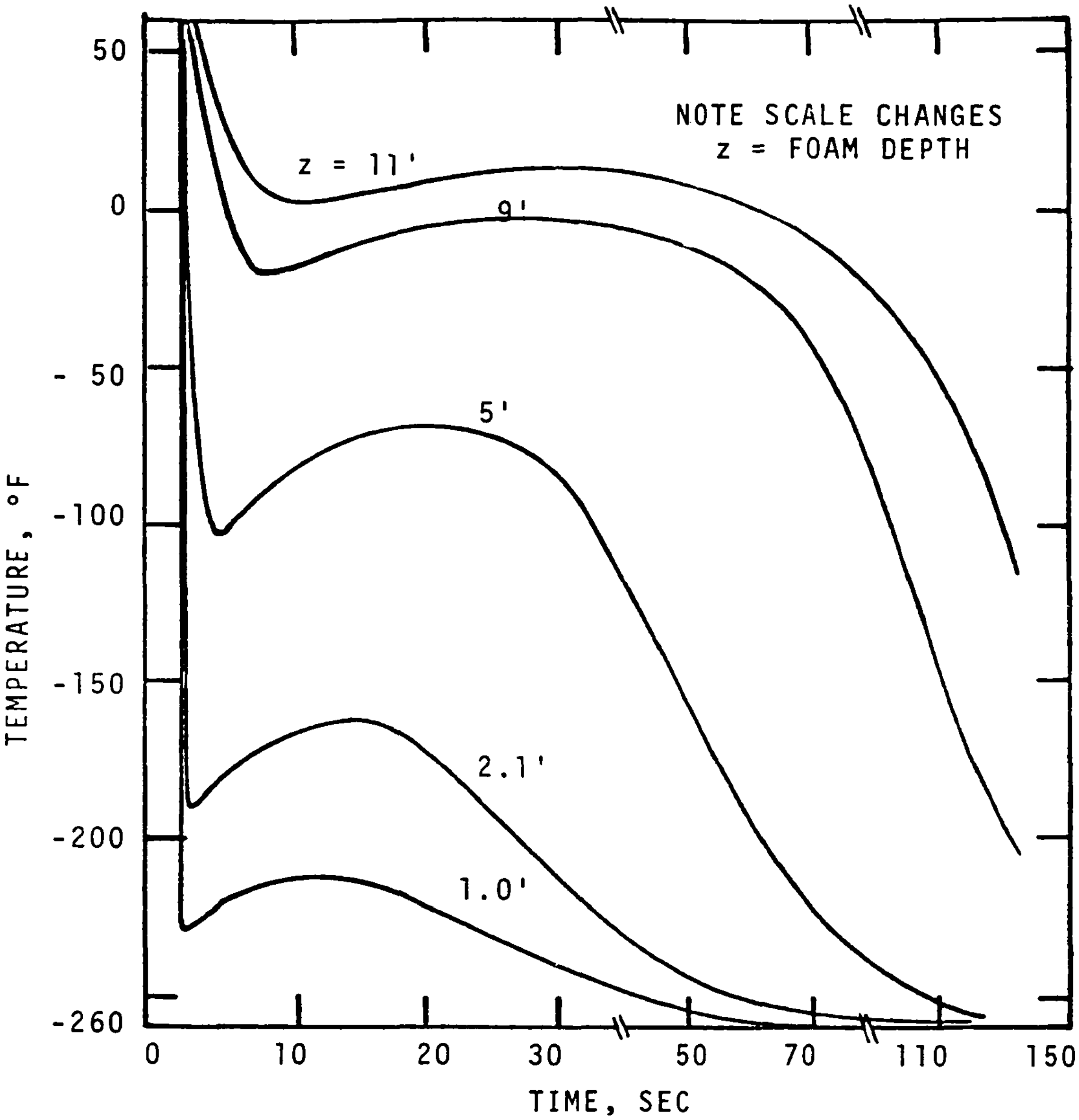

Figure VI-2. LNG Vapor Exit Temperature Versus Time for Run B-1.

of LNG on soil follows Model I-6 of Chapter IV, designated Run B-2, the resulting temperature profiles of LNG vapor in the 500:1 expansion foam are presented in Figure VI-3. These two figures indicate that boil-off rate is a significant factor on the change of vapor temperature inside the expanded foam. Figure VI-3 shows the effect of vapor flow rate on the effective foam duration time. The effective foam duration time is defined as the time interval during which the LNG vapor passing through the foam is higher than -170°F. As shown by Figure VI-3, to obtain a duration time of 60 seconds with a 500:1 expansion foam, Test 2 required a foam depth of 3.65 feet. Test 1 required a depth of 5.6 feet of foam, or an increase of 56 percent in foam coverage. It is noticeable that the effective duration time of Test 2 changes sharply with a small change in the thickness of foam when the thickness is from 1.5 feet to 2.0 feet. Beyond this region the rate of change of the effective duration time is reduced and is linear with foam thickness. Test 1 displays a similar performance wave as shown in Figure VI-3.

Run B-3 examines the effect of a time delay before the expanded foam is applied on the LNG spill, using the same conditions as Run B-2. The boundary conditions VI-27 and VI-28 for Equations V-5 and V-6 are changed to be

$$\begin{aligned} t = 0,\ & T_{fi} = T_\infty \\ & T_{gi} = T_L,\ i = 1,2,\ldots,N_z \end{aligned} \tag{VII-29}$$

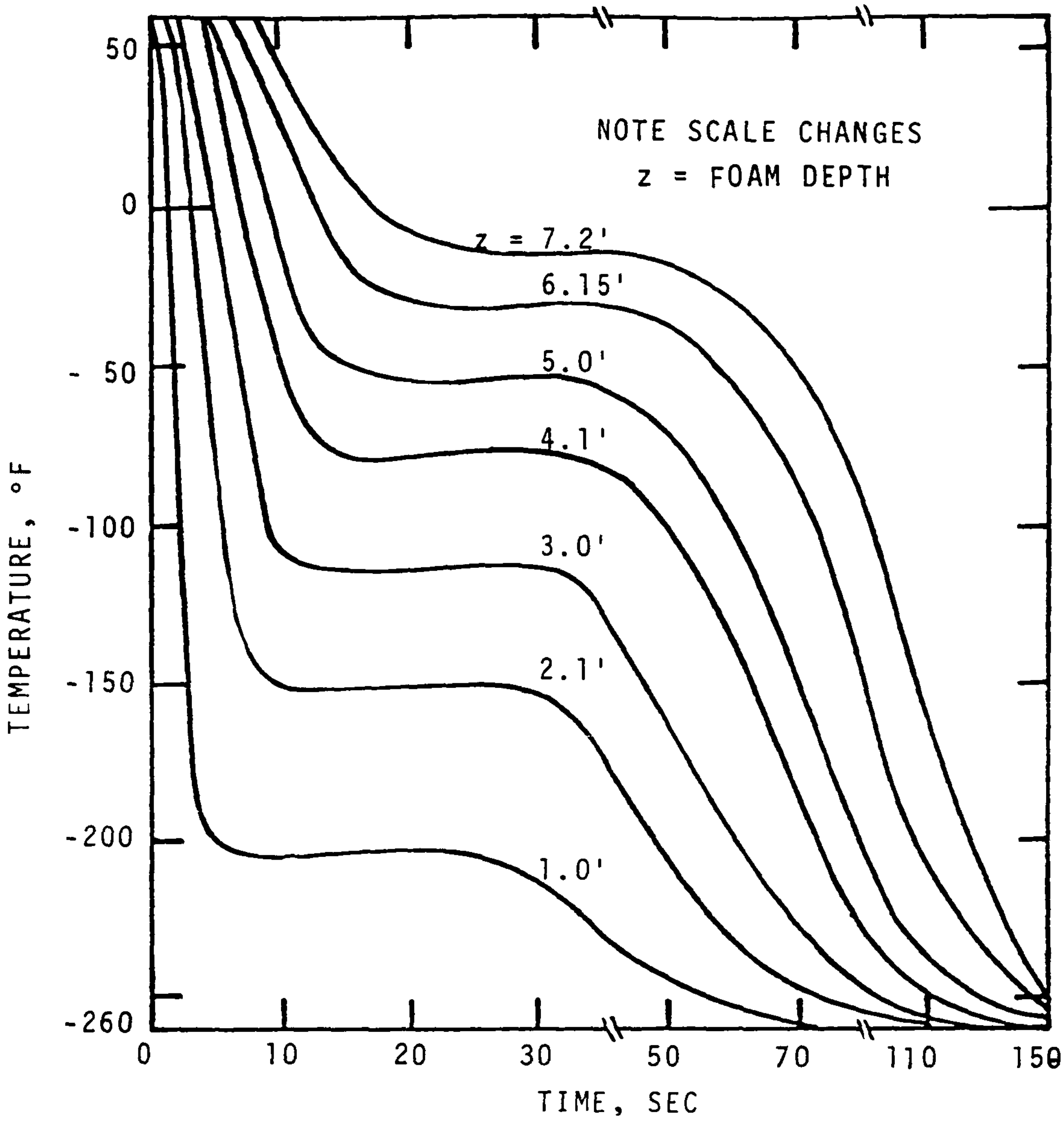

Figure VI -3. LNG Vapor Exit Temperature Versus Time Run B-2.

$$t > 0,\ T_{gi} = T_L,\ i = 0 \qquad \text{(VI-30)}$$

The numerical results of Run B-3 with a 10 second foam application delay are plotted in Figure VI-4 as temperature of vapor versus time with foam thicknesses as a parameter. Let the rate of applied foam be finite. For each time interval there is a new additional foam on the top until it reaches the required thickness. Because the simultaneous ordinary differential equations are solved by numerical integration, calculating the temperatures of vapor and foam at time $t + \Delta t$, the temperatures at time t should be specified in advance. For example, there are i sections of foam at time $i\ \Delta t$. The temperatures of sections from 1 to i at this time are the initial values for obtaining the temperatures of these sections at time $(i + 1)\Delta t$. The initial values of temperatures for the new additional section, $i + 1$, are assumed to be

$$T_{fi+1} = T_\infty \qquad \text{(VI-31)}$$

and

$$T_{gi+1} = T_{gi} \qquad \text{(VI-32)}$$

Due to the round off and truncation errors, the last assumption, Equation VI-32, makes the numerical integration method unstable when the foam application rate is low, even if the integration interval is very small. Therefore, Equation VI-32 should be modified to

$$T_{gi+1} = \omega \times T_{gi} \qquad \text{(VI-33)}$$

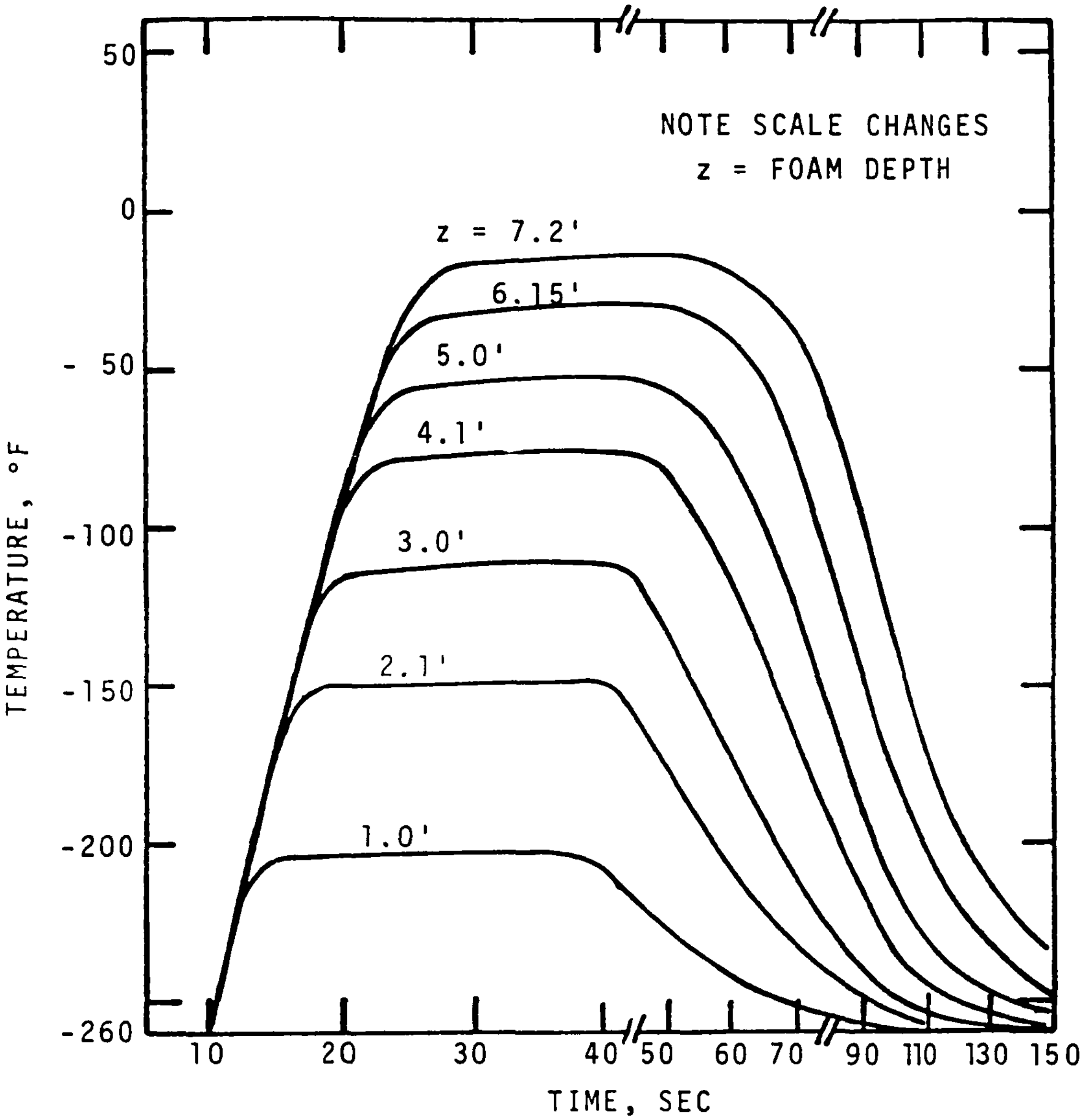

Figure VI-4. LNG Vapor Exit Temperature Versus Time for Run B-3.

where ω is a constant and less than 1. For example, ω is chosen to be 0.998 for the present study. The conditions of Runs B-4, B-5, B-6, and B-7 are the same as Run B-3 except for the foam application rate. Figures VI-5 through VI-8 show the temperature profiles versus time for these tests. There is a major discrepancy between the exact solutions shown in Figure VI-1 and the numerical solutions shown in Figure VI-2 or Figure VI-3. The discrepancy is that the exact solution has a discontinuity in the LNG vapor temperature. Actually no real flow system has a discontinuity in the temperature of the passing fluid. The discontinuous point can be smoothed out rapidly by molecular, eddy or Taylor diffusion. Therefore, it indicates that the partial differential equations, Equations VI-1 and VI-2, were obtained by neglecting the diffusion effect, and the equations from the physical discrete model represent the real situation more accurately. Further discussions of the exact solutions and numerical solution can be found in Rosenbrock and Storey's book (84).

Effect of Latent Heat

In order to evaluate quantitatively the effect of the latent heat of the frozen foam on its performance, it is necessary to compare the results of Runs B-7 and B-8. Because the conditions of these two runs are the same, except that no phase change is assumed in Run B-8, it is noticeable that

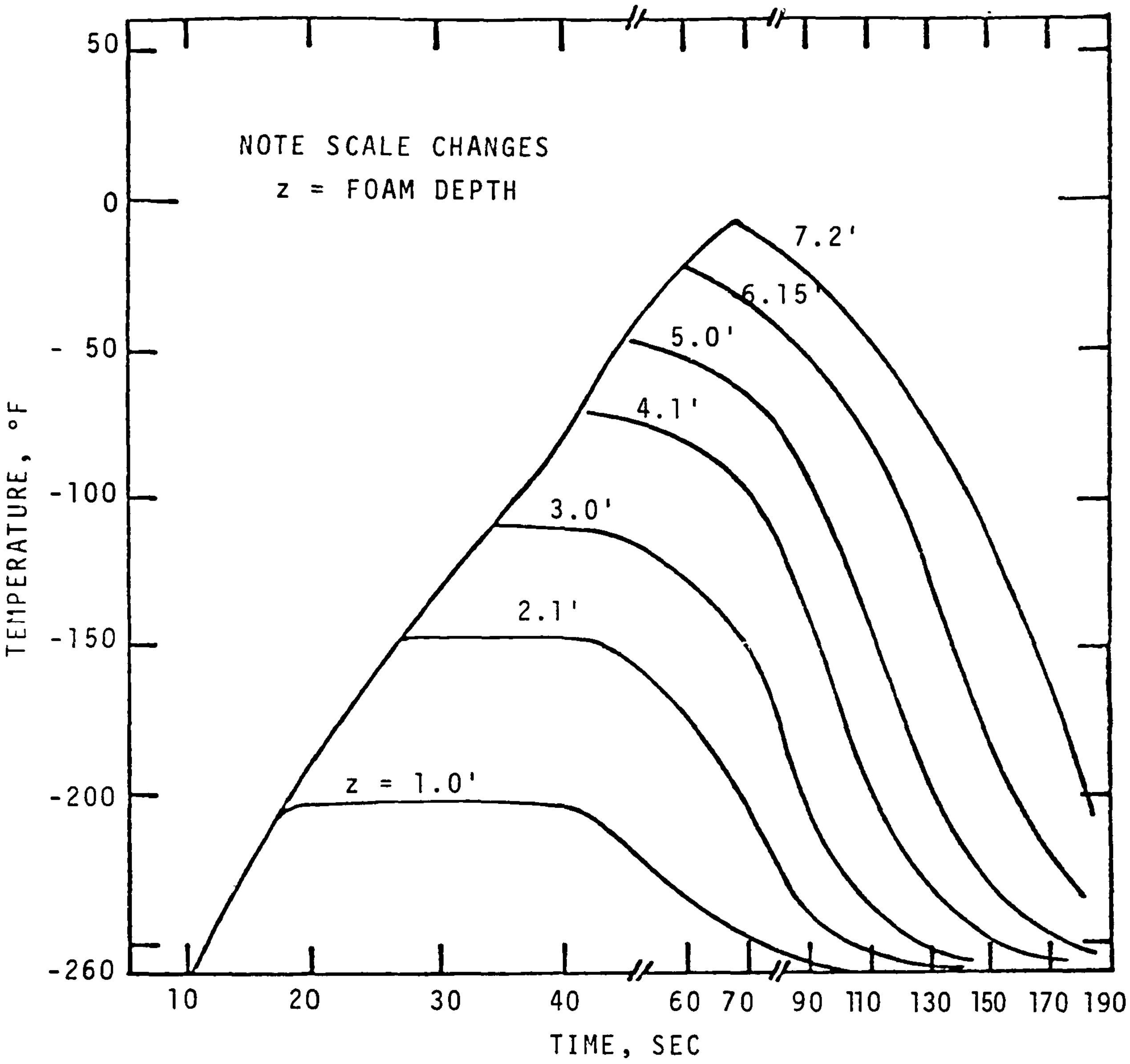

Figure VI-5. LNG Vapor Exit Temperature Versus Time for Run B-4.

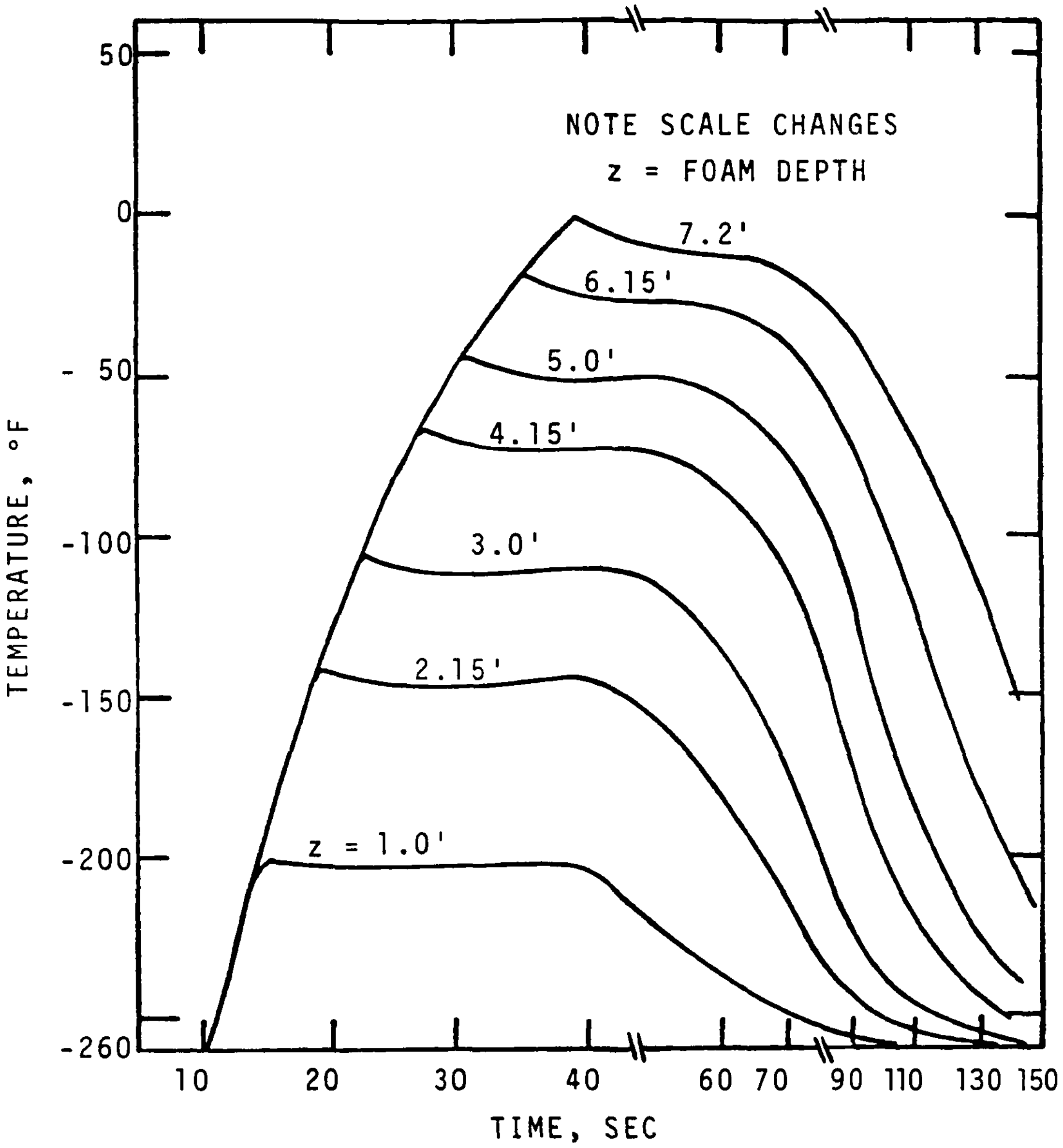

Figure VI-6. LNG Vapor Exit Temperature Versus Time for Run B-5.

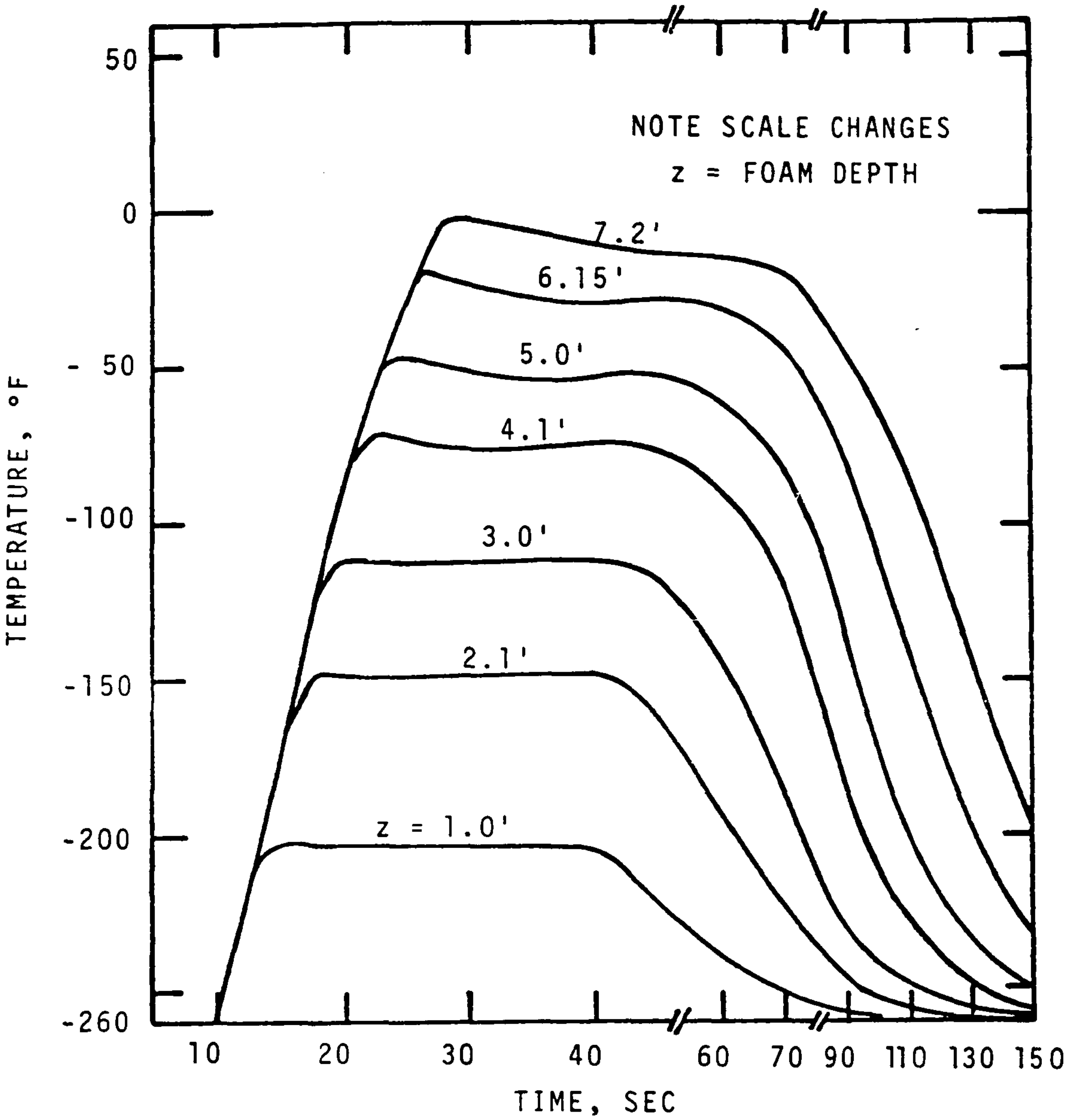

Figure VI-7. LNG Vapor Exit Temperature Versus Time for Run B-6.

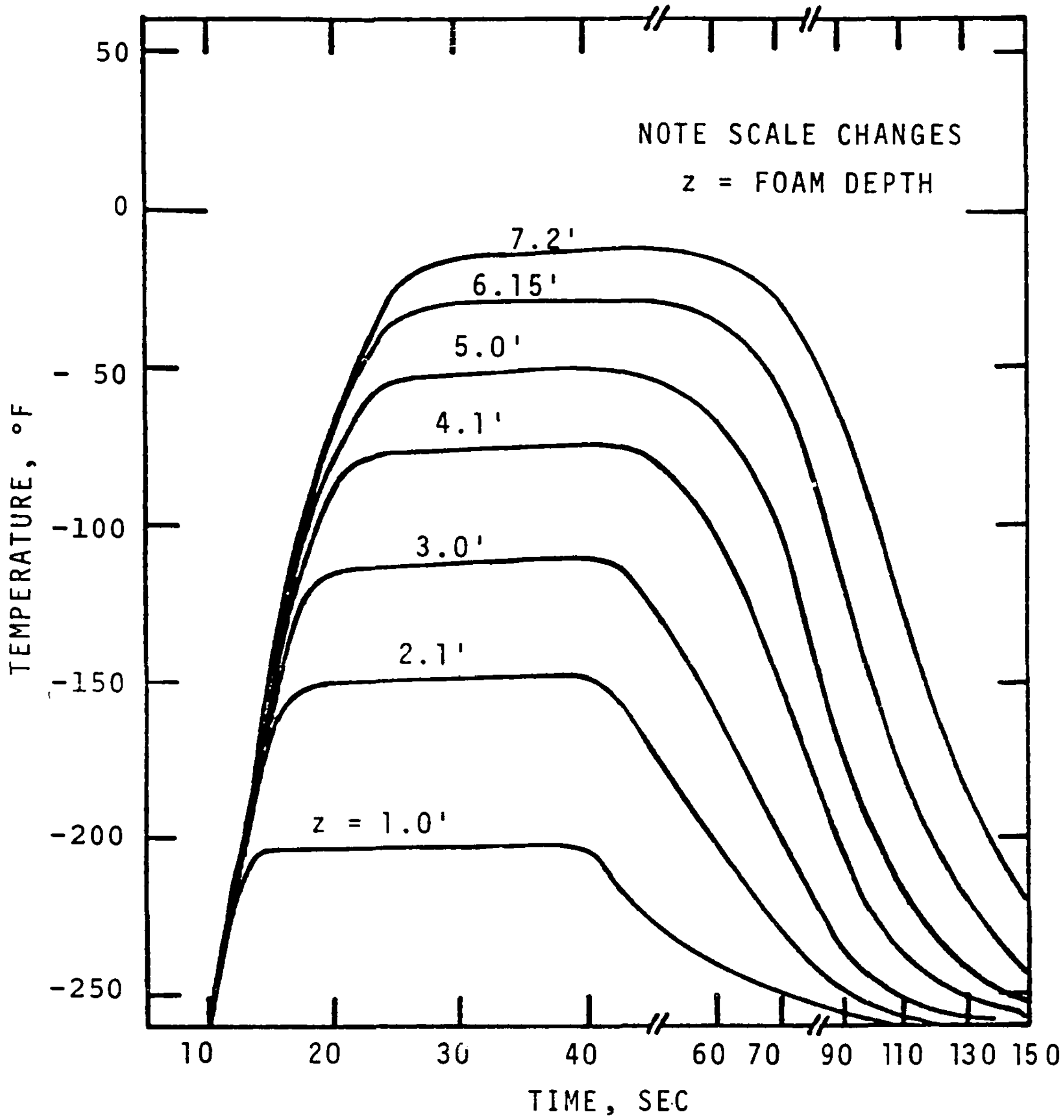

Figure VI-8. LNG Vapor Exit Temperature Versus Time for Run B-7.

each temperature profile of Run B-8 shown in Figure VI-9 increases to a higher temperature and then decreases monotonically. The temperature profiles of Run B-7 shown in Figure VI-8 have different characteristics. Each of these profiles increases to a higher temperature and stays approximately at the same temperature for a period of time. Due to the phase transition, the large amount of latent heat provides the heat source for the LNG vapor. Therefore, the latent heat keeps the LNG vapor warmer.

The plot of the effective foam duration times of Runs B-7 and B-8 is shown in Figure VI-10. The effective foam duration time is defined as the time interval during which the passing LNG vapor through the foam is higher than -170°F. The difference in duration time of these two runs is shown as a dotted line in this figure and the difference is from 25 seconds to 64 seconds for the thickness of foam from 1.5 feet to 8.0 feet. As can be seen from Figure VI-10, the efficiency of a fixed foam depth for increasing the LNG temperature would be increased at least 100 percent by the latent heat. In analyzing the required foam depth for a desired duration time it shows that the latent heat makes a 50 percent reduction of the foam depth. The freezing of a foam blanket not only supports the additional foam on the top but also makes the high expansion foam more efficient by providing a significant source of heat.

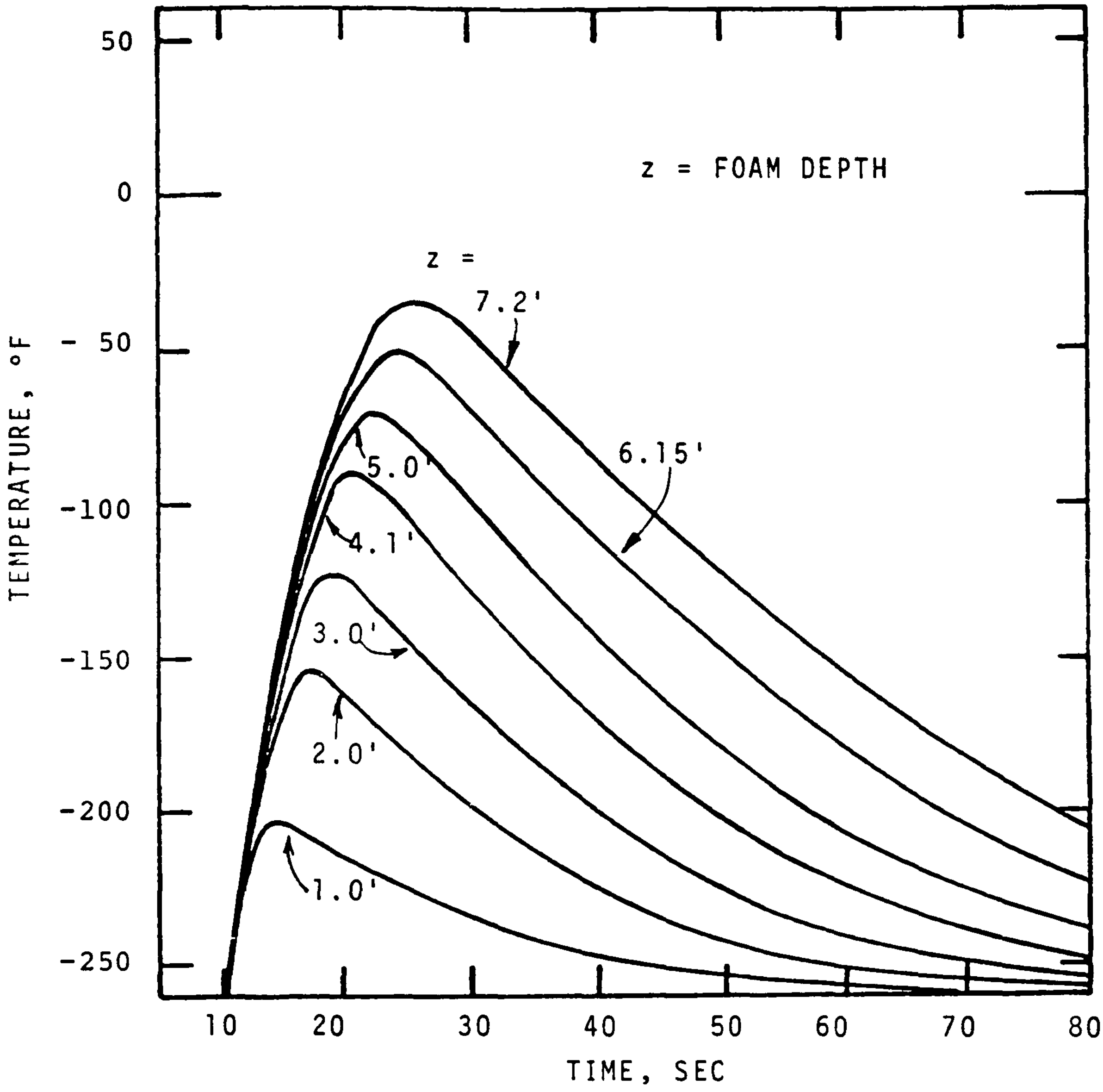

Figure VI-9. LNG Vapor Exit Temperature Versus Time for Run B-8.

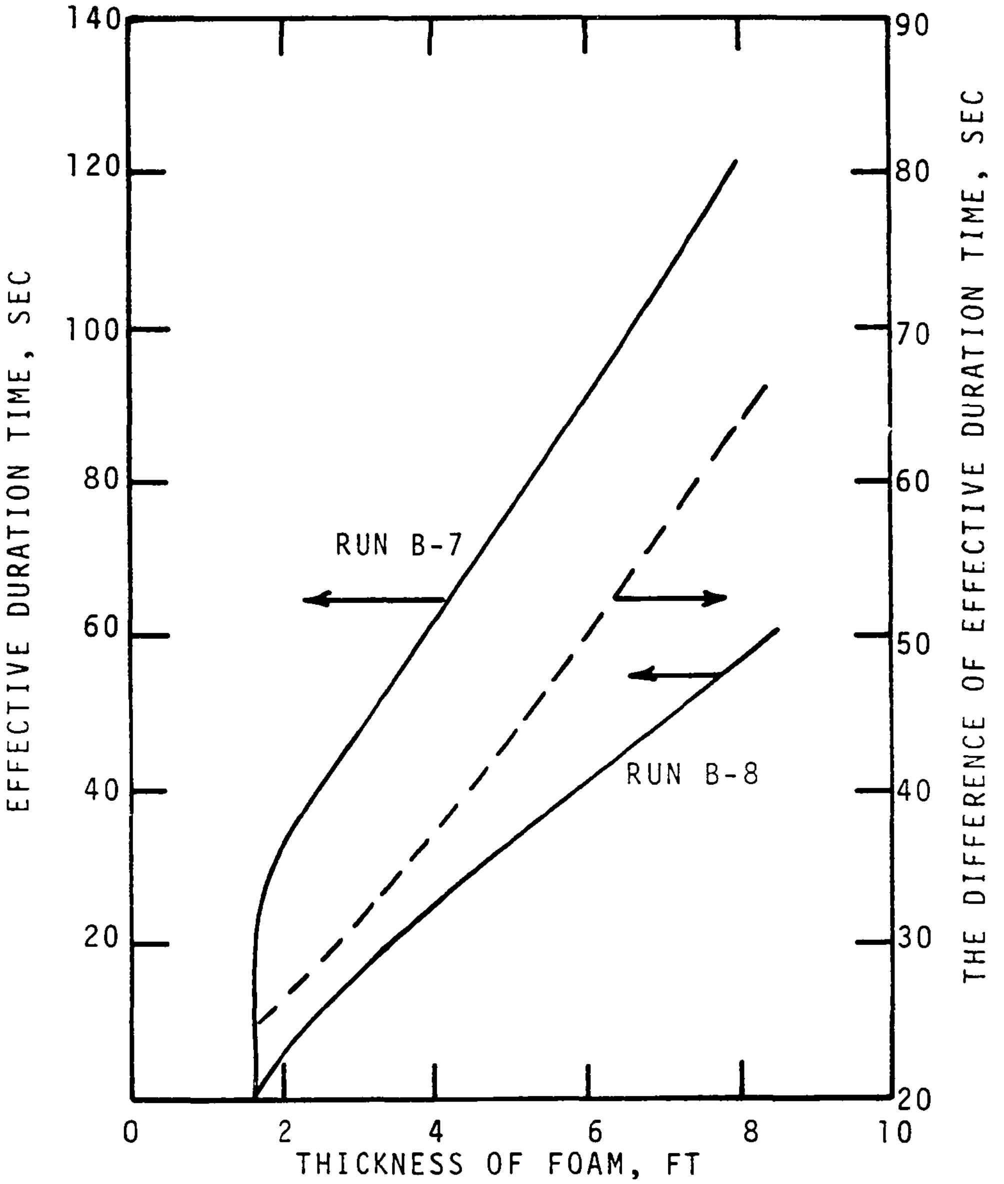

Figure VI-10. Comparison of the Effective Duration Time for Runs B-7 and B-8.

Effect of Vapor Flow Rate

In examining Figures VI-2 and VI-3, it is found that the boil-off rate is an important factor on the change of vapor temperature inside the high expansion foam. Figure VI-11 shows the duration times of Run B-1 and Run B-2. It is noticeable that the effective duration time of Run B-2 changes sharply with a small change in the thickness of foam when the foam depth is from 1.5 feet to 2.0 feet. Beyond this region, the plot of the effective duration time against foam thickness is almost a straight line. Run B-1 has the same general characteristic. As shown in Figure VI-11, Run B-2 gives a 28 sec longer duration time for a fixed thickness of foam. To get the same duration time, Run B-1 needs approximately a 2 feet thicker foam bed if the desired duration time is longer than 35 sec. For instance, to obtain a 60 sec duration time, Run B-2 required 3.65 feet depth of foam. Run B-1 required a depth of 5.6 feet of foam, or an increase of 55 percent of foam.

The effective duration time of Runs A-1 through A-4 of the simplest model are shown in Figure VI-12 for comparative purposes. The duration times of Runs A-1 and A-3 are discussed in this section. Because the vapor flow rate ratio of these two runs is 1:3 and the other parameter values are all the same, it is interesting to note that to maintain the same duration time, the required foam depth for Run A-3 is 300 percent thicker. However, this linear correspondence does

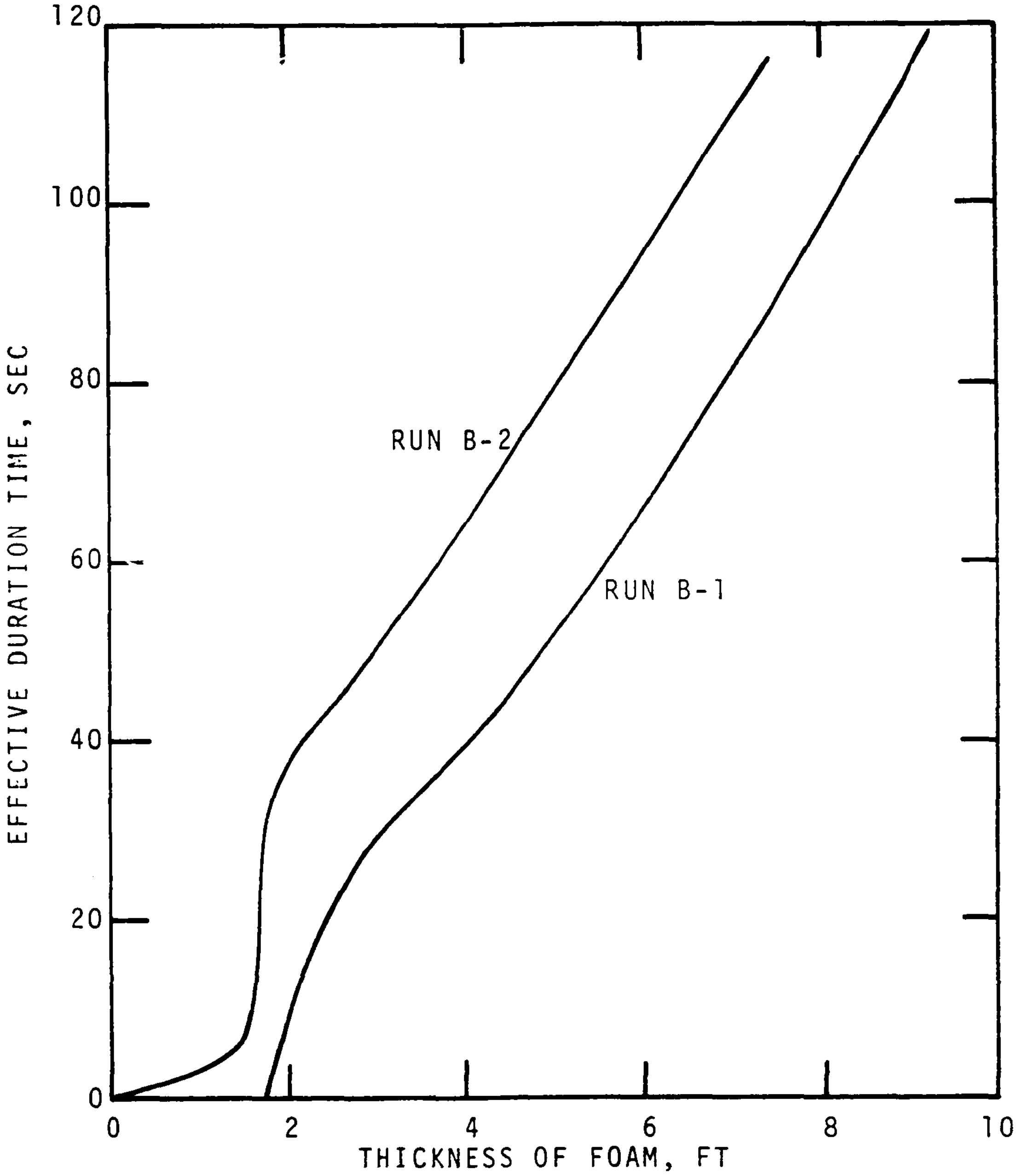

Figure VI-11. Comparison of the Effective Duration Time for Runs B-1 and B-2.

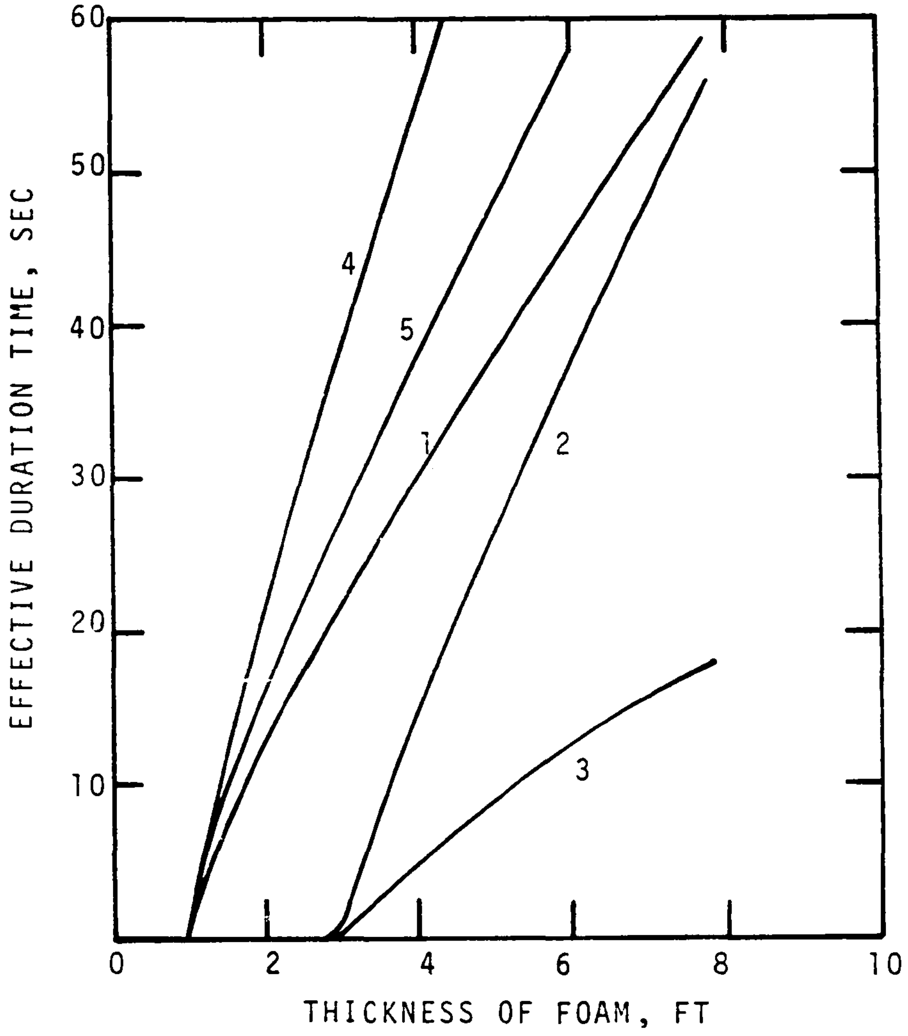

Figure VI-12. Comparisons of the Effective Duration Time for Runs A-1, 2, 3, 4 and 5. Numbers on Curves are Run Numbers.

not occur in the case of Run B-1 and Run B-2. Although the vapor flow rate ratios for Run B-1 and Run B-2 are from 30:1 to 1.5:1 at the initial period, i.e., less tha 15 seconds, the required foam depth ratios are from 1.2:1 to 1.8:1. Because of the evolved latent heat, the duration time ratios of nonlinear cases are not linearly proportional to the vapor flow rate ratios.

Effect of Foam Application Rate

The effective duration times of Runs B-3 through B-7 are plotted on Figure VI-13. As illustrated by this figure, an increasing foam application rate reduces the effective duration time. While the thickness of foam is less than 2 ft, the effective duration times are all about the same for all different application rates. However, the time of starting to keep the LNG vapor higher than -170°F, strongly depends upon the foam application rate as shown in Figure VI-14. The relationship is a hyperbolic function. Therefore, the performance difference becomes even more significant if the application rate is lower than 5 cfm/ft^2.

The plot of the duration time against the foam application rate with the thickness of foam as a parameter is shown in Figure VI-15. This figure will reveal that if the foam is thicker, then the application rate will be more important to make the foam more efficient. The duration time of the 6 feet depth of foam obtained by 100 cfm/ft^2 application rate

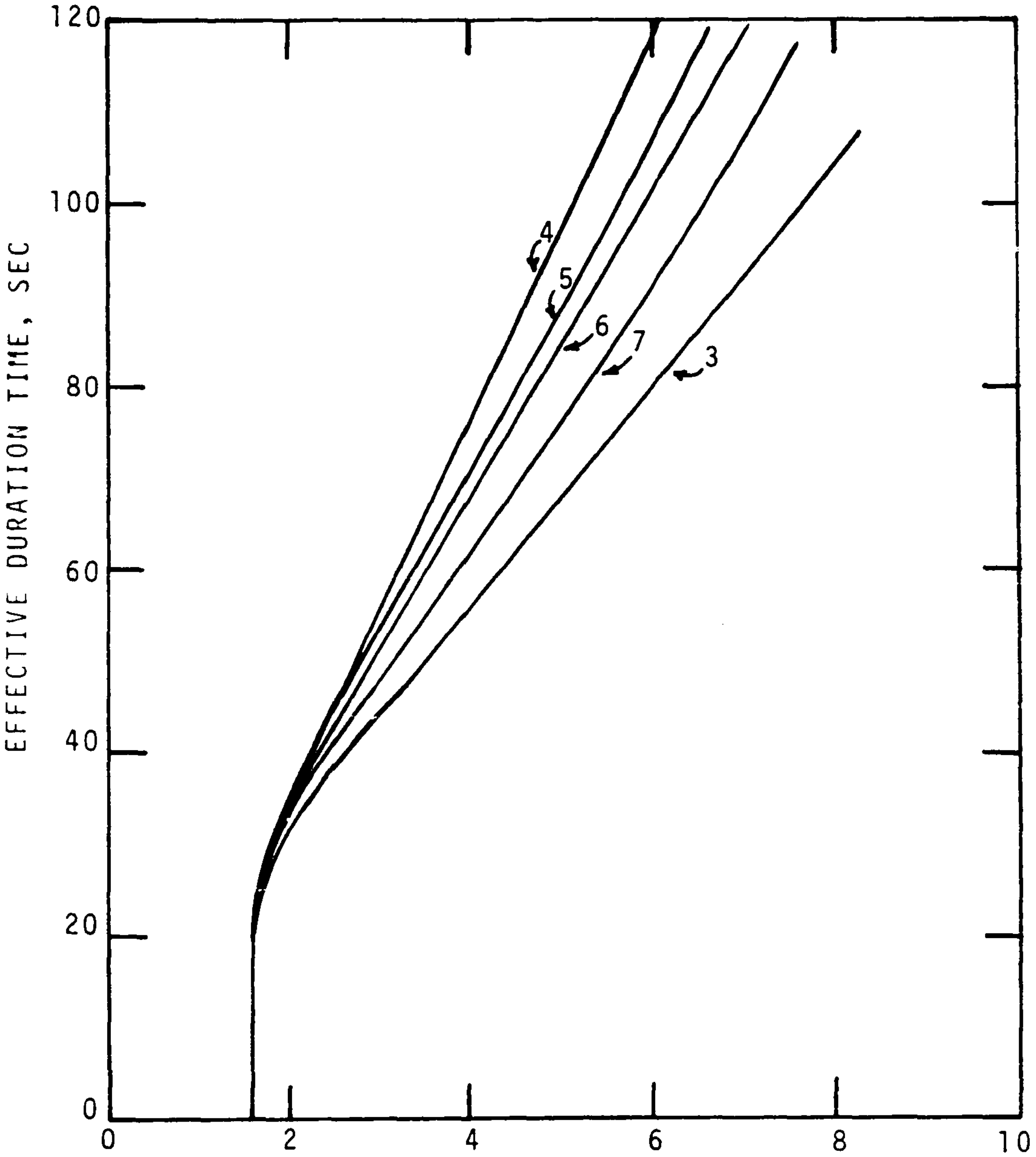

Figure VI-13. Comparisons of the Effective Duration Time for Runs B-3, 4, 5, 6, and 7. Numbers on Curves are Run Numbers.

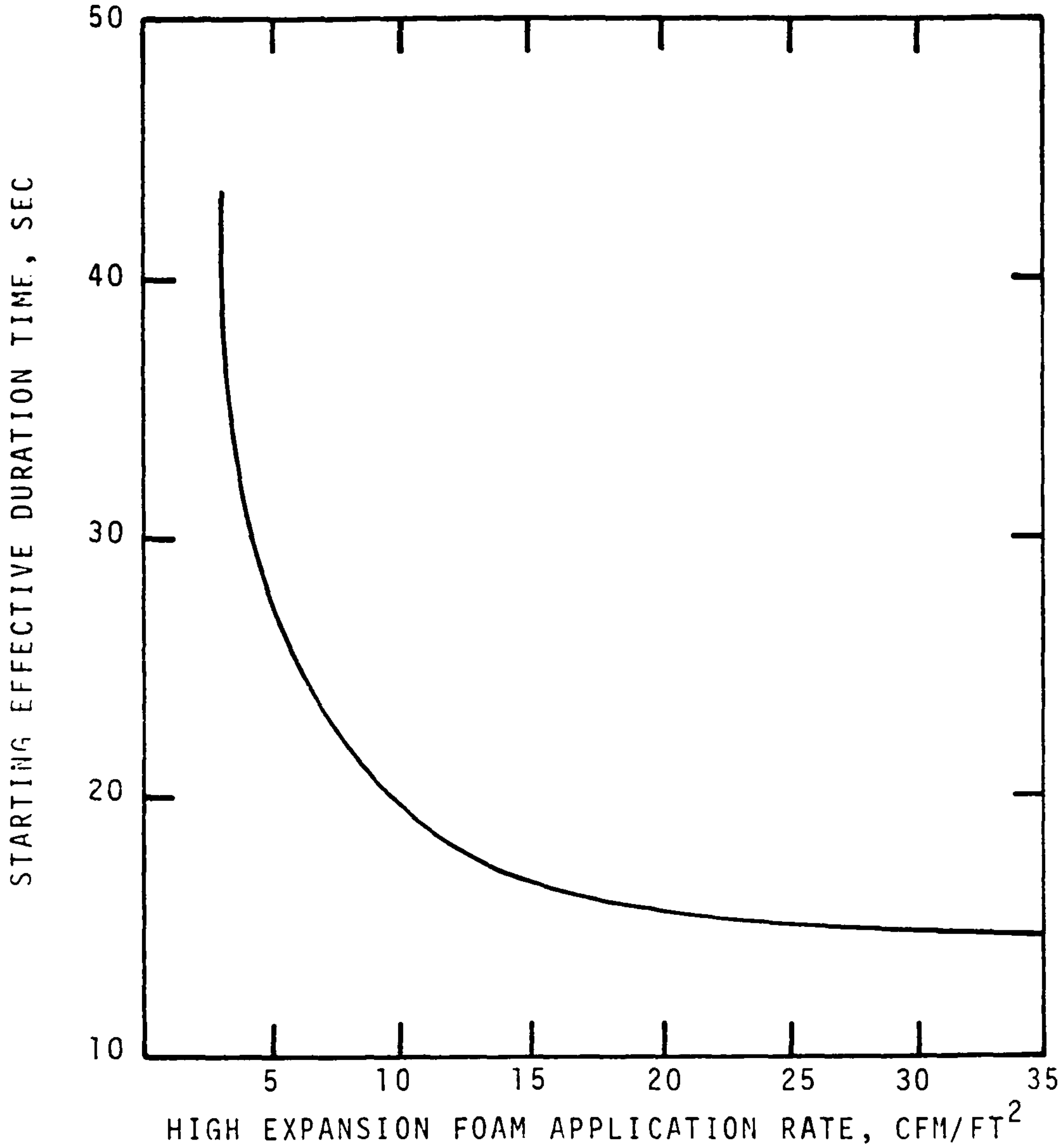

Figure VI -14. Effect of Foam Application Rate on the Starting Effective Durative Time.

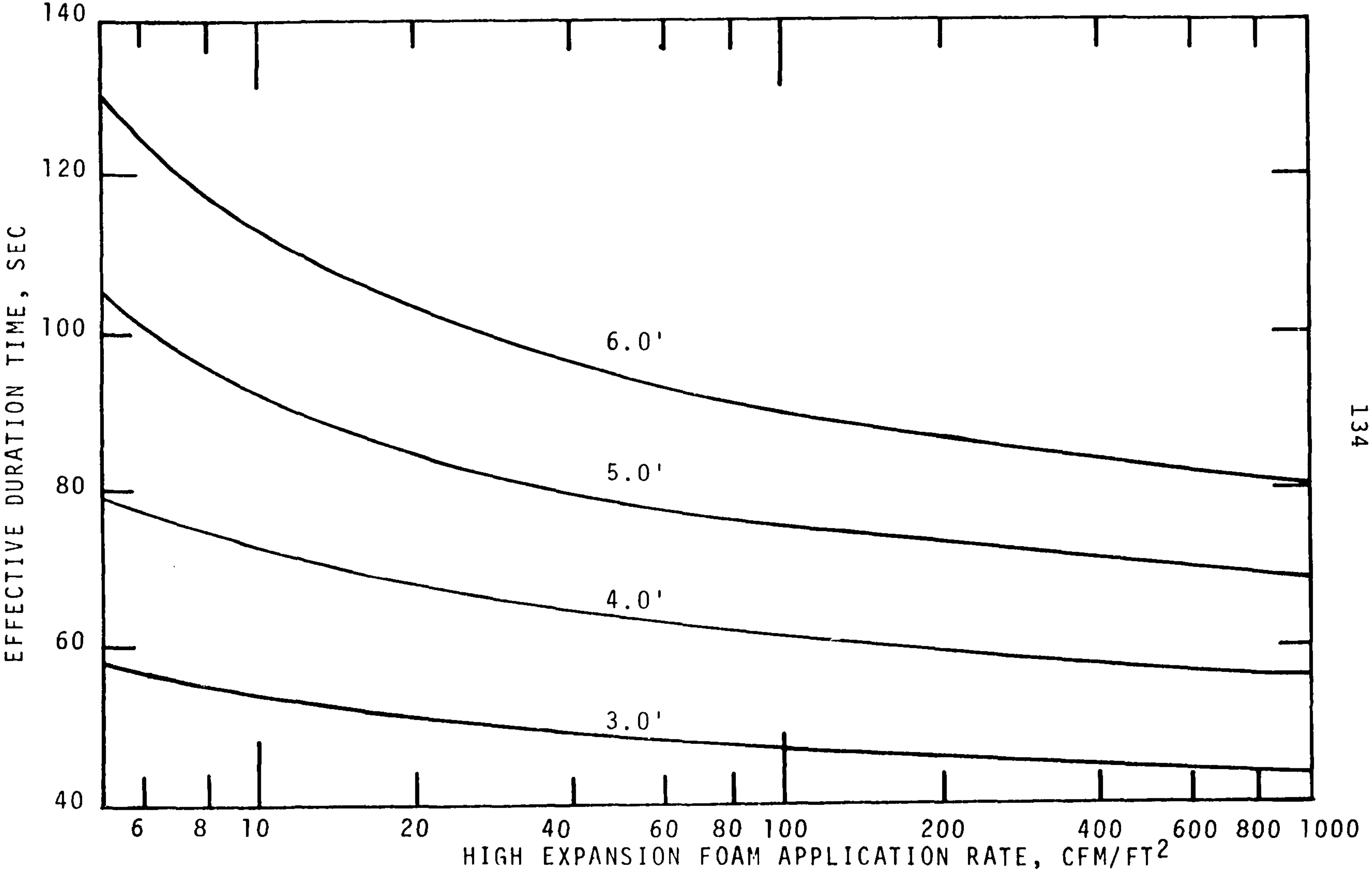

Figure VI-15. Effect of Foam Application Rate on the Effective Duration Time with Foam Thickness as Parameter.

is 90 sec. However, the 6 feet depth of foam has a 103 sec duration time if the application rate is 5 cfm/ft^2. There is an increase of 44 percent in the duration time for the 6 feet depth of foam, but for a 3 feet depth of foam the increase is only 22 percent.

As expected from these results, to control effectively the spilled LNG on land by using the high expansion foam, the initial application rate must be high enough until the foam is about 2 feet thick, after which the rate can be reduced.

Effect of Heat Transfer Coefficient

As mentioned in the previous section, the correlations given by Equations VI-22 and VI-23 or Equations VI-25 and VI-26 were employed to predict the overall heat transfer coefficient of the high expansion foam model. From Equations VI-22 and VI-23 or Equations VI-25 and VI-26 Figure VI-16 presents some of the overall heat transfer coefficients versus vapor flow rates with liquid flow rate as a parameter. Because the data are difficult to obtain, some contradictions are apparent between the results of these two investigations. As shown in Figure VI-16, under the same conditions the ratios of overall heat transfer coefficients obtained by the two different correlations are approximately 3:1. Equations VI-22 and VI-23 or Equations VI-25 and VI-26 were correlated for liquid flow rates exceeding 100 lb/ft^2-hr. But the liquid phase of the high expansion foam is stationary. As shown in

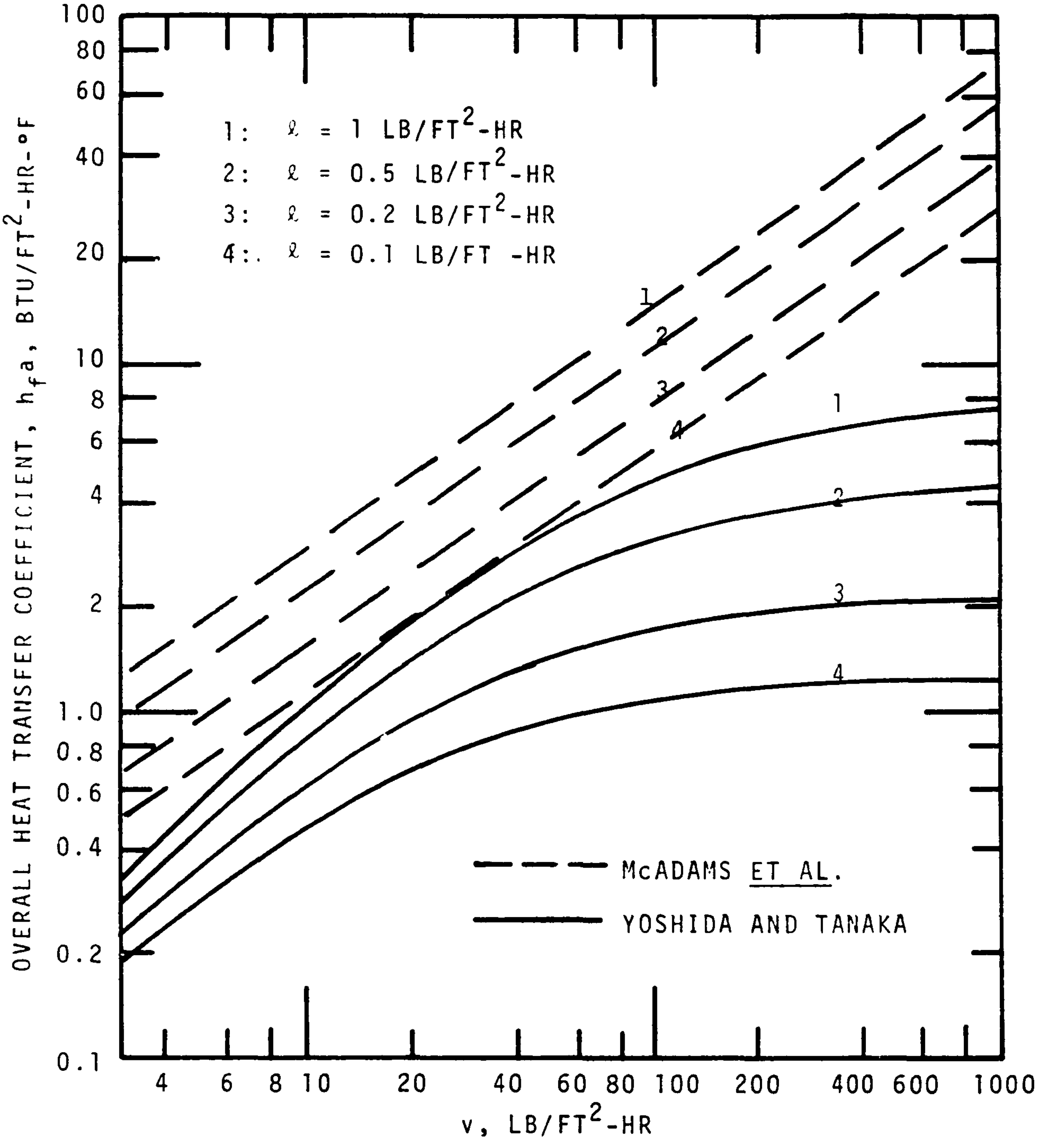

Figure VI-16. Overall Heat Transfer Coefficients.

Figure VI-16, the heat transfer coefficients are also liquid flow rate dependent. It was assumed that the heat transfer coefficients for the LNG vapor-water contact were obtained from Equations VI-22 and VI-23, or Equations VI-25 and VI-26 at a liquid flow rate of 1 lb/ft^2-hr. It is evident that the heat transfer coefficient between LNG vapor and high expansion foam must be investigated in the future.

Figure VI-17 is the plot of the comparison of the computed temperature profiles from Run B-7 and Run B-9. Since the overall heat transfer coefficients of Run B-9 are about one third of those of Run B-7, the heat transfer rate between LNG vapor and the high expansion foam for Run B-7 becomes somewhat higher. Consequently, the temperatures of the LNG vapor passing through the foam of Run B-7 are much higher than those of Run B-9 for time less than 60 sec. For instance, for Run B-9 the outlet temperature of LNG vapor passing through a 7.2 feet depth of foam is -110°F at t = 50 sec. The LNG vapor from Run B-7 is up to -12°F at the same depth of foam. From Figure VI-18 it can be seen that the larger heat transfer coefficients make foams with depths less than four feet more efficient. In contrast, if the depth of foam is more than four feet, the foam with the lower heat transfer coefficient is characterized by much higher duration time. From the temperature profiles in Figure VI-17 it seems that the latent heat of phase change dominates this characteristic. Although the

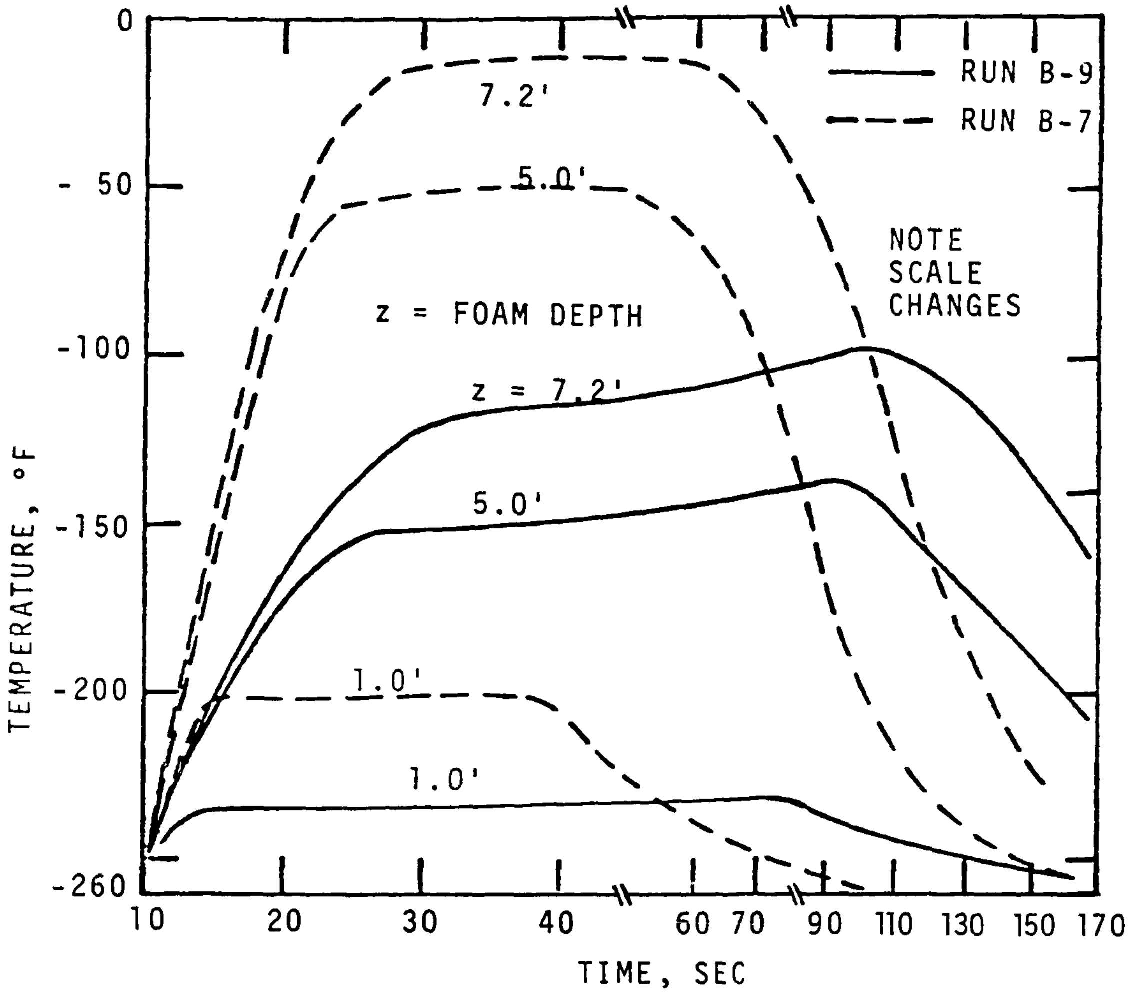

Figure VI -17. Comparisons of LNG Vapor Exit Temperature for Run B-7 and Run B-9 with Foam Thickness as a Parameter.

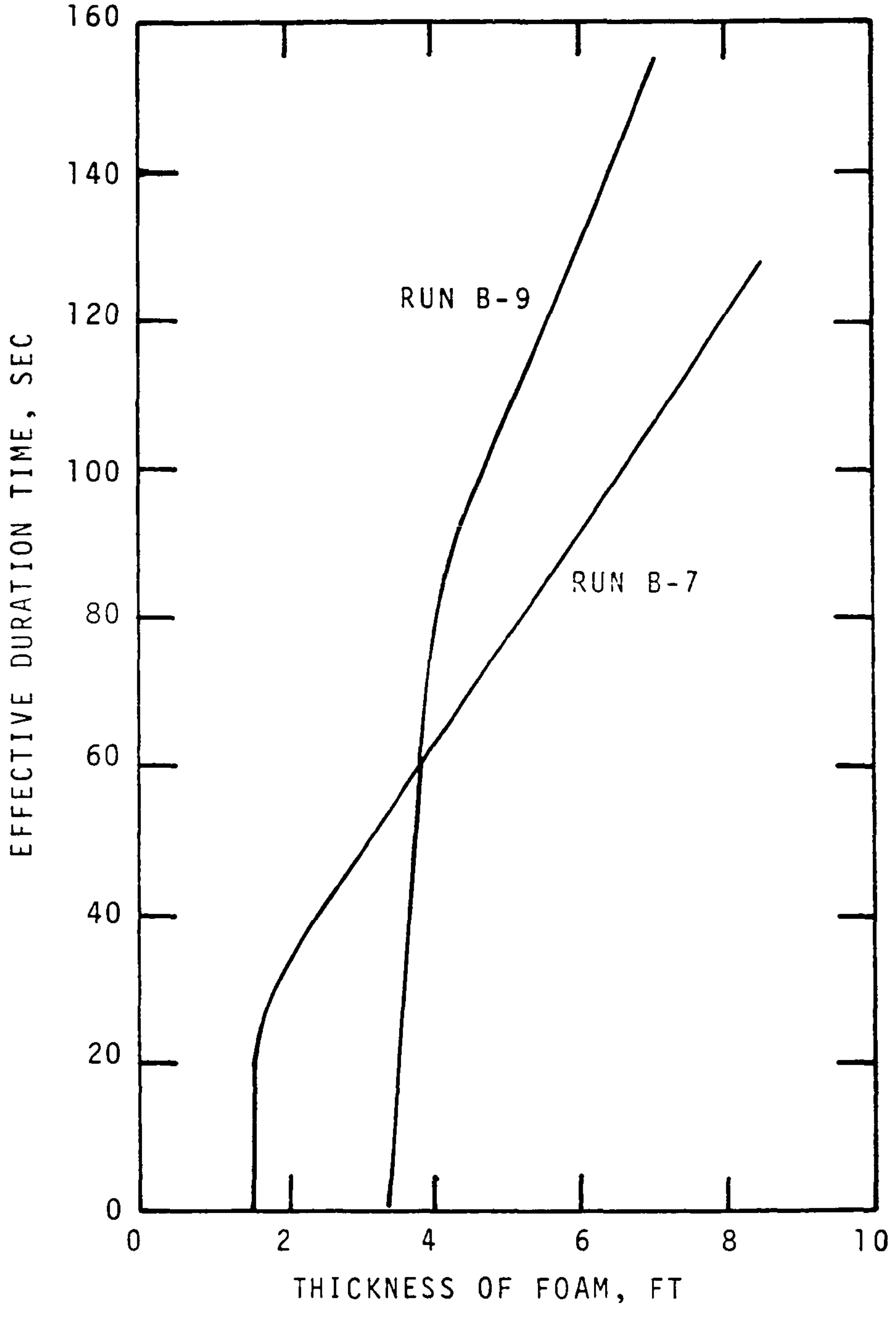

Figure VI-18. Comparison of the Effective Duration Time for Run B-7 and Run B-9.

resulting temperatures from the smaller heat transfer coefficient are lower, the profiles in Figure VI-17 indicate that the time of consuming the fixed amount of latent heat is due to the 3:1 heat transfer coefficient ratio. Hence, the total time of keeping LNG vapor higher than -170°F is longer. This is one more example which shows the contribution of latent heat for making the effective duration time of foam longer if the foam is thick enough to warm up the vapors to -170°F. Considering the simplest models shown in Figure VI-12, comparison of curves 1 and 2 indicates that the 3:1 heat transfer coefficient ratio does not make any significant difference in the effective duration time if the thickness of foam is more than 6 feet.

Other Effects

Figure VI-12 also depicts the influences of the properties of high expansion foam and LNG on the effective duration time of the simplest model. From the comparison of Runs A-1 and Run A-4, the effective duration time is increased by 70 to 80 percent due to 100 percent deviation in the thermal properties of high expansion foam. However, from Runs A-1 and A-5, a 100 percent increase in the density of LNG vapor results in a 25 percent increase of the effective duration time.

CHAPTER VII

CONCLUSIONS AND RECOMMENDATIONS FOR FURTHER STUDY

Conclusions

The proposed numerical method based on the quasilinearization technique is an effective tool to solve one- and two-dimensional heat or mass transfer problems with and without phase change. The problems with nonlinear boundary conditions and with composite material have been treated without any additional effect. The accelerating parameter has no influence on the convergence rate of the two-dimensional models.

The boiling heat transfer coefficient between LNG and soil is the most important factor in predicting the LNG boil-off rates in the short time region, i.e., the convective heat transfer control period. When the temperature difference between LNG and soil drops, the soil thermal properties dominate the accurate prediction of the LNG boil-off rates. The results of the models with temperature dependent boiling heat transfer coefficient and variable soil properties agrees with the experimental LNG spill tests on land.

The two-dimensional models show higher heat transfer rates than one-dimensional models due to the two-dimensional compensation heat transfer around the corner. It has been found that the thickness of polyurethane insulation from 1.5 to 2.0 inches on land can reduce the evaporation rates of LNG significantly.

A mathematical model for analyzing heat transfer between boil-off LNG vapors and high expansion foam is adequate for studying the effects of latent heat, vapor flow rate, and heat transfer coefficient on the performance of high expansion foam. The effective foam duration time was defined as the time interval in which the exit LNG vapor temperature was higher than -170°F, the buoyancy point of LNG vapors in the atmosphere.

The evaporation rate of LNG is much higher than the corresponding steady state rate within the first few minutes after a spill on land. Therefore, the time dependent boil-off rate should be included in the study of high expansion foam performance during the transient period. From the comparison of computer results of models with and without the transition heat, it has been shown that the latent heat of phase change would make a 100 percent difference in the effective foam duration time. The numerical results of the high expansion foam model has also shown that higher foam application rate is necessary to gain control of an LNG spill immediately. After the foam is thicker than 2 feet, the reduction in the foam application rate with increasing the depth of foam is required to obtain longer duration time.

Recommendations for Further Study

1. Investigate the following effects on the heat transfer rate between LNG and soil: the underground water movement, the permeability of LNG into soil and the increasing area due to the cracking of soil.
2. Study the moving boundary problems in cylindrical and spherical coordinates by using the proposed numerical method.
3. Take heat transfer data between LNG and high expansion foam.
4. Investigate the effect of increasing evaporation rate due to the applied high expansion foam on the high expansion foam performance.

NOMENCLATURE

a	a geometrical factor, ft
a_1	parameter
a_i	$= -c_i - b_i$ or defined by Equation III-74
$a_{i,j}$	$= -c_{i,j} - b_{i,j}$ or defined by Equation III-61
$\underline{A}_j$	a tridiagonal matrix whose diagonal entries are positive and off-diagonal entries are negative, defined by Equation III-32 or Equation III-48
$\underline{A}$	a tridiagonal matrix whose diagonal entries are positive and off-diagonal entries are negative, defined by Equation III-70
b_1	parameter
b_i	$= -2\bar{h}^2/[\bar{h}_i(\bar{h}_{i-1} + \bar{h}_i)]$ or defined by Equation III-74
$b_{i,j}$	$=-2\bar{h}\bar{g}/[\bar{h}_i(\bar{h}_{i-1} + \bar{h}_i)]$ or defined by Equation III-62
$b_{i,j}^{(i)}$	$= -2\bar{h}\bar{g}/[\bar{h}_i(\bar{h}_{i-1} + \bar{h}_i)] \quad k_o^{(i)} I^{(i)}/k_o I_o$
$\underline{B}_j$	an N_x-dimensional vector defined by Equation III-33
$\underline{B}$	an N_x-dimensional vector defined by Equation III-71
c	specific heat, Btu/ft^3-°F
c_1	parameter
c_p	specific heat, Btu/lb-°F
c_t	specific heat distribution function for the latent heat, Btu/ft^3-°F

c_i	$= -2\bar{h}^2/[\bar{h}_{i-1}(\bar{h}_{i-1} + \bar{h}_i)]$ or $= -2\overline{hg}/[\bar{h}_{i-1}(\bar{h}_{i-1} + \bar{h}_i)] \times k_o^{(1)} I^{(1)}/k_o I_o$
d_1	parameter
$d_{i,j}$	$= -f_{i,j} - e_{i,j}$
$\underline{D}_i$	a tridiagonal matrix whose diagonal entries are positive and off-diagonal entries are negative, defined by Equation III-38
$e_{i,j}$	$= -2\bar{h}\bar{g}/[\bar{g}_j(\bar{g}_{j-1} + \bar{g}_j)]$ or $= -2\bar{h}\bar{g}/[\bar{g}_j(\bar{g}_{j-1} + \bar{g}_j)] \times k_o^{(1)} I^{(1)}/k_o I_o$
erf x	$= \frac{2}{\sqrt{\pi}} \int_0^x e^{-x^2}\, dx$
erfc	$= \frac{2}{\sqrt{\pi}} \int_0^x e^{-x^2}\, dx$
$\underline{E}_i$	an N_y- dimensional vector defined by Equation III-39
E	total internal energy including latent heat and sensible heat, Btu/ft^3
E_t	internal distribution function for latent heat, Btu/ft^3
$E_{i,j}$	total internal energy of mesh region (i,j) at time t
$E_{i,j,0}$	total internal energy of mesh region (i,j) at time $t - \Delta t$
f	volume fraction occupied by vapor
$f(U_{i,j}^{(1)})$	the transformation of $u_{i,j}^{(2)}$ from $u^{(2)}$ domain to $u^{(1)}$ domain
$f(U_{i,j}^{(2)})$	the transformation of $u_{i,j}^{(1)}$ from $u^{(1)}$ domain to $u^{(2)}$ domain

$f_{i,j}$	$= -2\overline{hg}/[\bar{g}_{j-1}(\bar{g}_{j-1} + \bar{g}_j)]$ or $= -2\overline{hg}/[\bar{g}_{j-1}(\bar{g}_{j-1} + \bar{g}_j)] \times k_o^{(1)} I^{(1)}/k_o I_o$
F	dependent variable
$\bar{g}_j$	$= g_j/a$
$\bar{g}$	arbitrarily chosen from g_j
h	heat transfer coefficient, Btu/ft^2-hr-°F
h_i	mesh spacing in the x-direction (= $x_{i+1} - x_i$), ft
$\bar{h}_i$	h_i/a
$\bar{h}$	arbitrarily chosen from $\bar{h}_i$
h_a	constant in Equation III-41
h_b	constant in Equation III-41
$h_f a$	overall heat transfer coefficient, Btu/ft^2-hr-°F
$h_g a$	heat transfer coefficient of gas film, Btu/ft^2-hr-°F
$h_l a$	heat transfer coefficient of liquid film, Btu/ft^2-hr-°F
H	latent heat of phase change, Btu/ft^3
$\underline{H}$	an N x N matrix defined by Equation III-28
$\underline{H}_j$	a tridiagonal matrix whose diagonal entries are $a_{i,j}$ and off-diagonal entries are $b_{i,j}$ and $c_{i,j}$, $1 \le i \le N_x$
H_i	$= -h_a\, a(T_1 - T_2)^{h_b - 1}\bar{h}_i/k_o I$
I	$= \int_o^1 \alpha(\bar{u})\, d\bar{u}$
$I^{(i)}$	$= \int_o^1 \alpha^{(i)}\,(\bar{u}^{(i)})\, d\bar{u}^{(i)}$
$\underline{I}$	identity matrix
$J_o(x)$	zero order Bessel function of the first kind
k, k(T)	thermal conductivity, Btu/hr-ft-°F
k^+	defined by Equation II-9
k^-	defined by Equation II-10
$k^{(i)}$	thermal conductivity of component i, Btu/hr-ft-°F

ℓ	liquid flow rate, lb/ft^2-hr
L^{-1}	inversion of Laplace transformation
N	number of unknown values of $u_{i,j}$, $1\leq i<N_x$, $1\leq j<N_y$
N_x	number of mesh points in the x-direction
N_y	number of mesh points in the y-direction
N_z	number of mesh points in the z-direction
p	Laplace transformation variable corresponding to ξ
q	Laplace transformation variable corresponding to μ
$\bar{q}$	heat flux across the exposed boundary Btu/hr-ft^2
q_1, q_2	the rates of heat transferred by conduction or convection into a mesh region (i,j) through its sides 1 and 2, Btu/hr
q_3, q_4	the rates of heat transferred out of a mesh region (i,j) through its sides 3 and 4, Btu/hr
Q	volumetric rate of heat generated, Btu/ft^3
$\bar{Q}$	total heat flux, Btu/ft^2
r	radial distance, ft
r_o	radius of cylinder or sphere, ft
$\bar{r}$	$\int_0^{\gamma_o/\gamma} \frac{d\gamma}{\gamma^\eta}$, transformed coordinate
R	radial interface of the solid-liquid, ft
$\bar{R}$	$\int_0^{\gamma_o/\gamma} \frac{d\gamma}{\gamma^\eta}$, transformed coordinate
S	cross sectional area per unit length, ft^2/ft
i	defined by Equation III-68 and Equation III-74
$S_{i,j}$	defined by Equation III-24, Equation III-47 or Equation III-64

S	an N-dimensional vector whose entries are the known values of $S_{i,j}$, $1 \leq i \leq N_x$, $1 \leq j \leq N_y$
t	time, hr
t'	$= t - z\ [f\ (\rho_g c_g)_o / v_o c_{go}]$
T	temperature, °F
T_o	the temperature of soil surface, °F
T_1, T_2	two reference temperatures in the interested region, °F
T_L	boiling temperature of LNG, °F
T_∞	initial temperature of medium, °F
U	dimensionless temperature
$\bar{U}$	dimensionless temperature $[= (T - T_2)/(T_1 - T_2)]$
v	vapor flow rate, lb/ft^2-hr
$\underline{V}$	an N x N matrix defined by Equation III-29
$\underline{V}_i$	a tridiagonal matrix whose diagonal entries are $d_{i,j}$ and off-diagonal entries are $e_{i,j}$ and $f_{i,j}$, $1 \leq j \leq N_y$
w	transformation variable defined by Equation II-12
w_{ij}	defined by Equation III-45
x,y,z	cartesian coordinates
X	dimensionless temperature of high expansion foam $[= (T_f - T_\infty)/(T_L - T_\infty)]$
X(t)	the interfacial position of frozen and unfrozen soil
Y	dimensionless temperature of LNG vapor $[= (T_g - T_\infty)/(T_L - T_\infty)]$
$\bar{z}$	$x/\sqrt{t}$
Z	root of transcendental Equation IV-22

Greek Letters

α	thermal diffusivity (= k/c), ft^2/hr
$\alpha(\bar{U})$	defined by Equation III-6
β	$= (\alpha-1)/(\alpha+1)$
γ	accelerating parameter of alternating direction implicit procedure
δ	thickness of insulation, ft
$\bar{\delta}$	thickness of frozen layer, ft
δt	a short time period, hr
δT	half transition temperature interval, °F
$\delta T_f, \delta T_g$	small increment of T_f and T_g respectively
δz	small increment of z
$\Delta v, \Delta t, \Delta z$	increment of v, t, and z respectively
$\Delta\tau\ \Delta\hat{\tau}$	increment of τ and $\hat{\tau}$ respectively
ΔT	$= T_o - T_L$, °F
ε	defined by Equation II-15
ε'	defined by Equation III-19
η	parameter; $\eta=0$ for spherical coordinate; $\eta=1$ for cylindrical coordinate
ξ	$= z'(h_f a)/(v_o c_{go})$
μ	$= (h_f a)_o t'/[(\rho_f c_f)(1-f)]$
κ	$= \sqrt{\alpha_I/\alpha_S}$
α	$= k_S \kappa / k_I$
$\lambda_{i,j,l}$	defined by Equation II-6
ρ	density, lb/ft^3
τ	dimensionless time, $\tau = k_o t/c_o a^2$

$\hat{\tau}$	$= \tau/\bar{h}\bar{g}$ or $\tau/\bar{h}^2$
Γ_i^{n+1}	dimensionless temperature difference between nth iteration and n+1st iteration of $u_i = (u_i^{n+1} - u_i^n)$
$\Gamma_{i,j}^{n+1}$	dimensionless temperature difference between nth iteration and n+1st iteration of $u_{i,j} = (u_{i,j}^{n+1} - u_{i,j}^n)$
$\underline{\Gamma}_i^{n+1}$	a vector whose entries are the unknown values of $\Gamma_{i,j}^{n+1}$ falling on the ith grid-line parallel to the x-axis
$\underline{\Gamma}^{n+1}$	an N-dimensional vector whose entries are the U unknown values of $\Gamma_{i,j}^{n+1}$
$\Gamma_{i,j}^{*}$	dimensionless temperature change over the half iteration
$\underline{\Gamma}_j^{*}$	a vector whose entries are the unknown values of $\Gamma_{i,j}^{*}$ falling on the jth grid-line parallel to the y-axis
$\underline{\Gamma}^{*}$	an N-dimensional vector whose entries are the N unknown values of $\Gamma_{i,j}^{*}$
$\Gamma_{i,j}^{n}$	dimensionless temperature difference after nth iteration
$\underline{\Gamma}^{n}$	an N-dimensional vector whose entries are the known values of $\Gamma_{i,j}^{n}$
θ	dimensionless transition temperature $[=(T_t-T_\infty)/(T_\ell-T_\infty)]$
$\underline{\theta}$	an N-dimensional source vector
ϕ_i	defined by Equation III-68 or Equation III-74
$\phi_{i,j}$	defined by Equation III-23 or Equation III-63
$\underline{\phi}$	an N x N diagonal matrix whose diagonal entries are the values of $\phi_{i,j}$

ϕ	physical parameter; the ratio of the product of specific heat and maximum temperature difference and latent heat
ω	constant defined in Equation VII-33

Subscripts

f	refers to high expansion foam
g	refers to LNG vapor
i	evaluated at $x = x_i$ or $z = z_i$
j	evaluated at $y = y_j$
$i \pm 1/2$	evaluated at $x = x_i + 1/2h_i$ and $x = x_i - 1/2h_{i-1}$ respectively
$j \pm 1/2$	evaluated at $y = y_j + 1/2\, g_j$ and $y = y_j - 1/2g_{j-1}$ respectively
i,j	evaluated at point (x_i, y_j)
I	refers to insulation
S	refers to soil
t	phase transition
w	wall
0	reference
1	refers to frozen soil
2	refers to unfrozen soil

Superscripts

n	iteration level
$*$	the half iteration
h	time level; $t = h\Delta t$
(i)	refers to the i^{th} component

BIBLIOGRAPHY

1. Allen, D. N. de G., and Severn, R. T. "The Application of Relaxation Method to the Solution of Non-Elliptic Partial Differential Equations. III. Heat Conduction with Change of State, in Two Space Dimensions." *Quart. J. Mech. and Appl. Math.*, *15* (1962):53-62.

2. Aris, R., and Amundson, N. R. "Mathematical Methods in Chemical Engineer." *First Order Partial Differential Equations with Applications*, *Vol. 2*. Englewood Cliffs, NJ: Prentice-Hall, Inc., 1973.

3. Bankoff, S. G. *Advances in Chemical Engineering*, *Vol. 5*, T. B. Drew, *et al.*, eds. New York: Academic Press, 1964, pp. 75-150.

4. Bellman, R. E., and Kalaba, R. E. *Quasilinearization and Nonlinear Boundary-Value Problems*. New York: American Elsevier Publishing Company, Inc., 1965.

5. Boley, B. A. "A Method of Heat-Conduction Analysis of Melting and Solidifying Slabs." *J. Math. Phys.*, *15* (1961):300-313.

6. Boley, B. A. "A General Starting Solution for Melting and Solidifying Slabs." *Int. J. Engr. Sci.*, *6* (1968):89-111.

7. Boley, B. A. and Yagoda, H. P. "The Starting Solution for Two-Dimensional Heat Conduction Problems with Phase Change." *Quart. Appl. Math.*, *27* (1969):223-246.

8. Boley, B. A. "Uniqueness in a Melting Slab with Space and Time-Dependent Heating." *Quart. Appl. Math.*, *XXVII* (1970):481-487.

9. Boley, B. A., and Yagoda, H. P. "The Three-Dimensional Starting Solution for a Melting Slab." *Proc. Roy. Soc.* (London), *A-323* (1971):89-110.

10. Bonacina, C.; Comini, G.; Fasano; and Primicerio, M. "Numerical Solution of Phase-Change Problem." *Int. J. Heat Mass Transfer*, *16* (1973):1825-1832.

11. Brown, L. E. and Colver, C. P. "Nucleate and Film Boiling Heat Transfer to Liquefied Natural Gas." *Adv. Cry. Engr.*, *13* (1968):647-654.

12. Brown, L. E. Private Communication.

13. Budak, B. M.; Sobol'eva, E. N.; and Uspenskii, A. B. "A Difference Method with Coefficient Smoothing for the Solution of Stefan Problems." *Zh. Vychisl. Mat. Fize.*, *5* (1965):828-840.

14. Burgess, D., and Zabetakis, M. G. "Fire and Explosion Hazards Associated with Liquefied Natural Gas." J. S. Dept. Interior, Bur. Mines Report 6099 (1962).

15. Bulavin, P. E., and Kashcheev, V. M. "Solution of the Non-Homogeneous Heat Conduction Equation for Multi-layered Bodies." *Int. Chem. Engr.*, *5*, (1965):112-115.

16. Cannon, J. R., and Hill, C. D. "On the Movement of a Chemical Reaction Interface." *Indiana Univ. Math. J.*, 20 (1970):429-453.

17. Carnahan, B.; Luther, H. A.; and Wilkes, J. O. "*Applied Numerical Methods.*" New York: John Wiley & Sons, Inc., 1969, pp. 441-448.

18. Carslaw, H. S., and Jaeger, J. C. *Conduction of Heat in Solids.*" Oxford at the Clarendon Press, second edition, 1959.

19. Churchill, S. W. "Heat Transfer Rate and Temperature Field for Underground Storage Tanks." *Soc. Petrol. Eng. J.*, *2* (1962):23-32.

20. Churchill, S. W., and Evans, L. B. "Coefficient for Calculation of Freezing in a Semi-Infinite Region." *J. of Heat Transfer*, *93* (1971):234-236.

21. Churchill, S. W. "Conduction to an Insulated Cylinder from a Semi-Infinite Region." *J. of Heat Transfer*, *92* (1970:188-190.

22. Dana, P. R. Ph.D. Thesis, Iowa State University. Ames, Iowa, 1969.

23. Din, F., ed. *Thermodynamic Functions of Gases* Vol. 3. London: Butterworth, 1961.

24. Drake, E. M.; Harris, S. H.; and Reid, R. C. "Analysis of Vapor Dispersion Experiments." A.G.A. Project IS-3-1: LNG Safety Program Phase II, *Consequences of LNG Spills on Land*, November 1973.

25. Douglas, J., Jr., and Rachford, H. H., Jr. "On the Numerical Solution of Heat Conduction Problems in Two or Three Space Variables." *Trans. Amer. Math. Soc.*, *82* (1956):421-439.

26. Douglas, J., Jr.; Peaceman, D. W.; and Rachford, H. H., Jr. "A Method for Calculating Multi-Dimensional Immiscible Placement." Trans. AIME, 216 (1959):297-308.

27. Douglas, J., Jr., and Jones, B. F., Jr. "One Predictor-Corrector Method for Nonlinear Parabolic Differential Equation." J. Soc. Indust. Appl. Math., 11 (1963): 195-204.

28. Douglas, J., Jr., and Dupont, T. "Galerkin Methods for Parabolic Equations." SIAM J. Num. Anal., 7 (1970):575-626.

29. Elmas, M. "On the Solidification of a Warm Liquid Flowing over a Cold Wall." Int. J. Heat Mass Transfer, 13 (1970):1060-1062.

30. Friedman, A. "The Stefan Problem in Several Space Variables." Trans. of the Amer. Math. Soc. 133 (1968):51-87.

31. Furnas, C. C. "Heat Transfer from a Gas Stream to a Bed of Broken Solids." Trans. Am. Inst. Chem. Engr. 24 (1930):142-193.

32. Goldstein, S., ed. Modern Development in Fluid Dynamics," Vol. 1. Oxford: Oxford University Press, 1938.

33. Goodman, T. R. "The Heat-Balance Integral and Its Application to Problem Involving a Change of Phase." Trans. Am. Soc. Mech. Engrs., 80 (1958):335.

34. Goodman, T. R. "The Heat-Balance Integral--Further Consideration and Refinements." J. Heat Transfer, 83 (1961):83.

35. Goodman, T. R. "Application of Integral Methods to Transient Nonlinear Heat Transfer." Advances in Heat Transfer, Vol. 1 (1964):51.

36. Griffith, M. V., and Horton, G. K. "The Transient Flow of Heat Through a Two-Layer Wall." Proc. Phys. Soc., 58 (1946):481-487.

37. Grimado, P. B., and Boley, B. A. "A Numerical Solution for the Symmetric Melting of Spheres." Int. J. Num. Meth. in Engr., 2 (1970):175-188.

38. Gupta, J. P. "An Approximate Method for Calculating the Freezing Outside Spheres and Cylinders." Chem. Eng. Sci., 28 (1970):1629-1633.

39. Gupta, J. P., and Churchill, S. W. "A Model for the Migration of Moisture During the Freezing of West Sand." AIChE Symposium Series, 69, 131 (1973):192-198.

40. Guzelsu, A. N., and Cakmak, A. S. "Starting Solution for an Ablating Hollow Cyclinder." Int. J. Solids Structures, 6 (1970):1087-1102.

41. Habib, I. S. "Solidification of Semi-Transparent Materials by Conduction and Radiation." Int. J. Heat Mass Transfer, 14 (1971):2161-2164.

42. Habib, I. S. "Solidification of a Semitransparent Cylindrical Medium by Conduction and Radiation." J. of Heat Transfer, 95 (1973):37-41.

43. Hashemi, H. T. "Heat Conduction with Change of Phase. Ph.D. Thesis. University of Oklahoma, Norman, Oklahoma, 1965.

44. Hashemi, H. T., and Sliepcevich, C. M. "Numerical Solution of the Two-Dimensional Transient Temperature Distribution in Melting and Solidifying Composite Media." University of Oklahoma Research Institute, Norman, Oklahoma, 1966.

45. Hashemi, H. T., and Sliepcevich, C. M. "Heat Leak to In-Ground Storage of LNG." Chem. Eng. Prog., 63 (1967): 68-72.

46. Hashemi, H. T., and Sliepcevich, C. M. "Effect of Seepage Stream on Artificial Soil Freezing." J. Soil Mech. Found. Div., ASCE, 99 (1973):307-322.

47. Hensel, S. L., Jr., and Treybal, R. E. "Air-Water Contact-Adiabatic Humidification of Air with Water in a Packed Tower." Chem. Eng. Prog., 48 (1952):362-370.

48. Hougen, O. A., and Watson, K. M. Chem. Proc. Prin., Part III. New York: Wiley, 1947.

49. Humbert-Basset, R., and Montet, A. "Dispersion dans l'Atmosphere d'un Nuage Gazeux forme par Epandage de G. N. L. sur le Sol." Proceedings, Third International Conference on Liquefied Natural Gas, Washington, DC, September 24-28, 1972.

50. Imber, M., and Huang, P. N. S. "Phase Change in a Semi-Infinite Solid Thermal Properties." Int. J. Heat Mass Transfer, 16 (1973):1951-1954.

51. Jakob, M. "Heat Transfer," Volume 1. New York: John Wiley & Son, Inc., 1947, pp. 97.

52. Kehoe, P. "A Moving Boundary Problem with Variable Diffusivity." Chem. Eng. Sci., 27 (1972):1184-1185.

53. Kersten, M. S. "Thermal Properties of Soils." Bulletin No. 28, University of Minnesota, Minneapolis, Minnesota, 1949.

54. Khakimo, K. R. "Voprosy Teorii i Praktiki Iskusstvennogo Zamorazhivaniya Gruntov." Izdat elstvo Akademic Nauk Moscow, USSR, 1959. U. S. Department of Commerce, TT66-41051.

55. Kuo, M. T. "Filter Cake Washing Performance." AIChE Journal, 6 (1960):566-568.

56. Lame, G., and Clapeyron, B. P. E. "Memoire sur la solidification par refroidissement dun globe liquide." Ann Chimie Phys., 47 (1931):250-256.

57. Lapidus, L. Digital Computation for Chemical Engineers. New York: McGraw-Hill Company, 1962.

58. Lazaridis, A. "A Numerical Solution of the Multidimensional Solidification (or Melting) Problem." Int. J. Heat Mass Transfer, 13 (1970):1459-1477.

59. Lederman, J. M., and Boley, B. A. "Axi- symmetric Melting or Solidification of Circular Cylinders." Int. J. Heat Mass Transfer, 13 (1970):413-427.

60. Lee, E. S. Quasilinearization and Invariant Imbedding. New York: Academic Press, 1968.

61. Lee, Y. F., and Boley, B. A. "Melting of an Infinite Solid with a Spherical Cavity." Int. J. Engr. Sci., 11 (1973):1277-1295.

62. Lock, G. S. H. "On the Perturbation of the Ice-Water Layer Problem." Int. J. Heat Mass Transfer, 14 (1971): 642-644.

63. Lock, G. S. H. "On the Use of Asymptotic Solutions to Plane Ice-Water Problem." J. Glaciol, 8 (1969):285.

64. Lock, G. S. H.; Gunderson, J. R.; Quon, D.; and Donnelly, J. K. "A Study of One-Dimensional Ice Formation with Particular Reference to Periodic Growth and Decay." Int. J. Heat Mass Transfer, 12 (1969):1343-1352.

65. Lockwood, J. D., and Mulholland, G. P. "Diffusion through Laminated Composite Cylinders Subjected to a Circumferentially Varying External Heat Flux." J. of Heat Transfer, 95 (1973):487-491.

66. McAdams, W. H.; Pohlenz, J. B.; and St. John, R. C. "Transfer of Heat and Mass Between Air and Water in a Packed Tower." Chem. Eng. Prog., 45 (1949):241-252.

67. Meyer, G. H. "Multidimensional Stefan Problems." SIAM J. Num. Anal., 10 (1973):522-538.

68. Meyer, G. H. "Numerical Solution of Systems of Nonlinear Algebraic Equations." New York: Academic Press, Inc., 1973.

69. Mickley, H. S.; Sherwood, T. L,; and Reed, C. E. Applied Mathematics in Chemical Engineering. New York: McGraw Hill Book Company, Inc., 1957.

70. Muehlbauer, J. C., and Sunderland, J. E. "Heat Conduction with Freezing or Melting." Appl. Mech. Rev., 18 (1965):951-959.

71. Mulholland, G. P., and Cobble, M. H. "Diffusion through Composite Media." Int. J. Heat Mass Transfer, 15 (1972):147-160.

72. Neumann, F. Unpublished lectures (1835-40?). Reported by H. Weber in Die partiellen Differential Gleichunger der Mathematischen Physik, nach Riemann's Verlesungen, 4th ed., Vol. II. Berlin: Braunschweig, 1901, pp. 118-122.

73. Ozisik, M. N. Boundary Value Problems of Heat Conduction. Scranton, PA: International Textbook Company, 1968.

74. Parker, R. O., and Spata, J. K. "Downwind Travel of Vapors from Large Pools of Cryogenic Liquids." Proceedings, First International Conference on LNG, Paper No. 24, Chicago, 1968.

75. Parker, R. O. "Study of Downwind Vapor Travel from LNG Spills." Proceedings, A.G.A. Operating Section Distribution Conference, 1970, D267-D275.

76. Parlange, J. Y. "Theory of Water-Movement in Soils: I, One-dimensional Absorption." Soil Science, 111 (1971): 134-137.

77. Peaceman, D. W., and Rachford, H. H., Jr. "The Numerical Solution of Parabolic and Ellipitic Differential Equations." J. Soc. Indust. Appl. Math., 3 (1955): 28-41.

78. Pechoc, V. "Generalized Numerical Solution of Heat Equation with Moving Boundary Conditions." Collection Czechoslov. Chem. Commun., 36 (1971):3222-3235.

79. Pedroso, R. I., and Domoto, G. A. "Perturbation Solution for Spherical Solidification of Saturated Liquids." J. of Heat Transfer, 95 (1973):42-46.

80. Pedroso, R. I., and Domoto, G. A. "Exact Solution by Perturbation Method for Planar Solidification of a Saturated Liquid with Convection at the Wall." Int. J. Heat Mass Transfer, 16 (1973):1816-1819.

81. Perry, J. H. Chemical Engineer's Handbook, 4th ed. New York: McGraw-Hill, 1963.

82. Poots, G. "An Approximate Treatment of a Heat Conduction Problem Involving a Two-Dimensional Solidification Front." Int. J. Heat Mass Transfer, 5 (1962):339-348.

83. Ralston, A., and Wilf, H. S., eds. Mathematical Methods for Digital Computers. New York: John Wiley, 1960.

84. Rosenbrock, H. H., and Storey, C. Computational Techniques for Chemical Engineers. Oxford: Pergamon Press, 1966.

85. Rubinstein, L. I. The Stefan Problem. Riga: Latvia State University Computing Center, 1967.

86. Ruoff, A. L. "An Alternate Solution of Stefan's Problem." Quart. Appl. Math., 16 (1958):197-210.

87. Samarskii, A. A., and Moiseynko, B. D. "An Economic Continuous Calculation Scheme for the Stefan Multidimensional Problem." Zh. Vychisl, Mat. Mat. Fix., 5 (1965):816-827.

88. Savino, J. M., and Siegel, R. "An Analytical Solution for Solidification of a Moving Warm Liquid onto an Isothermal Cold Wall." Int. J. Heat Mass Transfer, 12 (1969):803-809.

89. Saylor, P. E., and Sebastin, J. D. "Calculation of Optimum Parameters for Alternating Direction Implicit Procedures." Comm, ACM, 16 (1973):663-635.

90. Schumann, T. E. W. "Heat Transfer: A Liquid Flowing Through a Porous Prism." J. of the Franklin Inst., 208 (1929):405:416.

91. Sciance, C. T.; Colver, C. P.; and Sliepcevich, C. M. "Pool Boiling of Methane Between Atmospheric Pressure and the Critical Pressure." Adv. Cry. Engr., Vol. 12. New York: Plenum Press, 1967, pp. 395-407.

92. Sciance, C. T.; Colver, C. P.; and Sliepcevich, C. M. "Nucleate Pool Boiling and Burnout of Liquefied Hydrocarbon Gases." Chem. Engr. Prog. Sym. Ser., 63, 77 (1967):109-114.

93. Sciance, C. T.; Colver, C. P.; and Sliepcevich, C. M. "Film Boiling Measurement and Correlation for Liquefied Hydrocarbon Gases." *Chem. Eng. Prog. Sym. Ser.*, *63*, 77 (1967):115-119.

94. Seider, W. D., and Churchill, S. W. "The Effect of Insulation on Freezing Front Motion." *Chem. Eng. Prog. Sym. Ser.*, *61*, 59 (1965):179-184.

95. Selim, M. S., and Seagrave, R. C. "Solution of Moving-Boundary Transport Problems in Finite Media by Integral Transformations. I. Problems with a Plane Moving Boundary." *Ind. Eng. Chem. Fund.*, *12* (1973): 1-8.

96. Selim, M. S., and Seagrave, R. C. "Solution of Moving-Boundary Transport Problems in Finite Media by Integral Transforms. II. Problems with a Cylindrical or Spherical Moving Boundary." *Ind. Eng. Chem. Fund.*, *12* (1973):9-13.

97. Selim, M. S., and Seagrave, R. C. "Solution of Moving-Boundary Transport Problems in Finite Media by Integral Transforms. III. The Elution Kinetics of the Copper Ammine Complex from a Cation-Exchange Resin." *Ind. Eng. Chem. Fund.*, *12* (1973):14-17.

98. Shanks, D. "Nonlinear Transformation of Divergent and Slowly Convergent Sequence." *J. of Math. and Phys.*, *34* (1955):1.

99. Shih, Y. P., and Tsay, S. Y.. "Analytical Solutions for Freezing a Saturated Liquid Inside or Outside Cylinders." *Chem. Eng. Sci.*, *25* (1971):809-816.

100. Shih, Y. P., and Chou, T. C. "Analytical Solutions for Freezing a Saturated Liquid Inside or Outside Spheres." *Chem. Eng. Sci.*, *26* (1971):1787-1793.

101. Stefan, J. "Ueber einige Problem der Theories des Warmeleitung, Sitzungsberichte Klasi." *Akad*. *Wissenschaften*, Vienna, 98, Part II (1889):473-484.

102. Tao, L. E. "Generalized Numerical Solutions of Freezing a Saturated Liquid in Cylinders and Spheres." *AIChE J.*, *13* (1967):165-169.

103. Tani, I. "On the Approximate Solution of the Laminar Boundary-Layer Equations." *J. Aero. Sci.*, *21* (1954):487.

104. Tien, L. C., and Churchill, S. W. "Freezing Front Motion and Heat Transfer Outside an Infinite Isothermal Cylinder." AIChE J., 11 (1965):790-793.

105. Tien, C. T. "Heat Transfer in Cryogenic Insulation." Cry. Tech., 7 (1971):157-159.

106. Tihonov, A. N., and Samarskii, A. A. The Equations of Mathematical Physics, 2nd ed., edited by Gittl. Moscow, 1953.

107. Tittle, C. W. "Boundary Value Problems in Composite Media: Quasi-Orthogonal Functions." J. Appl. Phys., 36 (1965):1486-1488.

108. Varga, R. S. Matrix Iterative Analysis. Englewood Cliffs, New Jersey: Prentice-Hall, Inc., 1962.

109. Vishnev, I. P. "General Relationship for Heat Transfer During Boiling of Cryogenic Liquids." Int. Chem. Engr., 14 (1974):8-15.

110. Voelker, D., and Doetsch, G. "Die Zweidimensionale Laplace Transformation." Verlag Birkhauser Basel, 1950.

111. Welker, J. R. Private communication, University Engineers, Inc., 1973.

112. Wesson, H. R.; Welker, J. R.; and Brown, L. E. "Control LNG-Spill Fires." Hydrocarbon Proc., 51, 12 (1972): 61-64.

113. Wesson, H. R.; Welker, J. R.; Brown, L. E.; and Sliepcevich, C. M. "Fight LNG Fires with Foam?" Hydrocarbon Proc., 52, 10 (1973):165-171.

114. Wilcox, D. C. "An Empirical Vapor Dispersion Law for LNG Spill." TRW Systems, Inc., Report on A.G.A. Project IS-33-4, 1971.

115. Wilkenson, J. H. Rounding Errors in Algebraic Processes. Englewood Cliffs, New Jersey: Prentice-Hall, 1963.

116. Yansinsky, J. B. "The Solution of Three Dimensional Composite Media with Heat Conduction Problems by Synthesis Methods." J. of Heat Transfer, 93 (1971): 221-228.

117. Yoshida, F., and Tanaka, T. "Air-Water Contact Operations in a Packed Column." Ind. and Eng. Chem., 43 (1951).

APPENDICES

APPENDIX A

BOIL-OFF RATES OF LNG

The calculated boil-off rates of LNG from Models I-4, I-5, I-6, I-9, I-10, II-1, and II-3 were fitted by the polynomial equations in terms of time, t (sec); i.e.,

$$v = a_1 + b_1t + c_1t^2 + d_1t^3 + e_1t^4$$

The parameters of polynomial equation for these models are summarized in the following tables.

TABLE A-1

PARAMETERS OF POLYNOMIAL EQUATION FOR MODEL I-4

a_1	b_1	c_1	d_1	e_1	Time Range sec
$0.326285\mathrm{x}10^{4}$	$-0.331840\mathrm{x}10^{5}$	$0.173353\mathrm{x}10^{7}$	$-0.291194\mathrm{x}10^{8}$	0.0	0.0-0.032568
$0.359463\mathrm{x}10^{4}$	$0.250312\mathrm{x}10^{4}$	$-0.911288\mathrm{x}10^{6}$	$0.994777\mathrm{x}10^{7}$	$-0.308135\mathrm{x}10^{8}$	0.032568-0.145336
$0.958670\mathrm{x}10^{3}$	$0.179217\mathrm{x}10^{5}$	$-0.146466\mathrm{x}10^{6}$	$0.391367\mathrm{x}10^{6}$	$-0.347031\mathrm{x}10^{6}$	0.145336-0.446688
$0.140094\mathrm{x}10^{4}$	$-0.192895\mathrm{x}10^{4}$	$0.155691\mathrm{x}10^{4}$	$-0.582525\mathrm{x}10^{3}$	$0.798412\mathrm{x}10^{2}$	0.446688-2.713716
$0.508689\mathrm{x}10^{3}$	$-0.929159\mathrm{x}10^{2}$	$0.968343\mathrm{x}10^{1}$	$-0.401818\mathrm{x}10^{0}$	$0.274528\mathrm{x}10^{-2}$	2.713716-11.22155
$0.582681\mathrm{x}10^{3}$	$-0.750153\mathrm{x}10^{2}$	$0.428642\mathrm{x}10^{1}$	$-0.846832\mathrm{x}10^{-1}$	0.0	11.22155-20.40478
$0.190714\mathrm{x}10^{3}$	$-0.513503\mathrm{x}10^{1}$	$0.884625\mathrm{x}10^{-1}$	$-0.771062\mathrm{x}10^{-3}$	$0.263519\mathrm{x}10^{-5}$	20.40478-85.39558
$0.941392\mathrm{x}10^{2}$	$-0.592306\mathrm{x}10^{0}$	$0.216377\mathrm{x}10^{-2}$	$-0.336582\mathrm{x}10^{-5}$	$0.127551\mathrm{x}10^{-8}$	85.39558-308.2785
$0.500192\mathrm{x}10^{2}$	$-0.907555\mathrm{x}10^{-1}$	$0.972457\mathrm{x}10^{-4}$	$-0.408699\mathrm{x}10^{-7}$	0.0	308.2785-781.5239
$0.335074\mathrm{x}10^{2}$	$-0.266942\mathrm{x}10^{-1}$	$0.120738\mathrm{x}10^{-4}$	$-0.202872\mathrm{x}10^{-8}$	0.0	781.5239-1984.427
$0.204687\mathrm{x}10^{2}$	$-0.577789\mathrm{x}10^{-2}$	$0.886115\mathrm{x}10^{-6}$	$-0.495699\mathrm{x}10^{-10}$	0.0	1984.427-7160.757

TABLE A-2

PARAMETERS OF POLYNOMIAL EQUATION FOR MODEL I-5

a_1	b_1	c_1	d_1	e_1	Time Range sec
0.144439×10^{3}	-0.115355×10^{3}	0.356293×10^{3}	-0.442447×10^{3}	0.180899×10^{3}	0.0-1.070820
0.131819×10^{3}	-0.693064×10^{1}	0.476931×10^{0}	-0.190807×10^{-1}	0.299651×10^{-3}	1.070820-23.97743
0.963589×10^{2}	-0.107637×10^{1}	0.866587×10^{-2}	-0.345985×10^{-4}	0.521820×10^{-7}	23.97743-245.5667
0.494242×10^{2}	-0.101942×10^{0}	0.139771×10^{-3}	-0.968674×10^{-7}	0.261152×10^{-10}	245.5667-1202.327
0.257058×10^{2}	-0.131016×10^{-1}	0.422738×10^{-5}	-0.670858×10^{-9}	0.405618×10^{-13}	1202.327-5835.597

TABLE A-3

PARAMETERS OF POLYNOMIAL EQUATION FOR MODEL I-6

a_1	b_1	c_1	d_1	e_1	Time Range sec
0.113927×10^{3}	-0.122130×10^{2}	0.219246×10^{2}	-0.124308×10^{2}	0.0	0.0-1.038132
0.112011×10^{3}	-0.100921×10^{1}	0.218382×10^{-1}	-0.344528×10^{-3}	0.0	1.038132-23.46839
0.107552×10^{3}	-0.485629×10^{0}	-0.629194×10^{-3}	0.106370×10^{-4}	0.0	23.46839-79.30079
0.112610×10^{3}	-0.695259×10^{0}	0.225888×10^{-2}	-0.276970×10^{-5}	0.0	79.30079-243.1943
0.679966×10^{2}	-0.183705×10^{0}	0.269047×10^{-3}	-0.148245×10^{-6}	0.0	243.1943-677.3759
0.604636×10^{2}	-0.114882×10^{0}	0.117946×10^{-3}	-0.565970×10^{-7}	0.101705×10^{-10}	677.3759-1984.427
0.204687×10^{2}	-0.577789×10^{-2}	0.886115×10^{-6}	$-0.495699 \times 10^{-10}$	0.0	1984.427-7160.757

TABLE A-4

PARAMETERS OF POLYNOMIAL EQUATION FOR MODEL I-9 WITH 0.045 INCHES POLYURETHANE INSULATION

a_1	b_1	c_1	d_1	e_1	Time Range sec
0.550315×10^{2}	-0.736577×10^{3}	0.698561×10^{4}	-0.373928×10^{5}	0.843824×10^{5}	0.0-0.139856
0.304821×10^{2}	-0.118080×10^{3}	0.258457×10^{3}	-0.205724×10^{3}	0.0	0.139856-0.484632
0.147529×10^{2}	-0.126973×10^{2}	0.933526×10^{1}	-0.227933×10^{1}	0.0	0.484632-1.761984
0.908225×10^{1}	-0.103449×10^{0}	0.143140×10^{-1}	-0.898984×10^{-3}	0.0	1.761984-5.540759
0.875276×10^{1}	-0.929283×10^{-2}	0.410491×10^{-4}	-0.642962×10^{-7}	0.0	5.540759-376.6318
0.812584×10^{1}	-0.131090×10^{-2}	0.198246×10^{-6}	-0.119238×10^{-10}	0.0	376.6318-7582.64

TABLE A-5

PARAMETERS OF POLYNOMIAL EQUATION FOR MODEL I-10 WITH 0.135 INCHES POLYURETHANE INSULATION

a_1	b_1	c_1	d_1	e_1	Time Range sec
0.114385×10^{3}	-0.229855×10^{4}	0.597661×10^{5}	-0.527858×10^{7}	0.108108×10^{9}	0.0-0.032306
0.636691×10^{2}	-0.896997×10^{3}	0.789323×10^{4}	-0.358773×10^{5}	0.649402×10^{5}	0.032306-0.162112
0.374831×10^{2}	-0.208590×10^{3}	0.703392×10^{3}	-0.115890×10^{4}	0.732648×10^{3}	0.162112-0.519552
0.156302×10^{2}	-0.162316×10^{2}	0.103241×10^{2}	-0.320240×10^{1}	0.379034×10^{0}	0.519552-2.911751
0.662263×10^{1}	-0.127935×10^{1}	0.157819×10^{0}	-0.871174×10^{-2}	0.178427×10^{-3}	2.911751-17.3995
0.259194×10^{1}	-0.113176×10^{-2}	0.341777×10^{-5}	-0.429199×10^{-8}	0.0	17.3995-376.6318
0.242445×10^{1}	-0.559928×10^{-4}	0.279173×10^{-8}	-0.968078×10^{-13}	0.0	376.6318-10092.23

TABLE A-6

PARAMETERS OF POLYNOMIAL EQUATION FOR MODEL I-10 WITH 0.045 INCHES POLYURETHANE INSULATION

a_1	b_1	c_1	d_1	e_1	Time Range sec
0.114385×10^{3}	-0.229855×10^{4}	0.597661×10^{5}	-0.527858×10^{7}	0.108108×10^{9}	0.0-0.032306
0.636691×10^{2}	-0.896997×10^{3}	0.789323×10^{4}	-0.358773×10^{5}	0.649402×10^{5}	0.032306-0.162112
0.315639×10^{2}	-0.129019×10^{3}	0.322238×10^{3}	-0.380553×10^{3}	0.171128×10^{3}	0.162112-0.744336
0.147529×10^{2}	-0.126973×10^{2}	0.933526×10^{1}	-0.227933×10^{1}	0.0	0.744336-1.761984
0.908225×10^{1}	-0.103449×10^{0}	0.143140×10^{-1}	-0.898984×10^{-3}	0.0	1.761984-5.540759
0.875276×10^{1}	-0.929283×10^{-2}	0.410491×10^{-4}	-0.642962×10^{-7}	0.0	5.540759-376.6318
0.812584×10^{1}	-0.131090×10^{-2}	0.198246×10^{-6}	$-0.119238 \times 10^{-10}$	0.0	376.6318-5782.64

TABLE A-7

PARAMETERS OF POLYNOMIAL EQUATION FOR MODEL I-10 WITH 1.224 INCHES POLYURETHANE INSULATION

a_1	b_1	c_1	d_1	e_1	Time Range sec
$0.114385\mathrm{x}10^{3}$	$-0.229855\mathrm{x}10^{4}$	$0.597661\mathrm{x}10^{5}$	$-0.527858\mathrm{x}10^{7}$	$0.108108\mathrm{x}10^{9}$	0.0-0.032306
$0.636691\mathrm{x}10^{2}$	$-0.896997\mathrm{x}10^{3}$	$0.789323\mathrm{x}10^{4}$	$-0.358773\mathrm{x}10^{5}$	$0.649402\mathrm{x}10^{5}$	0.032306-0.162112
$0.374831\mathrm{x}10^{2}$	$-0.208590\mathrm{x}10^{3}$	$0.703392\mathrm{x}10^{3}$	$-0.115890\mathrm{x}10^{4}$	$0.732648\mathrm{x}10^{3}$	0.162112-0.519552
$0.156301\mathrm{x}10^{2}$	$-0.162312\mathrm{x}10^{2}$	$0.103234\mathrm{x}10^{2}$	$-0.320156\mathrm{x}10^{1}$	$0.378672\mathrm{x}10^{0}$	0.519552-2.911751
$0.649930\mathrm{x}10^{1}$	$-0.117436\mathrm{x}10^{1}$	$0.130581\mathrm{x}10^{0}$	$-0.704768\mathrm{x}10^{-2}$	$0.144166\mathrm{x}10^{-3}$	2.911751-17.3995
$0.276138\mathrm{x}10^{1}$	$-0.905629\mathrm{x}10^{-1}$	$0.187719\mathrm{x}10^{-2}$	$-0.194143\mathrm{x}10^{-4}$	$0.779416\mathrm{x}10^{-7}$	17.3995-78.15238
$0.137441\mathrm{x}10^{1}$	$-0.111810\mathrm{x}10^{-1}$	$0.576346\mathrm{x}10^{-4}$	$-0.148629\mathrm{x}10^{-6}$	$0.149224\mathrm{x}10^{-9}$	78.14238-326.4802
$0.644131\mathrm{x}10^{0}$	$-0.116985\mathrm{x}10^{-2}$	$0.135087\mathrm{x}10^{-5}$	$-0.537292\mathrm{x}10^{-9}$	0.0	326.4802-953.0998
$0.291931\mathrm{x}10^{0}$	$-0.278300\mathrm{x}1\mathrm{o}^{-5}$	$0.130735\mathrm{x}10^{-9}$	0.0	0.0	953.0998-11642.39

TABLE A-8

PARAMETERS OF POLYNOMIAL EQUATION FOR MODEL I-10 WITH 1.944 INCHES POLYURETHANE INSULATION

a_1	b_1	c_1	d_1	e_1	Time Range sec
0.114385×10^{3}	-0.229855×10^{4}	0.597661×10^{5}	-0.527858×10^{7}	0.108108×10^{9}	0.0-0.032306
0.636691×10^{2}	-0.896997×10^{3}	0.789323×10^{4}	-0.358773×10^{5}	0.649402×10^{5}	0.032306-0.162112
0.374831×10^{2}	-0.208590×10^{3}	0.703392×10^{3}	-0.115890×10^{4}	0.732648×10^{3}	0.162112-0.519552
0.156301×10^{2}	-0.162312×10^{2}	0.103234×10^{2}	-0.320156×10^{1}	0.378672×10^{0}	0.519552-2.911751
0.649930×10^{1}	-0.117436×10^{1}	0.130581×10^{0}	-0.704768×10^{-2}	0.144166×10^{-3}	2.911751-17.3995
0.276138×10^{1}	-0.905629×10^{-1}	0.187719×10^{-2}	-0.194143×10^{-4}	0.779416×10^{-7}	17.3995-78.15238
0.137735×10^{1}	-0.112580×10^{-1}	0.583198×10^{-4}	-0.151011×10^{-6}	0.151674×10^{-9}	78.15238-326.4802
0.641081×10^{0}	-0.109764×10^{-2}	0.107361×10^{-5}	-0.394537×10^{-9}	0.0	326.4802-953.0998
0.415010×10^{0}	-0.315217×10^{-3}	0.149356×10^{-6}	$-0.246974 \times 10^{-10}$	0.0	953.0998-2247.335
0.186153×10^{0}	-0.359008×10^{-5}	0.325406×10^{-9}	$-0.992740 \times 10^{-14}$	0.0	2247.335-15494.83

TABLE A-9

PARAMETERS OF POLYNOMIAL EQUATION FOR MODEL II-1

a_1	b_1	c_1	d_1	e_1	Time Range sec
$0.194199\mathrm{x}10^{4}$	$-0.580700\mathrm{x}10^{4}$	$0.102887\mathrm{x}10^{6}$	$-0.592218\mathrm{x}10^{6}$	0.0	0.0-0.089881
$0.198863\mathrm{x}10^{4}$	$0.360727\mathrm{x}10^{4}$	$-0.861315\mathrm{x}10^{5}$	$0.306945\mathrm{x}10^{6}$	$-0.326926\mathrm{x}10^{6}$	0.089881-0.401688
$0.880894\mathrm{x}10^{3}$	$0.121696\mathrm{x}10^{4}$	$-0.351017\mathrm{x}10^{4}$	$0.191665\mathrm{x}10^{4}$	0.0	0.401688-0.965484
$0.119624\mathrm{x}10^{4}$	$-0.142171\mathrm{x}10^{4}$	$0.932509\mathrm{x}10^{3}$	$-0.207362\mathrm{x}10^{3}$	0.0	0.965484-1.843271
$0.469479\mathrm{x}10^{3}$	$0.205632\mathrm{x}10^{3}$	$-0.186177\mathrm{x}10^{3}$	$0.425618\mathrm{x}10^{2}$	$-0.307844\mathrm{x}10^{1}$	1.843271-5.56524
$0.314180\mathrm{x}10^{3}$	$0.135675\mathrm{x}10^{1}$	$-0.532581\mathrm{x}10^{1}$	$0.518617\mathrm{x}10^{0}$	$-0.146013\mathrm{x}10^{-1}$	5.56524-16.1107
$0.346889\mathrm{x}10^{3}$	$-0.116104\mathrm{x}10^{2}$	$-0.179965\mathrm{x}10^{0}$	$0.540131\mathrm{x}10^{-1}$	$-0.876146\mathrm{x}10^{-3}$	16.1107-28.91627
$0.244377\mathrm{x}10^{3}$	$-0.841251\mathrm{x}10^{1}$	$0.148719\mathrm{x}10^{0}$	$-0.934972\mathrm{x}10^{-3}$	0.0	28.91627-63.20518
$0.125703\mathrm{x}10^{3}$	$-0.136255\mathrm{x}10^{1}$	$0.936783\mathrm{x}10^{-2}$	$-0.317096\mathrm{x}10^{-4}$	$0.413127\mathrm{x}10^{-7}$	63.20518-263.3652
$0.588124\mathrm{x}10^{2}$	$-0.126971\mathrm{x}10^{1}$	$0.174138\mathrm{x}10^{-3}$	$-0.113033\mathrm{x}10^{-6}$	$0.273438\mathrm{x}10^{-10}$	263.3652-1528.847

TABLE A-10

PARAMETERS OF POLYNOMIAL EQUATION FOR MODEL II-3

a_1	b_1	c_1	d_1	e_1	Time Range sec
$0.114000\text{x}10^{3}$	$-0.751584\text{x}10^{1}$	$0.816311\text{x}10^{1}$	$-0.284283\text{x}10^{1}$	0.0	0.0-1.454723
$0.112085\text{x}10^{3}$	$-0.411311\text{x}10^{0}$	$-0.134107\text{x}10^{1}$	$0.109972\text{x}10^{-1}$	0.0	1.454723-9.94572
$0.135183\text{x}10^{3}$	$-0.502429\text{x}10^{1}$	$0.249547\text{x}10^{0}$	$-0.449544\text{x}10^{-2}$	0.0	9.945720-24.52534
$0.829351\text{x}10^{2}$	$0.152383\text{x}10^{1}$	$-0.523192\text{x}10^{-1}$	$0.442073\text{x}10^{-3}$	0.0	24.52534-55.03678
$0.979869\text{x}10^{2}$	$0.143261\text{x}10^{1}$	$-0.685087\text{x}10^{-1}$	$0.885819\text{x}10^{-3}$	$-0.379615\text{x}10^{-5}$	55.03678-87.79318
$0.156747\text{x}10^{3}$	$-0.171309\text{x}10^{1}$	$0.102444\text{x}10^{-1}$	$-0.233119\text{x}10^{-4}$	0.0	87.79318-162.3059
$0.101448\text{x}10^{3}$	$-0.522611\text{x}10^{0}$	$0.149725\text{x}10^{-2}$	$-0.162014\text{x}10^{-5}$	0.0	162.3059-358.1674
$0.673330\text{x}10^{2}$	$-0.166617\text{x}10^{0}$	$0.239155\text{x}10^{-3}$	$-0.130555\text{x}10^{-6}$	0.0	358.1675-621.1437
$0.362922\text{x}10^{2}$	$-0.232372\text{x}10^{-1}$	$0.714074\text{x}10^{-5}$	0.0	0.0	621.1437-1312.019

TABLE A-11

PARAMETERS OF POLYNOMIAL EQUATION FOR MODEL I-4-a

a_1	b_1	c_1	d_1	e_1	Time Range sec
0.113253×10^{3}	-0.407780×10^{1}	-0.167832×10^{0}	0.0	0.0	0.0-1.184507
0.111521×10^{3}	-0.246771×10^{1}	0.699692×10^{-1}	-0.151704×10^{-2}	0.0	1.184507-21.3199
0.116068×10^{3}	-0.233376×10^{1}	0.238622×10^{-1}	-0.901767×10^{-4}	0.0	21.3199-98.10719
0.556312×10^{3}	-0.342842×10^{0}	0.113168×10^{-2}	-0.137803×10^{-5}	0.0	98.10719-318.2507
0.337094×10^{2}	-0.850893×10^{-1}	0.121863×10^{-3}	-0.665941×10^{-7}	0.0	318.2507-660.2397
0.200093×10^{2}	-0.186799×10^{-1}	0.102389×10^{-4}	-0.219036×10^{-8}	0.0	660.2397-1556.819
0.114286×10^{2}	-0.340040×10^{-2}	0.572112×10^{-6}	$-0.362676 \times 10^{-10}$	0.0	1556.819-5912.277

TABLE A-12

PARAMETERS OF POLYNOMIAL EQUATION FOR MODEL I-4-b

a_1	b_1	c_1	d_1	e_1	Time Range sec
0.113791×10^{3}	-0.117552×10^{2}	0.214599×10^{2}	-0.130992×10^{2}	0.0	0.0-1.08612
0.111908×10^{3}	-0.144827×10^{1}	0.341604×10^{-1}	-0.620502×10^{-3}	0.0	1.08612-23.84747
0.108310×10^{3}	-0.867513×10^{0}	0.145984×10^{-2}	-0.957432×10^{-5}	0.0	23.84747-113.9147
0.839848×10^{2}	-0.551682×10^{0}	0.190279×10^{-2}	-0.243453×10^{-5}	0.0	113.9147-287.9638
0.462687×10^{2}	-0.111791×10^{0}	0.152326×10^{-3}	-0.794253×10^{-7}	0.0	287.9638-628.6677
0.291358×10^{2}	-0.293873×10^{-1}	0.169562×10^{-4}	-0.374347×10^{-8}	0.0	628.6677-1588.715
0.159067×10^{2}	-0.443916×10^{-2}	0.535195×10^{-6}	0.0	0.0	1588.715-3641.401
0.119025×10^{2}	-0.200610×10^{-2}	0.191781×10^{-6}	$-0.696886 \times 10^{-11}$	0.0	3641.401-10144.79

APPENDIX B

THE TRANSIENT HEAT CONDUCTION OF A TWO-LAYER SLAB WITH CONVECTIVE BOUNDARY CONDITION

The equations and boundary conditions describing Model I-8 are

$$c_I \frac{\partial T_I}{\partial t} = k_I \frac{\partial^2 u_I}{\partial x^2} \qquad \text{(B-1)}$$

$$c_s \frac{\partial T_I}{\partial t} = k_s \frac{\partial^2 u_s}{\partial x^2} \qquad \text{(B-2)}$$

$$T_I(x,0) = 0 = T_s(x,0) \qquad \text{(B-3)}$$

$$T_I = T_s \quad \text{at } x = \delta \qquad \text{(B-4)}$$

$$k_I \frac{\partial T_I}{\partial} = k_s \frac{\partial T_s}{\partial x} \quad \text{at } x = \delta \qquad \text{(B-5)}$$

$$k_I \left. \frac{\partial T_I}{\partial x} \right|_{x=0} = h(T_I - T_L) \quad \text{at } x = 0 \qquad \text{(B-6)}$$

$$T_s(\infty,t) = 0 \qquad \text{(B-7)}$$

Let $u_I = (T_I - T_\infty)/(T_L - T_\infty)$ and $u_s = (T_s - T_\infty)/(T_L - T_\infty)$. Then Equations B-1 and B-2 become

$$\frac{\partial u_I}{\partial t} = \alpha_I \frac{\partial^2 u_I}{\partial x^2} \qquad \text{(B-8)}$$

$$\frac{\partial u_s}{\partial x} = \alpha_s \frac{\partial^2 u_s}{\partial x^2} \qquad \text{(B-9)}$$

where $\alpha_I = k_I/c_I$ and $\alpha_s = k_s/c_s$. The boundary conditions are

$$u_I(x,0) = 0 = u_s(x,0) \qquad \text{(B-10)}$$

$$u_I = u_s \quad \text{at } x = \delta \qquad \text{(B-11)}$$

$$k_I \frac{\partial u_I}{\partial x} = k_s \frac{\partial u_s}{\partial x} \quad \text{at } x = \delta \qquad \text{(B-12)}$$

$$k_I \left.\frac{\partial u_I}{\partial x}\right|_{x=0} = h(u_I - 1) \quad \text{at } x = 0 \qquad \text{(B-13)}$$

$$u_s(\infty,t) = 0 \qquad \text{(B-14)}$$

Taking Laplace transformation with respect to t then

$$\frac{d\hat{u}_I}{dx^2} - \frac{p}{\alpha_I}\hat{u}_I = 0 \qquad \text{(B-15)}$$

$$\frac{d\hat{u}_s}{dx^2} - \frac{p}{\alpha_s}\hat{u}_s = 0 \qquad \text{(B-16)}$$

Thus

$$\hat{u}_I = A_1 e^{-\sqrt{p/\alpha_I}x} + B_1 e^{\sqrt{p/\alpha_I}x} \qquad \text{(B-17)}$$

$$\hat{u}_s = A_2 e^{-\sqrt{p/\alpha_s}x} \qquad \text{(B-18)}$$

The boundary conditions give

$$k_I \left.\frac{d\hat{u}_I}{dx}\right|_{x=0} = h(\hat{u}_I - \frac{1}{p}) \qquad \text{(B-19)}$$

Also

$$\frac{k_1}{k_2} = \frac{-\dfrac{A_2}{\sqrt{\alpha_2}}\, e^{-\delta\sqrt{p/\alpha_s}}}{-\dfrac{A_1}{\sqrt{\alpha_1}}\, e^{-\delta\sqrt{p/\alpha_I}} + \dfrac{B_1}{\sqrt{\alpha_1}}\, e^{\delta\sqrt{p/\alpha_I}}} \qquad \text{(B-20)}$$

and

$$A_1\, e^{-\delta\sqrt{p/\alpha_I}} + B_1\, e^{\delta\sqrt{p/\alpha_I}} = A_2\, e^{-\delta\sqrt{p/\alpha_s}} \qquad \text{(B-21)}$$

These result in

$$B_1 = \frac{-h}{\gamma k_I p}\left(\frac{1}{e^{2\delta\sqrt{p/\alpha_I}}}\right)\left(\frac{1}{\left(\sqrt{\dfrac{p}{\alpha_I}} + \dfrac{h}{k_I}\right) + \left(\sqrt{\dfrac{p}{\alpha_I}} - \dfrac{h}{k_I}\right)\gamma^{-1}\, e^{-2\delta\sqrt{p/\alpha_I}}}\right) \qquad \text{(B-22)}$$

where

$$\gamma = \frac{k_s\sqrt{\alpha_I} + k_I\sqrt{\alpha_s}}{k_s\sqrt{\alpha_I} - k_I\sqrt{\alpha_s}}$$

$$A_1 = \frac{h}{k_I p}\, \frac{1}{\sqrt{\dfrac{p}{\alpha_I}} + \dfrac{h}{k_I}} \left\{ 1 - \frac{1}{\gamma\, e^{2\delta\sqrt{p/\alpha_I}}} \times \frac{\sqrt{\dfrac{p}{\alpha_I}} - \dfrac{h}{k_I}}{\left(\sqrt{\dfrac{p}{\alpha_I}} + \dfrac{h}{k_I}\right) + \left(\sqrt{\dfrac{p}{\alpha_I}} - \dfrac{h}{k_I}\right)\gamma^{-1}\, e^{-2\delta\sqrt{p/\alpha_I}}} \right\} \qquad \text{(B-23)}$$

$$A_2 = -\frac{2\sqrt{\alpha_s}}{p}\, e^{-\delta(-\sqrt{p/\alpha_s} + \sqrt{p/\alpha_I})} \times \left(\frac{\lambda}{\gamma\left[\left(\sqrt{\dfrac{p}{\alpha_I}} + \dfrac{h}{k_I}\right) + \left(\sqrt{\dfrac{p}{\alpha_I}} - \dfrac{h}{k_I}\right)\gamma^{-1}\, e^{-2\delta\sqrt{p/\alpha_I}}\right]}\right) \qquad \text{(B-24)}$$

where $\lambda = (k_s\sqrt{\alpha_I} - k_I\sqrt{\alpha_s})^{-1}$.

Hence,

$$\hat{u}_I = \frac{h}{k_I p} \frac{1}{\sqrt{\frac{p}{\alpha_I}} + \frac{h}{k_I}} \left\{ 1 - \frac{1}{\gamma\ e^{2\delta\sqrt{p/\alpha_I}}} \right.$$

$$\left. \times \frac{\sqrt{p/\alpha_I} - h/k_I}{(\sqrt{\frac{p}{\alpha_I}} + \frac{h}{k_I}) + (\sqrt{\frac{p}{\alpha_I}} - \frac{h}{k_I})\gamma^{-1}\ e^{-2\delta\sqrt{p/\alpha_I}}} \right\} e^{-\sqrt{p/\alpha_I}\ x}$$

$$- \frac{h}{\gamma k_I p e^{2\delta\sqrt{p/\alpha_I}}} \frac{1}{(\sqrt{\frac{p}{\alpha_I}} + \frac{h}{k_I}) + (\sqrt{\frac{p}{\alpha_I}} - \frac{h}{k_I})\gamma^{-1} e^{-2\delta\sqrt{p/\alpha_I}}}$$

$$\times\ e^{\sqrt{p/\alpha_I}\ x} \qquad \text{(B-25)}$$

and

$$\hat{u}_s = - \frac{2\sqrt{\alpha_s}}{p}\ e^{-\delta(-\sqrt{p/\alpha_s} + \sqrt{p/\alpha_I})}$$

$$\times \frac{\lambda}{\gamma} \frac{e^{-\sqrt{p/\alpha_s}\ x}}{(\sqrt{\frac{p}{\alpha_I}} + \frac{h}{k_I}) + (\sqrt{\frac{p}{\alpha_I}} - \frac{h}{k_I})\gamma^{-1} e^{-2\delta\sqrt{p/\alpha_I}}} \qquad \text{(B-26)}$$

Since $\gamma^{-1}\ e^{-2\gamma\sqrt{p/\alpha_I}}$ is essentially less than unity, so $\hat{u}_I$ and $\hat{u}_s$ can be expressed by a power series.

Therefore,

$$\hat{u}_I = \frac{h}{k_I p}\,\frac{e^{-\sqrt{p/\alpha_I}\;x}}{\sqrt{\frac{p}{\alpha_I}} + \frac{h}{k_I}} - \frac{h}{\gamma k_I p}\, e^{(-\sqrt{p/\alpha_I}\;x\; -\; 2\sqrt{p/\alpha_I}\;\delta)}\,\frac{\sqrt{\frac{p}{\alpha_I}} - \frac{h}{k_I}}{\sqrt{\frac{p}{\alpha_I}} + \frac{h}{k_I}}$$

$$\times \left\{ \frac{1}{\sqrt{\frac{p}{\alpha_I}} + \frac{h}{k_I}} - \frac{\sqrt{\frac{p}{\alpha_I}} - \frac{h}{k_I}}{[\sqrt{\frac{p}{\alpha_I}} + \frac{h}{k_I}]^2}\,\gamma^{-1}\,e^{-2\sqrt{p/\alpha_I}\;\delta} \right.$$

$$\left. + \frac{(\sqrt{\frac{p}{\alpha_I}} - \frac{h}{k_I})^2}{(\sqrt{\frac{p}{\alpha_I}} + \frac{h}{k_I})^3}\,\gamma^{-2}\,e^{-4\sqrt{p/\alpha_I}\;\delta} + \ldots \right\}$$

$$- \frac{h}{\gamma k_I p}\, e^{\sqrt{p/\alpha_I}x - 2\sqrt{p/\alpha_I}\delta} \left\{ \frac{1}{\sqrt{\frac{p}{\alpha_I}} + \frac{h}{k_I}} - \frac{\sqrt{\frac{p}{\alpha_I}} - \frac{h}{k_I}}{(\sqrt{\frac{p}{\alpha_I}} + \frac{h}{k_I})^2}\,\gamma^{-1} e^{-2\sqrt{p/\alpha_I}\delta} \right.$$

$$\left. + \frac{(\sqrt{\frac{p}{\alpha_I}} - \frac{h}{k_I})^2}{(\sqrt{\frac{p}{\alpha_I}} + \frac{h}{k_I})^3}\,\gamma^{-2}\,e^{-4\sqrt{p/\alpha_I}\;\delta} + \ldots \right\} \quad \text{(B-27)}$$

$$\hat{u}_s = \frac{2h\sqrt{\alpha_I}}{p}\,\frac{\lambda}{\gamma} \left\{ \frac{e^{-\sqrt{p/\alpha_s}(x-\delta+\sqrt{\alpha_s/\alpha_I}\delta)}}{\sqrt{\frac{p}{\alpha_s}} + \frac{h}{k_I}\sqrt{\frac{\alpha_I}{\alpha_s}}} - \frac{1}{\gamma}\,\frac{e^{-\sqrt{p/\alpha_s}(x-\delta+3\sqrt{\alpha_s/\alpha_I}\delta)}}{\sqrt{\frac{p}{\alpha_s}} + \frac{h}{k_I}\sqrt{\frac{\alpha_I}{\alpha_s}}} \right.$$

$$\left. - \frac{2\,\frac{h}{k_I}\sqrt{\frac{\alpha_I}{\alpha_s}}\;e^{-\sqrt{p/\alpha_s}(x-\delta+3\sqrt{\alpha_s/\alpha_I}\;\delta)}}{\gamma\;(\sqrt{\frac{p}{\alpha_s}} + \frac{h}{k_I}\sqrt{\frac{\alpha_I}{\alpha_s}})^2} + \ldots \right\} \quad \text{(B-28)}$$

From the above expressions it is found that the successive exponentials have coefficients which are complicated functions of $\sqrt{p/\alpha_s}$. Therefore, there are no simple series for u_I and u_s. But only the first few terms of u_I and u_s can be written down immediately. Thus u_I and u_s are

$$
\begin{aligned}
u_I = {} & \operatorname{erfc} \frac{x}{2\sqrt{\alpha_I t}} - e^{\frac{h}{k_I}x+\alpha_I t\frac{h^2}{k_I^2}} \operatorname{erfc} \left(\frac{x}{2\sqrt{\alpha_I t}} + \frac{h}{k_I}\sqrt{\alpha_I t}\right) \\
& - \frac{1}{\gamma}\Bigg(\operatorname{erfc} \frac{x+2\delta}{2\sqrt{\alpha_I t}} - e^{\frac{h}{k_I}(x+2\delta)+\alpha_I t\frac{h^2}{k_I^2}} \operatorname{erfc} \left(\frac{x+2\delta}{2\sqrt{\alpha_I t}} + \frac{h}{k_I}\sqrt{\alpha_I t}\right)\Bigg) \\
& - \frac{1}{\gamma}\Bigg(\operatorname{erfc} \frac{-x+2\delta}{2\sqrt{\alpha_I t}} - e^{\frac{h}{k_I}(-x+2\delta)+\alpha_I t\frac{h^2}{k_I^2}} \operatorname{erfc} \left(\frac{-x+2\delta}{2\sqrt{\alpha_I t}} + \frac{h}{k_I}\sqrt{\alpha_I t}\right)\Bigg) \\
& + \frac{1}{\gamma^2}\Bigg(\operatorname{erfc} \frac{-x+4\delta}{2\sqrt{\alpha_I t}} - e^{\frac{h}{k_I}(-x+4\delta)+\alpha_I t\frac{h^2}{k_I^2}} \operatorname{erfc} \left(\frac{-x+4\delta}{2\sqrt{\alpha_I t}} + \frac{h}{k_I}\sqrt{\alpha_I t}\right)\Bigg) \\
& + \frac{2}{\gamma}\Bigg(\operatorname{erfc} \frac{x+2\delta}{2\sqrt{\alpha_I t}} - \frac{2h}{k_I}\left(\frac{\alpha_I t}{\pi}\right)^{1/2} e^{-(x+2\delta)^2/4\alpha_I t} \\
& \qquad - \left[1 - \frac{h}{k_I}(x+2\delta) - \frac{2h^2}{k_I^2}\alpha_I t\right] e^{\frac{h}{k_I}(x+2\delta)+\alpha_I t\frac{h^2}{k_I^2}} \\
& \qquad\qquad \times \operatorname{erfc}\left(\frac{x+2\delta}{2\sqrt{\alpha_I t}} + \frac{h}{k_I}\sqrt{\alpha_I t}\right)]\Bigg) \\
& - \frac{2}{\gamma^2}\Bigg(\operatorname{erfc} \frac{-x+4\delta}{2\sqrt{\alpha_I t}} - \frac{2h}{k_I}\left(\frac{\alpha_I t}{\pi}\right)^{1/2} e^{-(-x+4\delta)^2/4\alpha_I t} \\
& \qquad - \left[1 - \frac{h}{k_I}(-x+4\delta) - \frac{2h^2}{k_I^2}\alpha_I t\right] e^{\frac{h}{k_I}(-x+4\delta)+\alpha_I t\frac{h^2}{k_I^2}} \\
& \qquad\qquad \times \operatorname{erfc}\left(\frac{-x+4\delta}{2\sqrt{\alpha_I t}} + \frac{h}{k_I}\sqrt{\alpha_I t}\right)\Bigg) \\
& + \ldots \qquad\qquad \text{(B-29)}
\end{aligned}
$$

$$
\begin{aligned}
u_s = \frac{2k_I\sqrt{\alpha_s}\ \lambda}{\gamma}\Bigg\{ & \operatorname{erfc}\frac{x-\delta+\sqrt{\frac{\alpha_s}{\alpha_I}}\ \delta}{2\sqrt{\alpha_s t}} - e^{\frac{h}{k_I}\sqrt{\frac{\alpha_I}{\alpha_s}}\left(x-\delta+\sqrt{\frac{\alpha_s}{\alpha_I}}\ \delta\right)+\alpha_I t\frac{h^2}{k_I^2}} \\
& \qquad \times\ \operatorname{erfc}\left[\frac{x-\delta+\sqrt{\frac{\alpha_s}{\alpha_I}}\ \delta}{2\sqrt{\alpha_s t}} + \frac{h}{k_I}\ \sqrt{\alpha_I t}\right] \\
& - \frac{1}{\gamma}\Bigg\{\operatorname{erfc}\frac{x-\delta+3\sqrt{\frac{\alpha_s}{\alpha_I}}\ \delta}{2\sqrt{\alpha_s t}} - e^{\frac{h}{k_I}\sqrt{\frac{\alpha_I}{\alpha_s}}\left(x-\delta+3\sqrt{\frac{\alpha_s}{\alpha_I}}\delta\right)} \\
& \qquad \times\ \operatorname{erfc}\left[\frac{x-\delta+3\sqrt{\frac{\alpha_s}{\alpha_I}}\ \delta}{2\sqrt{\alpha_s t}} + \frac{h}{k_I}\ \sqrt{\alpha_I t}\right]\Bigg\} \\
& - \frac{2}{\gamma}\Bigg\{\operatorname{erfc}\frac{x-\delta+3\sqrt{\frac{\alpha_s}{\alpha_I}}\ \delta}{2\sqrt{\alpha_s t}} - \frac{h\sqrt{\alpha_I}}{k_I\sqrt{\alpha_s}}\ \left(\frac{\alpha_s t}{\pi}\right)^{1/2}\ e^{-\left(x-\delta+3\sqrt{\frac{\alpha_s}{\alpha_I}}\delta\right)^2/4\alpha_s t} \\
& \quad - \left(1 - \frac{h}{k_I}\sqrt{\frac{\alpha_s}{\alpha_I}}\ \left(x-\delta+3\sqrt{\frac{\alpha_s}{\alpha_I}}\delta\right) - \frac{h^2}{k_I^2}\sqrt{\frac{\alpha_s}{\alpha_I}}\ \alpha_s t\right) \\
& \qquad \times\ e^{\frac{h}{k_I}\sqrt{\frac{\alpha_I}{\alpha_s}}\left(x-\delta+3\sqrt{\frac{\alpha_s}{\alpha_I}}\delta\right)+\alpha_I t\frac{h^2}{k_I^2}} \\
& \quad \times\ \operatorname{erfc}\left[\frac{x-\delta+3\sqrt{\frac{\alpha_s}{\alpha_I}}\ \delta}{2\sqrt{\alpha_s t}} + \frac{h}{k_I}\ \sqrt{\alpha_I t}\right]\Bigg\}\ +\ldots\Bigg\} \qquad \text{(B-30)}
\end{aligned}
$$

APPENDIX C

FLOW DIAGRAM FOR SOLVING ONE- AND TWO-DIMENSIONAL HEAT CONDUCTION PROBLEMS WITH PHASE CHANGE

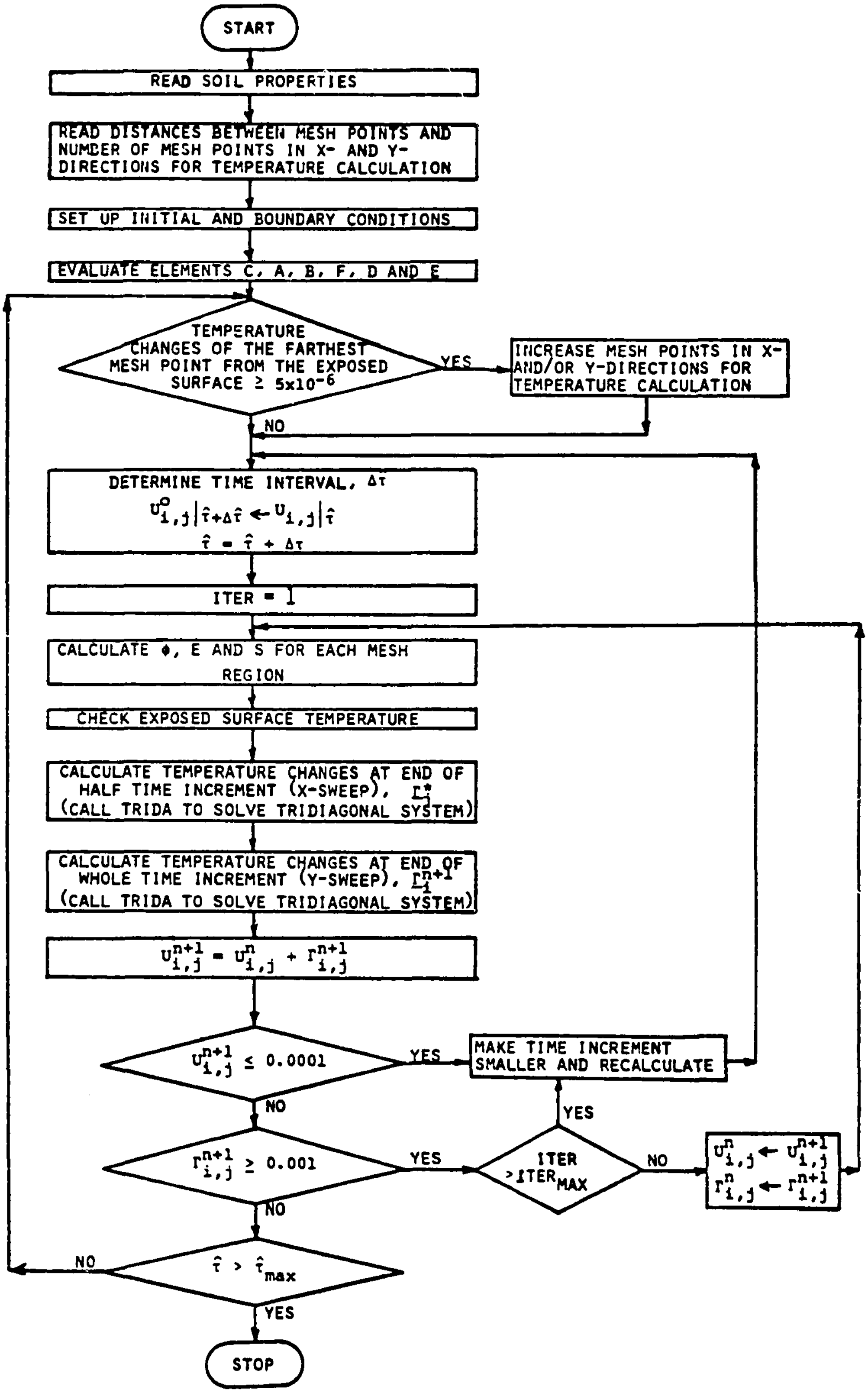
START
READ SOIL PROPERTIES
READ DISTANCES BETWEEN MESH POINTS AND NUMBER OF MESH POINTS IN X- AND Y-DIRECTIONS FOR TEMPERATURE CALCULATION
SET UP INITIAL AND BOUNDARY CONDITIONS
EVALUATE ELEMENTS C, A, B, F, D AND E
TEMPERATURE CHANGES OF THE FARTHEST MESH POINT FROM THE EXPOSED SURFACE $\geq 5\times10^{-6}$
YES
INCREASE MESH POINTS IN X- AND/OR Y-DIRECTIONS FOR TEMPERATURE CALCULATION
NO
DETERMINE TIME INTERVAL, $\Delta\tau$
$U^{o}_{i,j}\big|_{\hat{\tau}+\Delta\hat{\tau}} \leftarrow U_{i,j}\big|_{\hat{\tau}}$
$\hat{\tau} = \hat{\tau} + \Delta\tau$
ITER = 1
CALCULATE ϕ, E AND S FOR EACH MESH REGION
CHECK EXPOSED SURFACE TEMPERATURE
CALCULATE TEMPERATURE CHANGES AT END OF HALF TIME INCREMENT (X-SWEEP), Γ^{*}_{i} (CALL TRIDA TO SOLVE TRIDIAGONAL SYSTEM)
CALCULATE TEMPERATURE CHANGES AT END OF WHOLE TIME INCREMENT (Y-SWEEP), Γ^{n+1}_{i} (CALL TRIDA TO SOLVE TRIDIAGONAL SYSTEM)
$U^{n+1}_{i,j} = U^{n}_{i,j} + \Gamma^{n+1}_{i,j}$
$U^{n+1}_{i,j} \leq 0.0001$
YES
MAKE TIME INCREMENT SMALLER AND RECALCULATE
NO
$\Gamma^{n+1}_{i,j} \geq 0.001$
YES
YES
ITER $>$ ITER$_{MAX}$
NO
$U^{n}_{i,j} \leftarrow U^{n+1}_{i,j}$
$\Gamma^{n}_{i,j} \leftarrow \Gamma^{n+1}_{i,j}$
NO
NO
$\hat{\tau} > \hat{\tau}_{max}$
YES
STOP